

NASA/TM—2001-210901



High Temperature, Slow Strain Rate Forging of Advanced Disk Alloy ME3

Timothy P. Gabb and Kenneth O'Connor
Glenn Research Center, Cleveland, Ohio

August 2001

The NASA STI Program Office . . . in Profile

Since its founding, NASA has been dedicated to the advancement of aeronautics and space science. The NASA Scientific and Technical Information (STI) Program Office plays a key part in helping NASA maintain this important role.

The NASA STI Program Office is operated by Langley Research Center, the Lead Center for NASA's scientific and technical information. The NASA STI Program Office provides access to the NASA STI Database, the largest collection of aeronautical and space science STI in the world. The Program Office is also NASA's institutional mechanism for disseminating the results of its research and development activities. These results are published by NASA in the NASA STI Report Series, which includes the following report types:

- **TECHNICAL PUBLICATION.** Reports of completed research or a major significant phase of research that present the results of NASA programs and include extensive data or theoretical analysis. Includes compilations of significant scientific and technical data and information deemed to be of continuing reference value. NASA's counterpart of peer-reviewed formal professional papers but has less stringent limitations on manuscript length and extent of graphic presentations.
- **TECHNICAL MEMORANDUM.** Scientific and technical findings that are preliminary or of specialized interest, e.g., quick release reports, working papers, and bibliographies that contain minimal annotation. Does not contain extensive analysis.
- **CONTRACTOR REPORT.** Scientific and technical findings by NASA-sponsored contractors and grantees.

- **CONFERENCE PUBLICATION.** Collected papers from scientific and technical conferences, symposia, seminars, or other meetings sponsored or cosponsored by NASA.
- **SPECIAL PUBLICATION.** Scientific, technical, or historical information from NASA programs, projects, and missions, often concerned with subjects having substantial public interest.
- **TECHNICAL TRANSLATION.** English-language translations of foreign scientific and technical material pertinent to NASA's mission.

Specialized services that complement the STI Program Office's diverse offerings include creating custom thesauri, building customized data bases, organizing and publishing research results . . . even providing videos.

For more information about the NASA STI Program Office, see the following:

- Access the NASA STI Program Home Page at <http://www.sti.nasa.gov>
- E-mail your question via the Internet to help@sti.nasa.gov
- Fax your question to the NASA Access Help Desk at 301-621-0134
- Telephone the NASA Access Help Desk at 301-621-0390
- Write to:
NASA Access Help Desk
NASA Center for Aerospace Information
7121 Standard Drive
Hanover, MD 21076

NASA/TM—2001-210901



High Temperature, Slow Strain Rate Forging of Advanced Disk Alloy ME3

Timothy P. Gabb and Kenneth O'Connor
Glenn Research Center, Cleveland, Ohio

National Aeronautics and
Space Administration

Glenn Research Center

August 2001

Acknowledgments

The authors wish to acknowledge the many helpful discussions with David Mourer at General electric Aircraft Engines. The tests were performed at Wyman-Gordon Forgings, Houston R&D lab, by mike Powell, while the subsequent heat treatments were performed by Jim Smith, under the direction of William Konkel.

Available from

NASA Center for Aerospace Information
7121 Standard Drive
Hanover, MD 21076

National Technical Information Service
5285 Port Royal Road
Springfield, VA 22100

Available electronically at <http://gltrs.grc.nasa.gov/GLTRS>

High Temperature, Slow Strain Rate Forging of Advanced Disk Alloy ME3

Timothy P. Gabb and Kenneth O'Connor
National Aeronautics and Space Administration
Glenn Research Center
Cleveland, Ohio 44135

Introduction

The advanced disk alloy ME3 was designed in the HSR/EPM disk program to have extended durability at 1150-1250F in large disks. This was achieved by designing a disk alloy and process producing balanced monotonic, cyclic, and time-dependent mechanical properties, combined with robust processing and manufacturing characteristics. The resulting baseline alloy, processing, and supersolvus heat treatment produces a uniform, relatively fine mean grain size of about ASTM 7, with as-large-as (ALA) grain size of about ASTM 3 (ref. 1).

There is a long term need for disks with higher rim temperature capabilities than 1250F. This would allow higher compressor exit (T3) temperatures and allow the full utilization of advanced combustor and airfoil concepts under development. Several approaches are being studied that modify the processing and chemistry of ME3, to possibly improve high temperature properties. Promising approaches would be applied to subscale material, for screening the resulting mechanical properties at these high temperatures. An obvious path traditionally employed to improve the high temperature and time-dependent capabilities of disk alloys is to coarsen the grain size (ref. 2, 3). A coarser grain size than ASTM 7 could potentially be achieved by varying the forging conditions and supersolvus heat treatment (ref. 4).

The objective of this study was to perform forging and heat treatment experiments (“thermomechanical processing experiments”) on small compression test specimens of the baseline ME3 composition, to identify a viable forging process allowing significantly coarser grain size targeted at ASTM 3-5, than that of the baseline, ASTM 7.

Material and Procedure

Specimen machining, testing, and heat treatments were performed by Wyman-Gordon Forgings, Houston, Texas. A 1.1” thick cross-section of extrusion SMK05398 was removed using an abrasive disk saw. Specimen blanks were then electrodischarge machined along a 4.5” diameter circle centered in the cross section. Twenty right circular cylinder (RCC) specimens having a diameter of 0.50” and length of 0.75” were then machined. Six double cone (DC) specimens were also machined according to Fig. 1 (ref. 5). The matrix of test conditions for the RCC and DC specimens is shown in Table 1. RCC specimens were tested at 3 temperatures 2025, 2050, and 2075F using 3 strain rates of 0.0001, 0.0003, and 0.001 sec⁻¹, after being pre-soaked at the test temperature for times of either 1 or 10 h. This represented a 3x3x2 full factorial statistical test matrix. Additional RCC tests were performed at the mid temperature 2050F and strain rate 0.003 sec⁻¹: after a pre-soak of 5h to represent the centerpoint of the test matrix, and after

an extended pre-soak of 24h. All RCC tests were continued to an upset of at least 50%, and true strain of 0.70. DC specimens were tested at the 2 extreme temperatures of 2025 and 2075F and 2 extreme strain rates of 0.0001 and 0.001 sec⁻¹ after a 10h presoak, giving a 2x2 test matrix. Additional DC tests were performed at the mid temperature 2050F and strain rate 0.003 sec⁻¹ after a pre-soak of 5h as for the RCC matrix centerpoint, and after an extended pre-soak of 24h. All DC tests were continued to an upset of 50%.

After the tests, all specimens were sliced into four quarters. Single quarters of each specimen were heat treated together on a tray in a resistance heated furnace using a “direct heatup” (DH) supersolvus heat treatment of 2140F/1h and then air cooled. Other quarters were given a “pre-annealed” (PA) supersolvus heat treatment consisting of a subsolvus pre-anneal of 2075F/1h, followed by an extended supersolvus treatment of 2140F/3h. Heat treated and as-forged quarters were then sectioned, metallographically prepared, and swab etched for 3 minutes using Kallings reagent. Five fields near the center of the forging specimen were measured to determine mean grain size in each case, using a circular overlay grid according to ASTM E112. The largest grain observed on each metallographic section was measured for as-large-as (ALA) grain size according to ASTM E930. Statistical evaluations of flow stress and grain sizes were then performed. The test datum of 2050F/0.0003s⁻¹/24h presoak was not used in the statistical evaluations, as it would unbalance the statistical matrix designed around presoak times of 1 and 10h. Controlled variables were orthogonally scaled to standardized form in all cases using the relationship $v_i' = (v_i - v_{\text{mean}}) / (0.5 * (v_{\text{max}} - v_{\text{min}}))$. This produced a range for each standardized variable of -1 to +1. This gave standardized variables for temperature (T'), presoak time (P'), and log strain rate (log(R)') of:

$$T' = (T - 2050) / 25 \quad P' = (P - 5.5) / 4.5 \quad \log(R)' = (\log(R) + 3.5) / 0.5$$

After regression model equations were selected, major effects, residuals, and predicted confidence intervals were examined for each response.

Results and Discussion

Forging Stress-Strain Response

Typical engineering stress-strain curves are shown for RCC tests, and load-displacement curves for DC tests are shown in Fig. 2. Flow stress at a true strain of 0.5 for each RCC test was employed in detailed analyses. Scatter plots of this flow stress (S) vs. temperature (T), pre-soak time (P) and strain rate (R) are shown in Fig. 3. Strong dependencies of flow stress on temperature and strain rate are obvious. Reverse stepwise selection linear regression of log(stress) on log(strain rate), temperature, pre-soak time, and their interactive products were performed, using an F-to-enter=4. The resulting linear regression equation was:

$$\log(\text{stress}) = -.240553 + 0.041239T' + 0.018252P' + 0.554102\log(R)' \quad (1)$$

with a correlation coefficient $R^2_{\text{adj}} = .984$ and rms error = 0.03434. The complete statistical output is included in Appendix A-1. Plots of the resulting predicted and observed log(stress) vs. pre-soak time and vs. log(strain rate) showed only random error. A plot

of predicted and observed log(stress) vs. temperature is also shown in A-1. A systematic divergence at intermediate temperature is obvious, suggesting a non-linear dependence of log(stress) on temperature. Therefore, reverse stepwise selection regressions were performed including the squares of each variable. The resulting nonlinear regression equation was:

$$\log(\text{stress})=381.044539-0.371578T'+0.000091T'^2+0.019031P'+0.563907\log(R)' \quad (2)$$

with a higher correlation coefficient $R^2_{\text{adj}}=.995$ and lower rms error=0.0194. The plot of predicted and observed log(stress) vs. temperature showed improved agreement (A-2). This equation indicated flow stress generally increased with presoak time and strain rate, but the dependence varied with temperature. In the temperature range of 2025 to 2050F, flow stress only slightly increased with temperature. Such a temperature response would be preferable in a production process. But at higher temperatures, flow stress increased more sharply with temperature.

It is highly preferable that the alloy exhibit superplastic flow during a forging process. This allows complete flow of the material into all forging die cavities with uniform strain and strain rates in the disk alloy, and minimizes the buildup of stresses in the dies. Superplastic flow is present when a material exhibits high strain rate sensitivity (m), as usually defined by the relationship $\sigma=K(d\varepsilon/dt)^m$. A material is considered superplastic in deformation conditions where a strain rate sensitivity m of at least 0.3 is observed. The strain rate sensitivity m was determined by fitting a second order polynomial to the log(stress) data as a function of log(strain rate) for each temperature and pre-soaks of 1 and 10h. The first derivative was then taken and evaluated at each tested strain rate. It should be cautioned that only three strain rates were tested for each temperature and pre-soak. Therefore, the second order polynomial fit used three data points to estimate 3 constants, resulting in 0 degrees of freedom and a perfect fit through the data. This did not allow an estimate of the remaining rms standard deviation between the experimental data and the curve fit. The resulting equation constants are in Table 2, and strain rate sensitivities are included in Table 1. The material exhibited superplastic flow for all conditions evaluated.

Grain Size Response

1. As-Forged

Images of the typical microstructures observed in all specimens in the as-forged state are compared in Fig. 4-9. Macrostructures appeared uniform in all cases. Scatter plots of as-forged mean grain size (AFG) versus temperature (T), pre-soak time (P), and log(strain rate) (R) are shown in Fig. 3. Dependencies of grain size on temperature and strain rate are obvious. Reverse stepwise linear regression of mean ASTM grain size number on temperature, pre-soak time, log(strain rate), and their interactive products were performed, using an F-to-enter=4. The resulting linear regression equation was:

$$\text{AFG}=11.294737-0.416667T'$$

with a correlation coefficient $R^2_{\text{adj}}=0.6598$ and rms error=0.2408. The complete statistical output is given in Appendix B. Plots of the resulting predicted and observed

mean grain size vs. pre-soak time and vs. log(strain rate) showed only random error (A-3). The accompanying plot of predicted and observed mean grain size vs. temperature showed a systematic divergence at intermediate temperature, suggesting a non-linear dependence of mean grain size on temperature as observed for flow stress. Therefore, additional reverse stepwise regressions were performed including the squares of each variable. The resulting nonlinear regression equation was:

$$\text{AFG}=11.486292-0.415313T' -0.077218P'+0.091960R'-0.100000T'P'+0.088773T'R'-0.301556(T')^2 \quad (3)$$

with a higher correlation coefficient $R^2_{\text{adj}}=0.9072$ and lower rms error=0.1258. The plot of predicted and observed grain size vs. temperature showed improved agreement with random remaining error. These results mirrored the flow stress analysis in the respect that within a temperature range of 2025-2050F, as-forged grain size did not strongly increase with temperature. This would be a favorable temperature response range for production considerations.

2. Direct Heatup (DH) vs. Pre-Annealed (PA) Heat Treatment Response

Images of the typical macrostructures and microstructures observed in all specimens after DH and PA heat treatments are compared in Fig. 10-29. During forging, disks could have significant localized variations in strain rate, based on forging shape and material flow characteristics. During solution heat treatment, disks could have significant localized variations in solution time at temperature and subsequent cooling rate based on forging section thickness and mass, along with production practices. The microstructures are therefore compared at constant forging temperature and pre-soak time, to inspect the variations in grain size due to forging strain rate and solutioning time. Macroscopic variations of grain size with location are obvious for long presoaks, slow strain rates, and higher temperatures, especially at 2075F. Some of the variations in grain size were localized near the surface and might be machined away from a disk forging. However, the grain size variations for higher temperatures extended nearly across the entire specimen cross section. The RCC and DC specimens tested at 2075F often had over 100% larger grains in the center of the specimen, than near the sides. This excessive grain growth, while not classifiable as true critical grain growth at high strain rates (ref. 5), was definitely not conducive to a uniform supersolvus heat treatment grain size response desired in this study.

Grain sizes were consistently measured near the center of the cross section of each specimen. Scatter plots of averaged DH and PA mean grain size and ALA grain size are shown versus temperature (T), pre-soak time (P), and log(strain rate) (R) are shown in Fig. 30. Dependencies of grain size on temperature and strain rate are obvious. Regression analyses were therefore employed.

Two approaches were used to analyze this data. The first approach C evaluated the stability of grain size response with the Constraint that the two solution heat treat types DH and PA could be used to simulate expected random cause heat treatment process variations. The average and standard deviation between DH and PA mean grain sizes and the average between DH and PA ALA grain sizes were first analyzed in

approach C. The C analyses therefore had 19 data points for each of averaged grain size, standard deviation of grain size, and averaged ALA grain size.

The second approach U used solution time as a fourth Unconstrained process variable. From a practical standpoint, solution time variations could be due to furnace run-to-run dwell time variations, material location in a disk, and location of a disk on a tray of multiple disks within a furnace. Note that approach U ignored the contribution of the pre-anneal step of the PA heat treatment on resulting grain size. Approach U assumed that the grain size differences between DH and PA heat treatments were primarily due to only solution time, which for a disk can be measured with embedded thermocouples and modeled as a function of location for any disk shape. The U analyses therefore had 38 data points for each of mean grain size, standard deviation of grain size, and ALA grain size. The evaluations below indicated solution time did not significantly affect mean grain size, ALA grain size, and standard deviation of grain size.

Reverse stepwise selection linear regression of mean grain size (G) on the standardized variables and their interactive products were performed, using an F-to-remove=3.9. The resulting linear regression equations (A-4C and A-4U) were:

$$G=3.577042-1.008333T'-0.325844P' \quad R^2_{adj}=0.8251, \text{ rms error}=0.403 \quad (4C)$$

$$G=3.550790-1.000000T'-0.314903P' \quad R^2_{adj}=0.7394, \text{ rms error}=0.5077 \quad (4U)$$

These equations both indicated ASTM grain size number decreased (grain size increased) with increasing temperature and presoak time.

Linear regression of ALA grain size on the standardized variables and their interactive products were also performed, using an F-to-remove=3.9. The resulting linear regression equations were:

$$ALA=-0.499171-1.066667T'-0.428152P'+0.197674R' \quad R^2_{adj}=0.8700, \quad (5C)$$

$$\text{rms error}=0.3756$$

$$ALA=-0.496379-1.062500T'-0.425361P'+0.206261R'-0.179167 T'P' \quad (5U)$$

$$R^2_{adj}=0.8467, \text{ rms error}=0.4122$$

The complete statistical output is given in Appendix A-5C and A-5U. Plots of the resulting predicted and observed mean and ALA grain size vs. temperature, pre-soak time and vs. log(strain rate) showed only random error. The equations both indicated that ALA grain size coarsened with increasing temperature, presoak time, and decreasing strain rate. Equation 5U indicated an additional interactive contribution of combining high temperature and long presoak times gave coarser ALA grain sizes.

The regressions of standard deviation of supersolvus grain size (SDG) gave mixed results:

$$SDG=-.357895 \quad R^2_{adj}=0.0000, \text{ rms error}=0.2969 \quad (6C)$$

$$\text{Log}(SDG)=-1.172359+0.394899T'-0.192353R'-0.259390T'R' \quad R^2_{adj}=0.4186 \quad (6U)$$

$$\text{rms error}=0.4417$$

The complete statistical output is given in Appendix A-6C and A-6U. Plots of the resulting predicted and observed standard deviation of grain size vs. temperature, pre-soak time and vs. log(strain rate) showed only random error. While the rms error was larger using approach 6U, this equation did provide guidance in what variables controlled SDG. The standard deviation of grain size increased with temperature and decreased with strain rate, with their additional interactive contribution decreasing standard deviation.

Selection of Modified Forging Conditions

The equations generated to describe flow stress, mean as-forged grain size, as well as supersolvus heat treated mean, standard deviation, and ALA grain sizes could now be used to allow selection of modified forging conditions. It was clear that the target grain size of ASTM 3-5 could easily be attained using various combinations of temperature, presoak, and strain rate. The flow stresses were all acceptably low, and the material remained superplastic in all conditions evaluated. However, the uniformity goal was a key discriminator. The variation in grain size observed across the TMP specimens and across specimens with varied strain rates and presoaks clearly increased with temperature. Further, the ALA grain size coarsened unacceptably at high temperatures. These trends all pointed to the lower temperature of near 2025F as preferable. Flow stress and as-forged grain size was relatively stable between 2025 and 2050F. Heat treated grain size and ALA grain size only moderately increased with increasing presoak time at 2025F, as opposed to the larger changes at 2050 and 2075F. ALA grain size became finer with increasing strain rate.

The statistical software was used to determine optimal conditions for minimized ALA grain size in equ. 5C and 5U, and for minimized standard deviation of heat treated grain size in equ. 6U. The optimal conditions were 2025F/1h presoak/ 0.001 s^{-1} strain rate. However, a constant presoak time of 1h would not be possible in a section greater than 1" thick, due to variations in heat up time in a furnace. Heat up times can vary by 1 hour between a surface and midsection. So a longer presoak time would be necessary to allow for such heat up effects. An intermediate presoak of 5h was selected for several reasons. This time should minimize the effects of the above heat up time variations according to the regressions, and therefore be practical to use as an aim in a variety of forging shapes. A 5 h presoak time would also fit best into the statistical test matrix design, giving a tightened full factorial of two temperatures 2025 and 2050F by 3 presoak times of 1, 5, and 10h. The conditions of 2025F/5h presoak/ 0.001 s^{-1} were therefore entered into the above equations.

The resulting regression equation predictions of flow stress, as-forged grain size, mean supersolvus grain size, standard deviation of supersolvus grain size, and ALA supersolvus grain size are listed for the selected conditions of 2025F/5h presoak/ 0.001 s^{-1} with 95% confidence intervals in Table 3. The predictions and confidence intervals were all judged acceptable and will be compared to experimental results when these conditions are employed to forge and heat treat 20 pound subscale pancakes.

Summary and Conclusions

A series of forging experiments were performed with subsequent supersolvus heat treatments, in search of suitable forging conditions producing ASTM 3-5 supersolvus grain size. High forging temperatures of 2025F to 2075F and slow strain rates of 0.0001 to 0.001s⁻¹ were used, after presoaks of 1h to 24h. Two supersolvus heat treatments were then used having solution times of 1h or 3h. The findings can be summarized as follows:

- 1) The material displayed superplastic response under all tested conditions.
- 2) Forging flow stress increased with strain rate, but did not significantly increase with temperature from 2025-2050F.
- 3) As-forged grain size coarsened with decreasing strain rate and increasing presoak time, but did not significantly vary with temperature from 2025 to 2050F.
- 4) Heat treated mean and ALA grain size coarsened with increasing temperature, presoak time, and decreasing strain rate.
- 5) The forging temperature of 2075F gave very nonuniform supersolvus grain sizes.
- 6) The forging conditions of 2025F/5h presoak/0.001s⁻¹ strain rate were selected, based on grain size uniformity, standard deviation, ALA, and processing window, for evaluations on subscale pancakes.

It can be concluded from this work that:

- 1) Forging at high temperatures of 2025-2050F at moderately slow strain rates can produce consistent supersolvus grain sizes of ASTM 4-5 in ME3 disk alloy.
- 2) The supersolvus grain sizes do not significantly vary with solution times of 1 to 3h or with the introduction of a subsolvus pre-anneal before solutioning.
- 3) The forging temperature of 2075F should be avoided for this alloy if uniform grain size is desired.

References

1. Enabling Propulsion Materials Program Final Technical Report, Vol. 5: Task K - Long Life Compressor/Turbine Disk Material, Contract NAS3-26385, NASA Glenn Research Center, May 2000.
2. K. R. Bain, "Development of Damage Tolerant Microstructures in Udimet 720", Superalloys 1984, ed. M. Gell, et. al., The Minerals, Metals, and Materials Society, Warrendale, PA, 1984, pp. 13-22.
3. J. Gayda, R. V. Miner, T. P. Gabb, "On the Fatigue Crack Propagation Behavior of Superalloys at Intermediate Temperatures", Superalloys 1984, ed. M. Gell, C. S. Kortovich, R. H. Bricknell, W. B. Kent, J. F. Radavich, The Minerals, Metals, and Materials Society, Warrendale, PA, 1984, pp. 733-742.
4. M. Soucail, M. Harty, H. Octor, "The Effect of High Temperature Deformation on Grain Growth in a P/M Nickel-Base Superalloy", Superalloys 1996, ed. R. D. Kissinger, et. al., The Minerals, Metals, and Materials Society, Warrendale, PA, 1996, pp.663-666.
5. E.Huron, S. Srivatsa, E. Raymond, "Control of Grain Size Via Forging Strain Rate Limits for R'88DT", Superalloys 2000, ed. T. M. Pollock, R. D. Kissinger, R. R. Bowman, K. A. Green, M. McLean, S. L. Olson, J. J. Schirra, The Minerals, Metals, and Materials Society, Warrendale, PA, 2000, pp. 49-58.

Table 1. Test conditions and results.

Temp	Presoak	StrainRate	log	Stress	log	m	As-forged GS	PA heat treat GS	PA heat treat GS	PA heat treat GS	DH heat treat GS	DH heat treat GS	DH heat treat GS	PA+ DH heat treat GS	PA+ DH heat treat GS	PA+ DH heat treat GS
F	h	sec ⁻¹	StrainRate	ksi	Stress		Mean	Mean	Stan Dev	ALA	Mean	Stan Dev	ALA	Mean	ALA	Stan Dev
2025	1	0.0001	-4	0.73	-0.14	0.44	11.5	4.5	0.2	0.5	5.0	0.1	1.0	4.8	0.8	0.4
2025	1	0.0003	-3.5229	1.25	0.097	0.54	11.5	5.7	0.3	0.5	4.8	0.2	0.0	5.3	0.3	0.6
2025	1	0.001	-3	2.56	0.408	0.65	11.6	4.8	0.2	1.0	4.9	0.4	1.3	4.9	1.1	0.1
2025	10	0.0001	-4	1.04	0.017	0.6	11.7	3.9	0.2	0.0	3.6	0.2	0.0	3.8	0.0	0.2
2025	10	0.0003	-3.5229	1.99	0.299	0.58	11.7	3.7	0.4	0.0	4.7	0.2	0.0	4.2	0.0	0.7
2025	10	0.001	-3	3.97	0.599	0.56	11.6	4.3	0.1	0.5	4.3	0.2	0.5	4.3	0.5	0.0
2050	1	0.0001	-4	0.69	-0.16	0.55	11.6	3.8	0.3	-0.5	4.6	0.4	0.3	4.2	-0.1	0.6
2050	1	0.0003	-3.5229	1.28	0.107	0.58	11.7	4.1	0.3	0.5	4.2	0.3	0.5	4.2	0.5	0.1
2050	1	0.001	-3	2.61	0.417	0.61	11.7	3.9	0.1	-0.5	3.2	0.3	0.3	3.6	-0.1	0.5
2050	5	0.0003	-3.5229	1.65	0.217		11.4	3.7	0.3	-0.5	2.9	0.2	-0.3	3.3	-0.4	0.6
2050	10	0.0001	-4	0.97	-0.01	0.65	11.1	3.3	0.6	-0.5	2.3	0.3	-1.0	2.8	-0.8	0.7
2050	10	0.0003	-3.5229	1.91	0.281	0.58	11.5	3.7	0.3	-0.5	4.2	0.5	0.0	4.0	-0.3	0.4
2050	10	0.001	-3	3.66	0.563	0.5	11.4	3.4	0.2	-1.3	3.3	0.3	-0.5	3.4	-0.9	0.1
2050	24	0.0003	-3.5229	2.51	0.4		10.7	3.0	0.4	0.0	2.0	0.2	-1.5	2.5	-0.8	0.7
2075	1	0.0001	-4	0.89	-0.05	0.53	10.8	2.4	0.2	-1.5	2.4	0.7	-1.5	2.4	-1.5	0.0
2075	1	0.0003	-3.5229	1.61	0.207	0.55	10.8	3.1	0.7	-1.0	3.4	0.4	-0.8	3.3	-0.9	0.2
2075	1	0.001	-3	3.17	0.501	0.57	11.1	3.1	0.5	-0.5	2.0	0.3	-1.0	2.6	-0.8	0.8
2075	10	0.0001	-4	1.32	0.121	0.62	10.5	2.7	0.7	-2.8	2.7	0.5	-3.0	2.7	-2.9	0.0
2075	10	0.0003	-3.5229	2.44	0.387	0.5	10.5	2.3	1.0	-2.0	1.1	0.6	-2.3	1.7	-2.1	0.8
2075	10	0.001	-3	4.1	0.613	0.36	10.9	2.5	0.2	-2.0	2.5	0.2	-1.8	2.5	-1.9	0.0

Table 2. Constants for the polynomial equations fit for flow stress versus strain rate:
 $\log_{10}(\text{flow stress})=C1+C2*\log_{10}(\text{strain rate})+C3\log_{10}(\text{strain rate})^2$

Temp(F)	Presoak(h)	C1	C2	C3
2025	1	3.31306	1.28579	0.10584
2025	10	2.13958	0.46248	-0.017
2050	1	2.5019	0.78306	0.02932
2050	10	1.37482	0.04075	-0.0766
2075	1	2.43396	0.71377	0.02316
2075	10	0.55153	-0.4049	-0.1282

Table 3. Equation predictions and confidence intervals for the selected forging conditions of 2025F/5h presoak/0.001s⁻¹ strain rate.

	log	Flow Stress	As- Forged	Heat Treat	Heat Treat	Heat Treated	Heat Treated	Stand. Dev.	Stand. Dev.
	flow stress	ksi	Grain Size	Grain Size	Grain Size	ALA G.S.	ALA G.S.	Grain Size	Grain Size
Equation	2		3	4C	4U	5C	5U	6C	6U
Lower 95%	0.45	2.84	11.2	4.2	4.2	0.2	0.3		0.1
Predicted	0.49	3.10	11.6	4.6	4.6	0.8	0.8	0.2	0.2
Upper 95%	0.53	3.38	12.0	5.1	5.0	1.4	1.3		0.4

Fig. 1. Schematic drawing of double cone (DC) compression specimen.

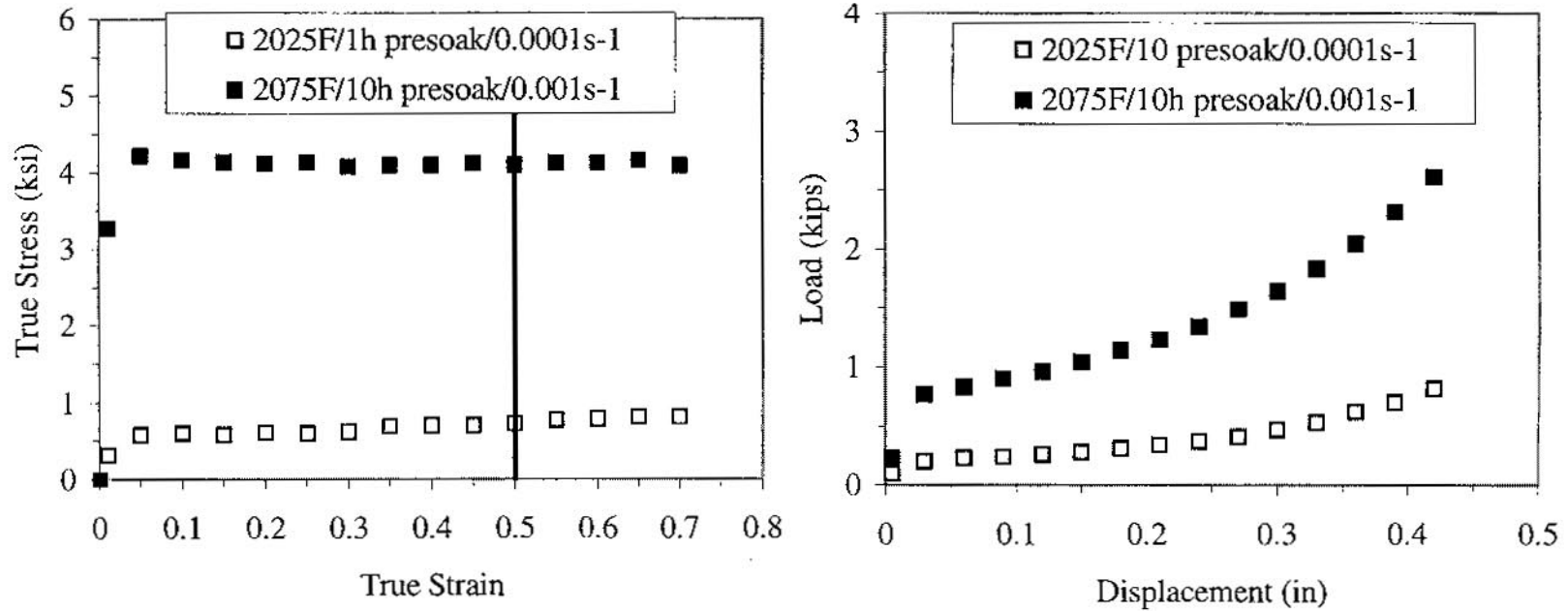
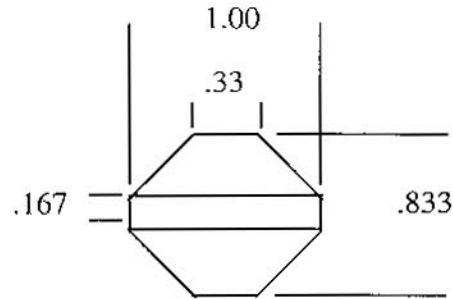


Fig. 2. Comparison of a) stress-strain curves during compression testing of RCC specimens, b) load-displacement curves during compression testing of DC specimens.

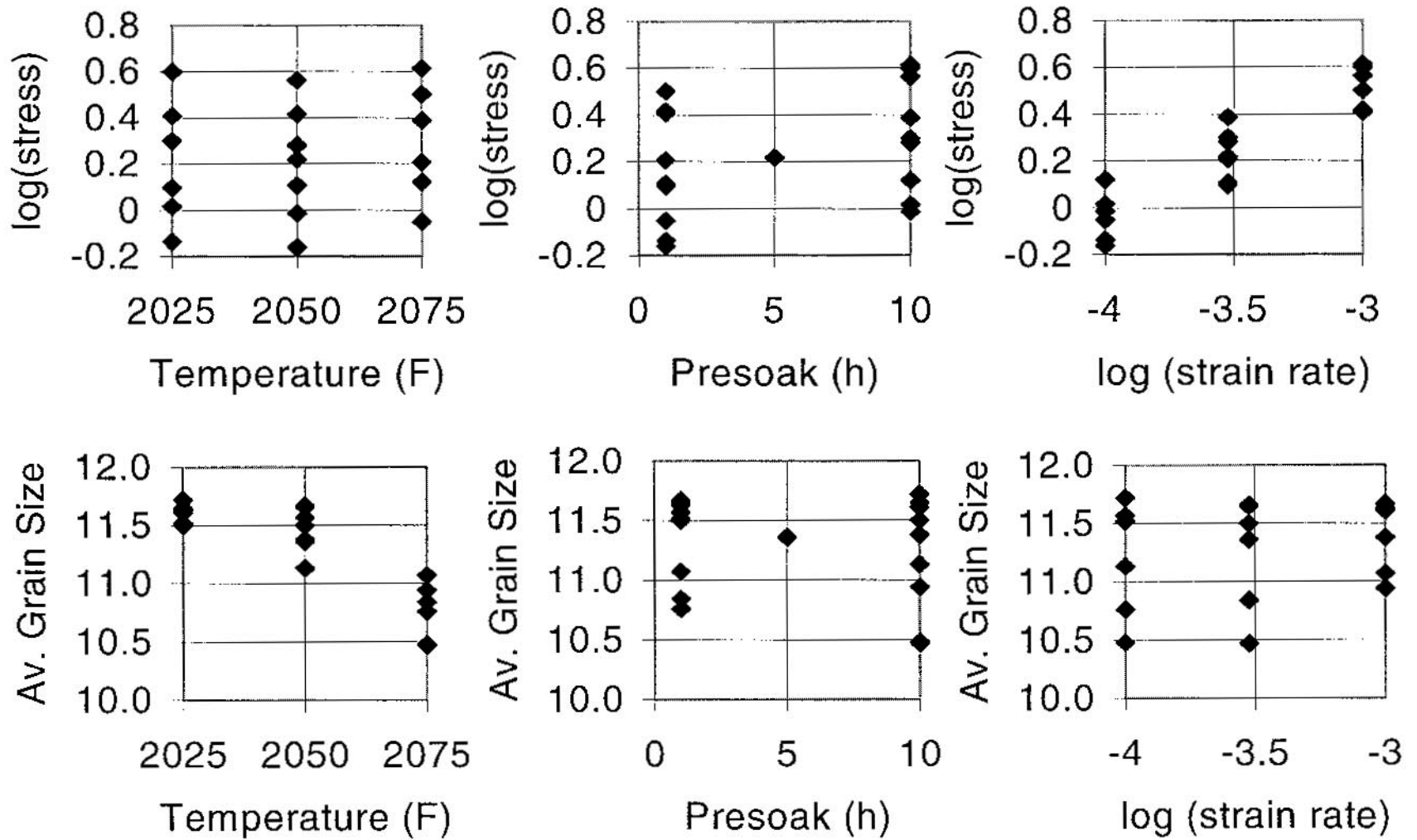


Fig. 3. Scatter plots of flow stress and as-forged average grain size vs. temperature, presoak time, and strain rate.

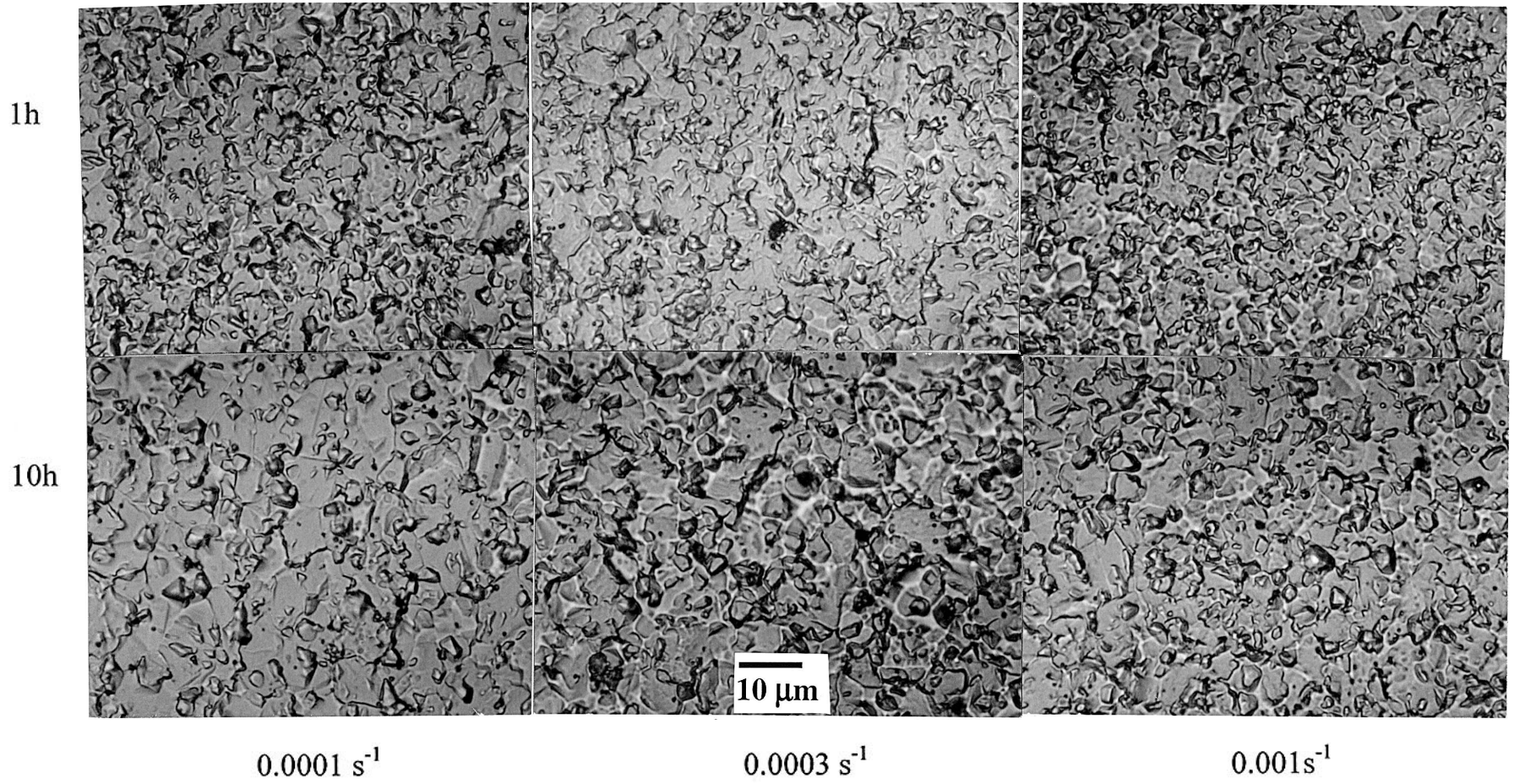


Fig. 4. Comparison of as-forged microstructures observed in RCC specimens after forging at 2025F.

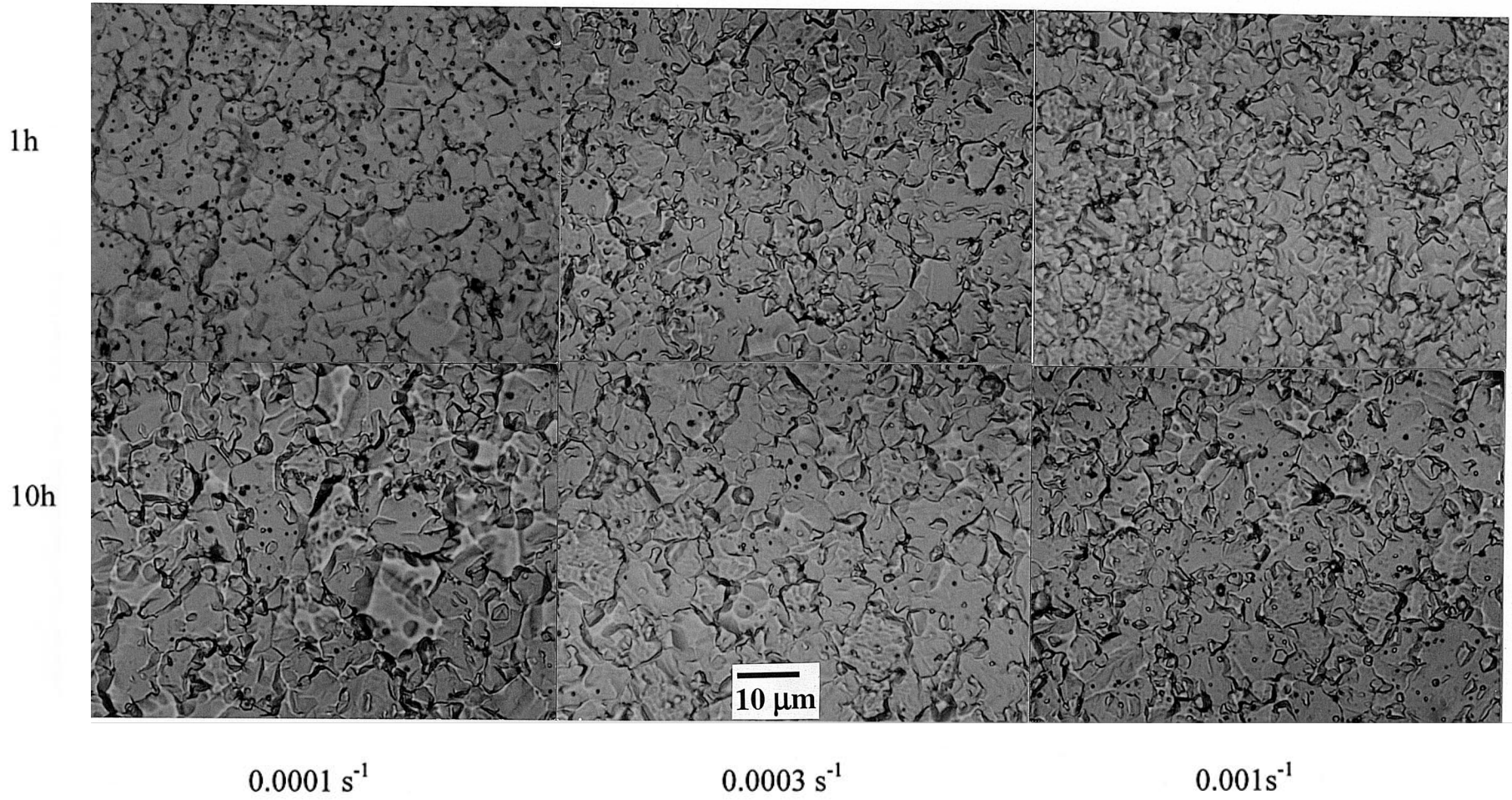


Fig. 5. Comparison of as-forged microstructures observed in RCC specimens after forging at 2050F.

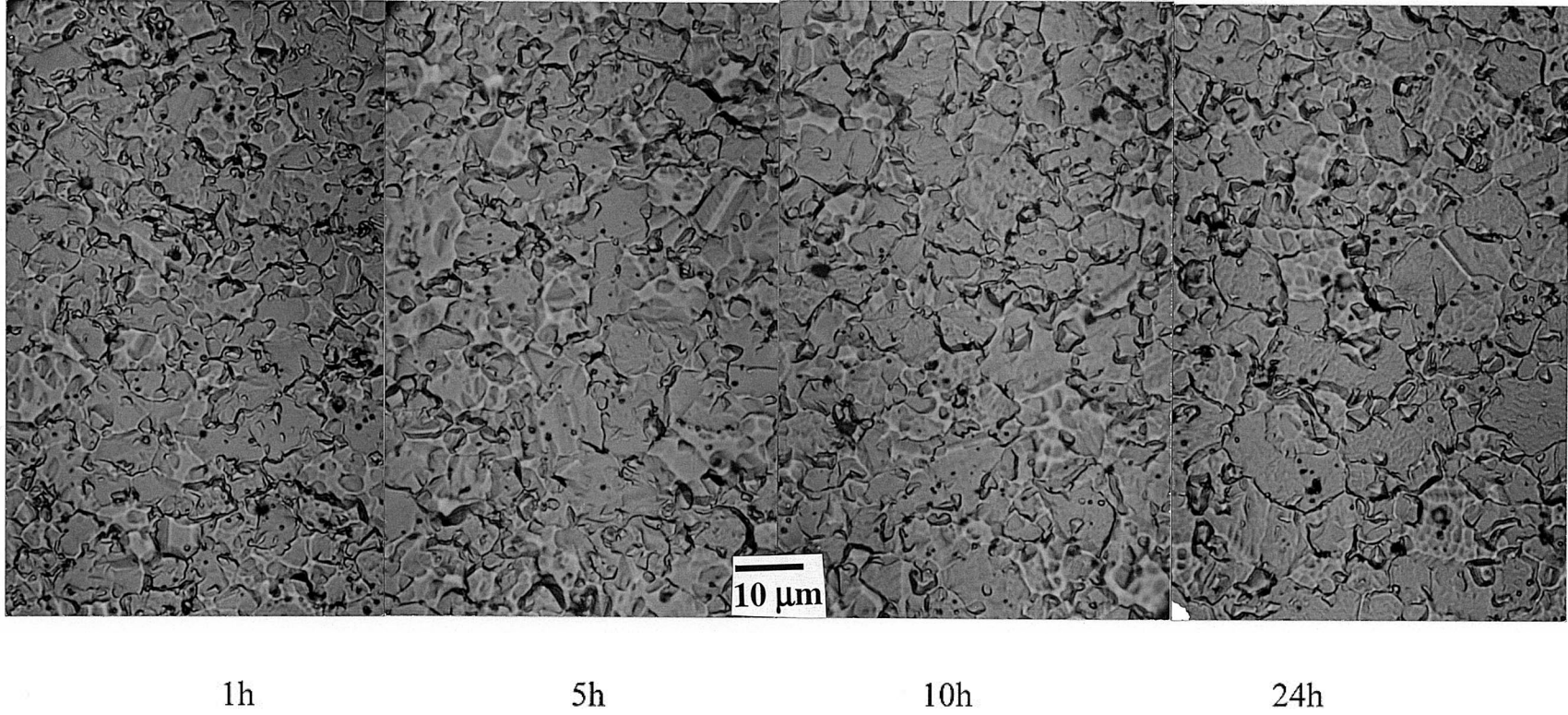


Fig. 6. Comparison of as-forged microstructures observed in RCC specimens after forging at 2050F/0.0003s⁻¹.

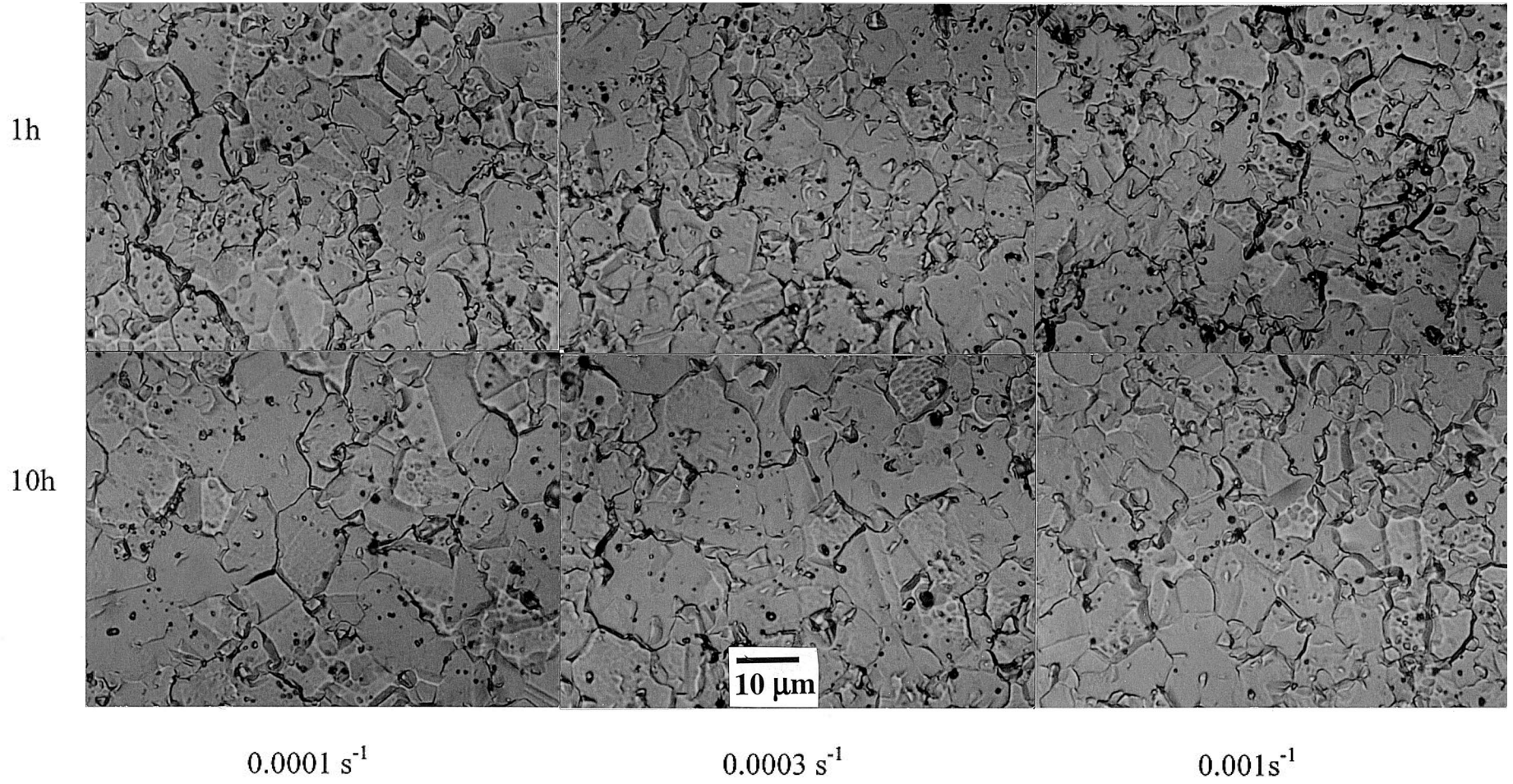
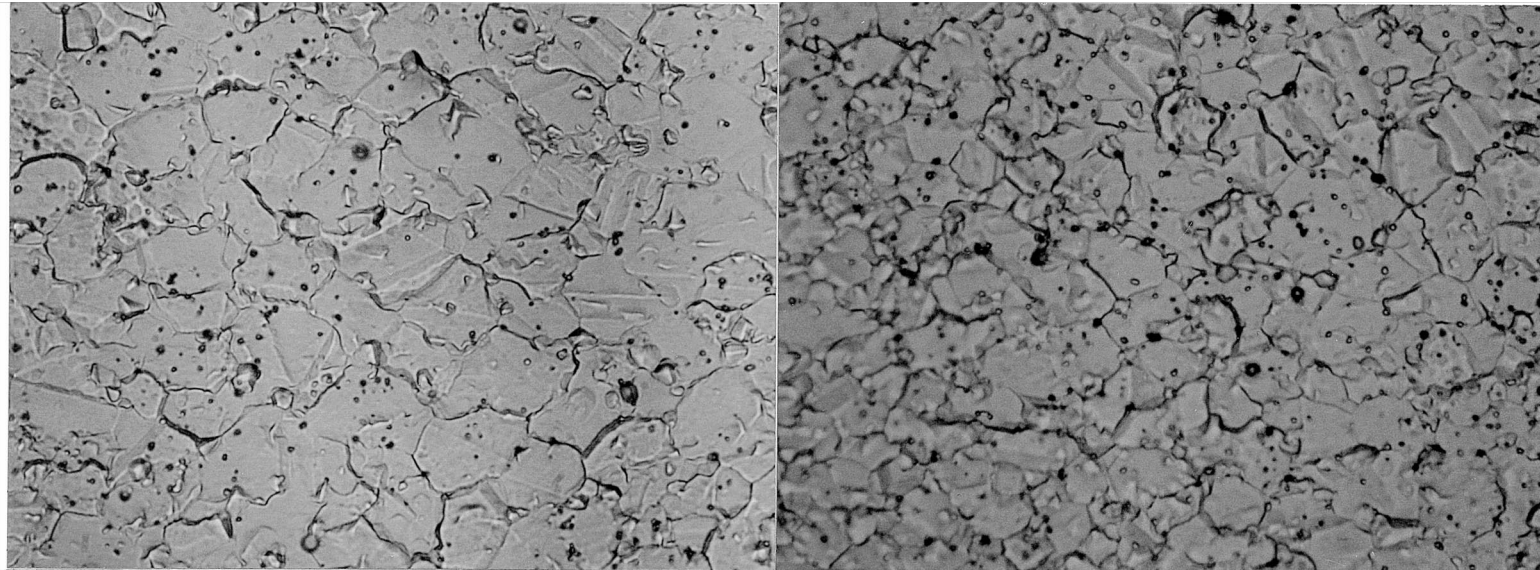
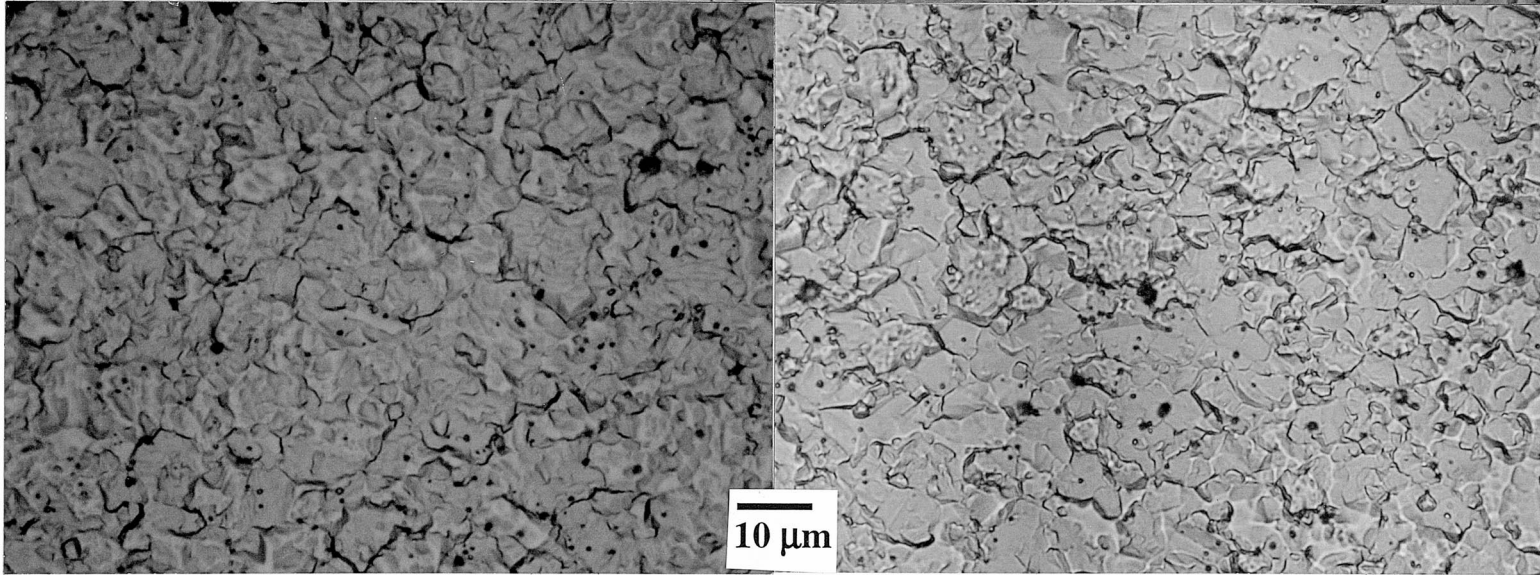


Fig. 7. Comparison of as-forged microstructures observed in RCC specimens after forging at 2075F.

2075



2025



0.0001 s⁻¹

0.001 s⁻¹

Fig. 8. Comparison of as-forged microstructures observed in DC specimens 10hr presoak.

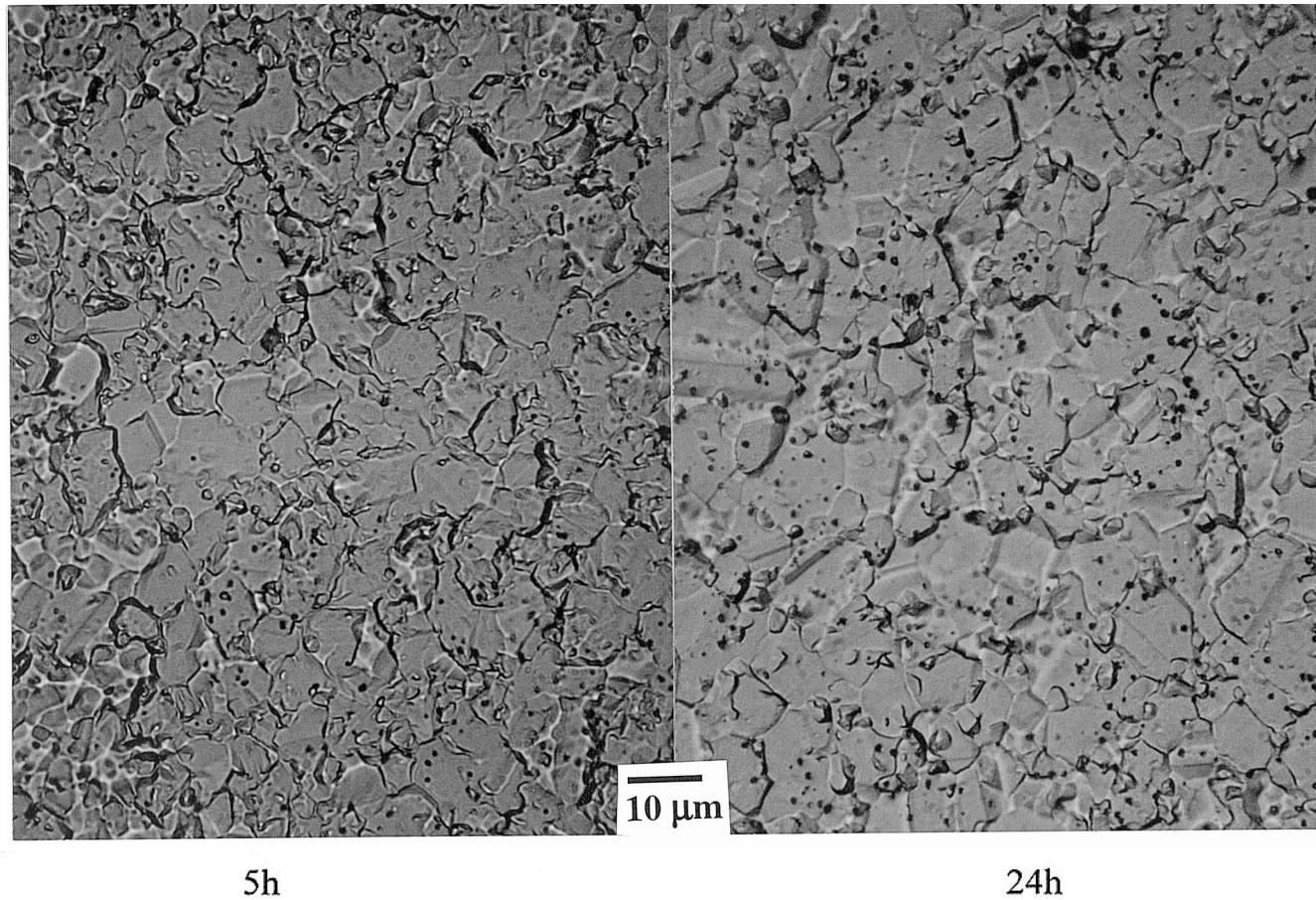
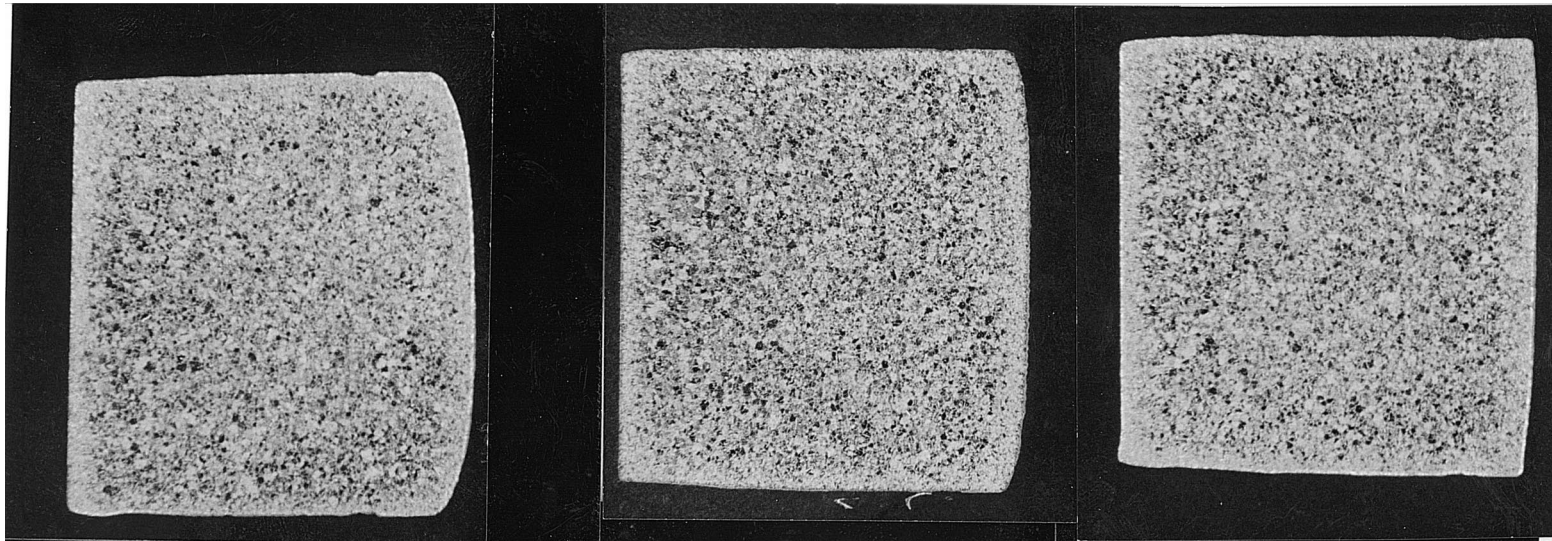
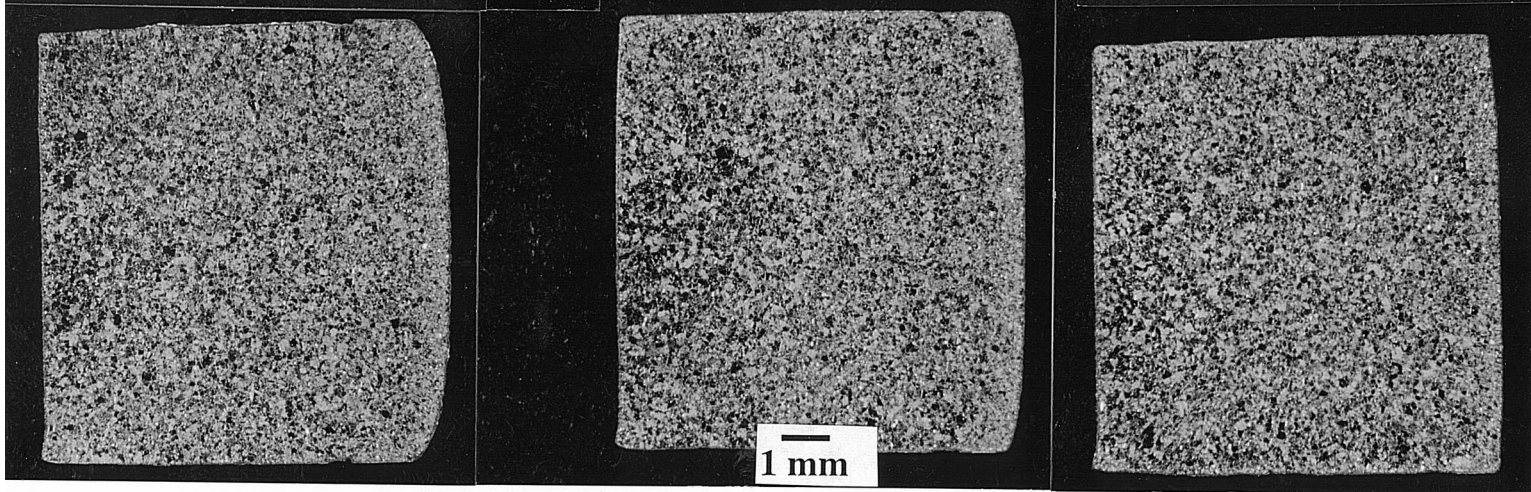


Fig. 9. Comparison of as-forged microstructures observed in DC specimens after forging at 2050F/0.0003 s⁻¹ approximate strain rate.

PA



DH



0.0001 s⁻¹

0.0003 s⁻¹

0.001 s⁻¹

Fig. 10. Comparison of macrostructures observed in RCC specimens after forging at 2025F/1h presoak.

PA

19

DH

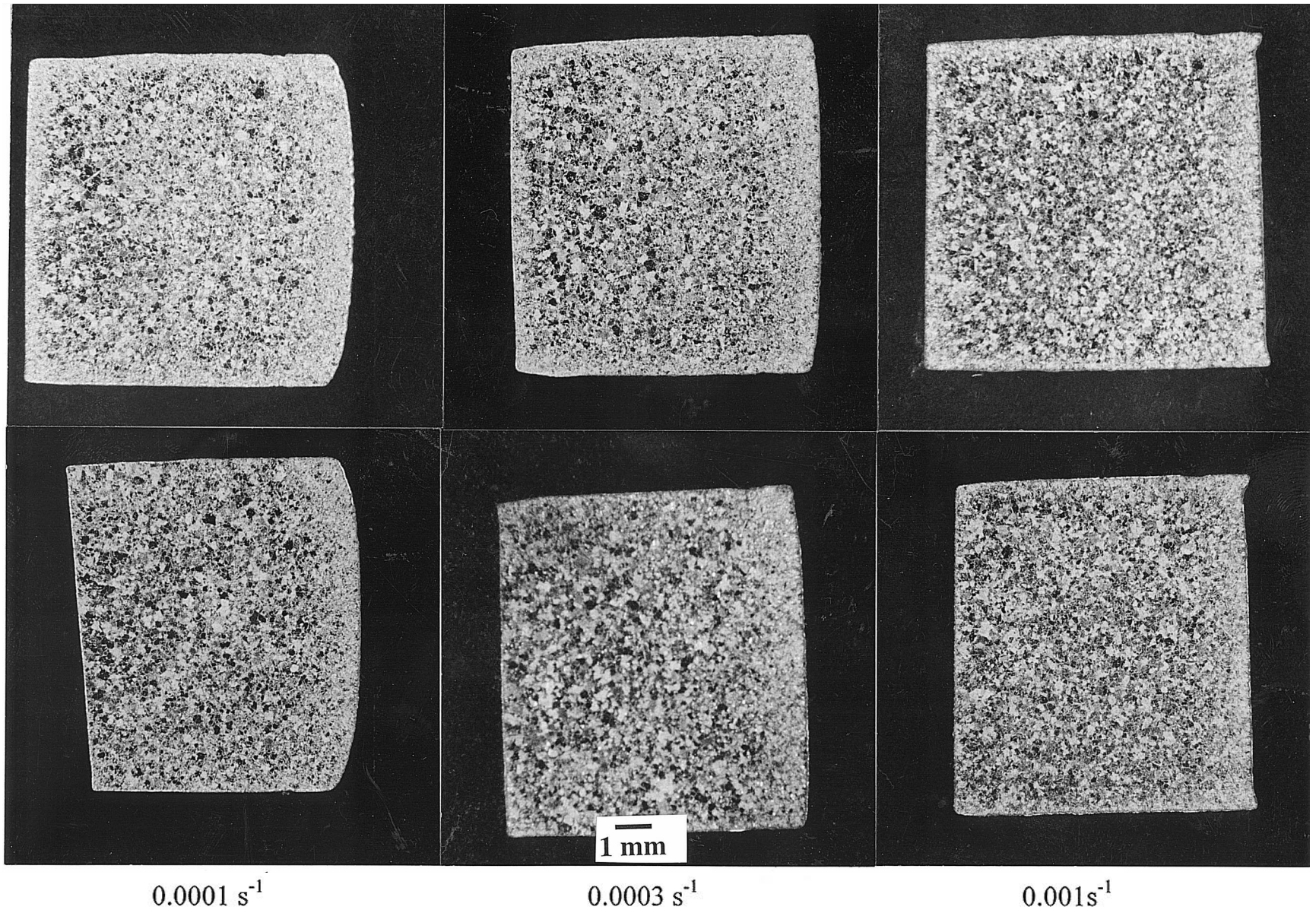


Fig. 11. Comparison of macrostructures observed in RCC specimens after forging at 2025F/10h presoak..

PA

DH

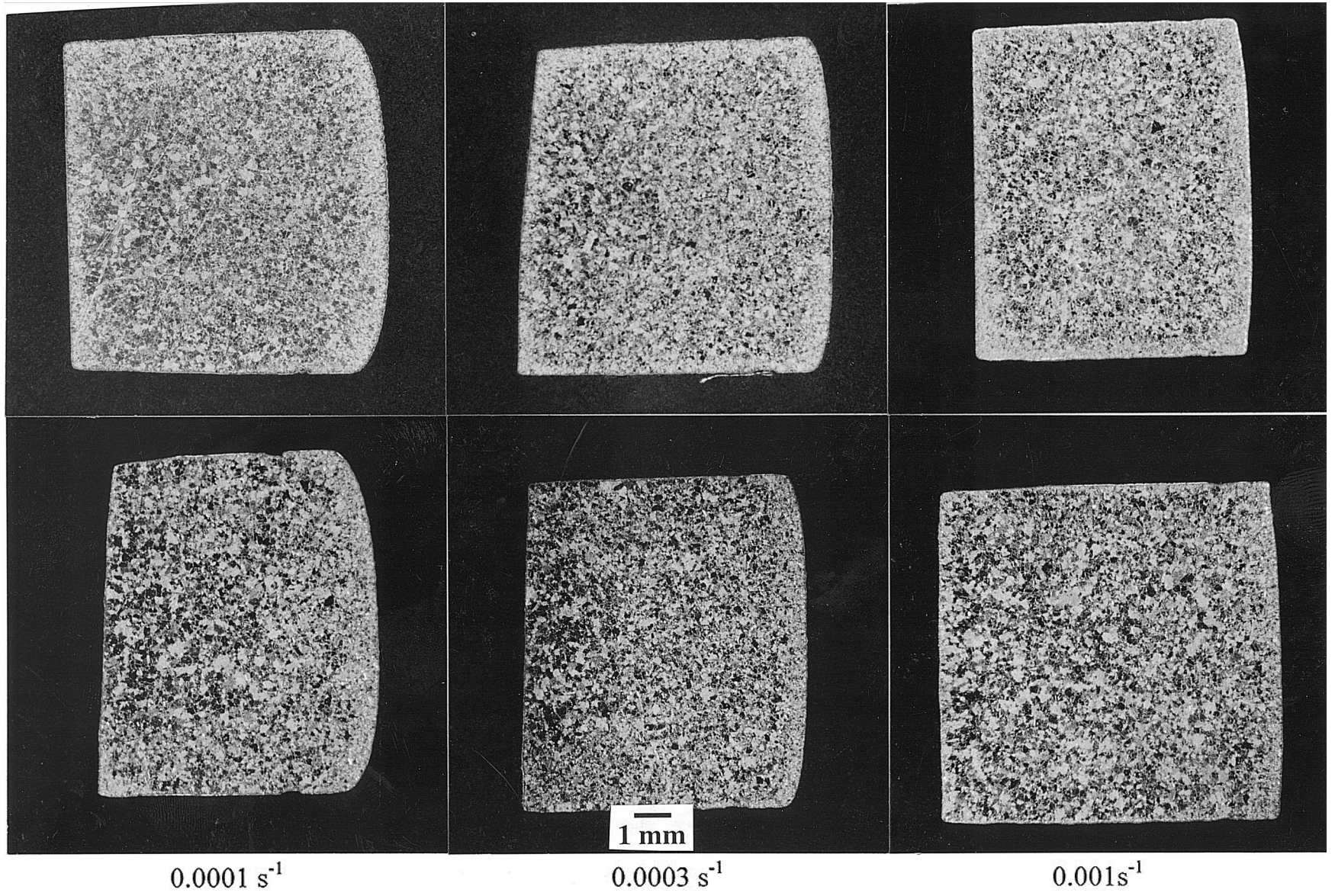


Fig. 12. Comparison of macrostructures observed in RCC specimens after forging at 2050F/1h presoak.

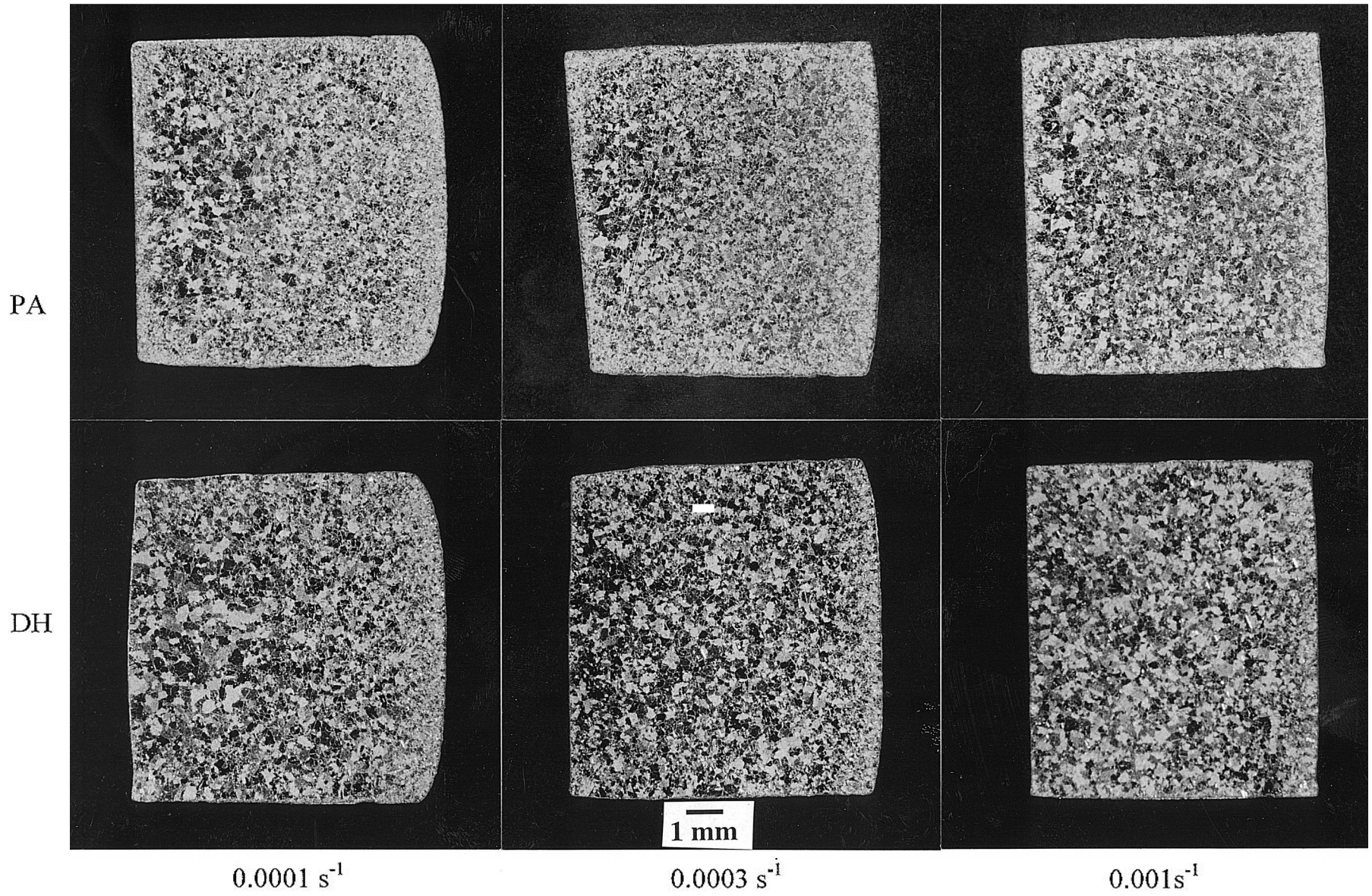


Fig. 13. Comparison of macrostructures observed in RCC specimens after forging at 2050F/10h presoak.

PA

DH

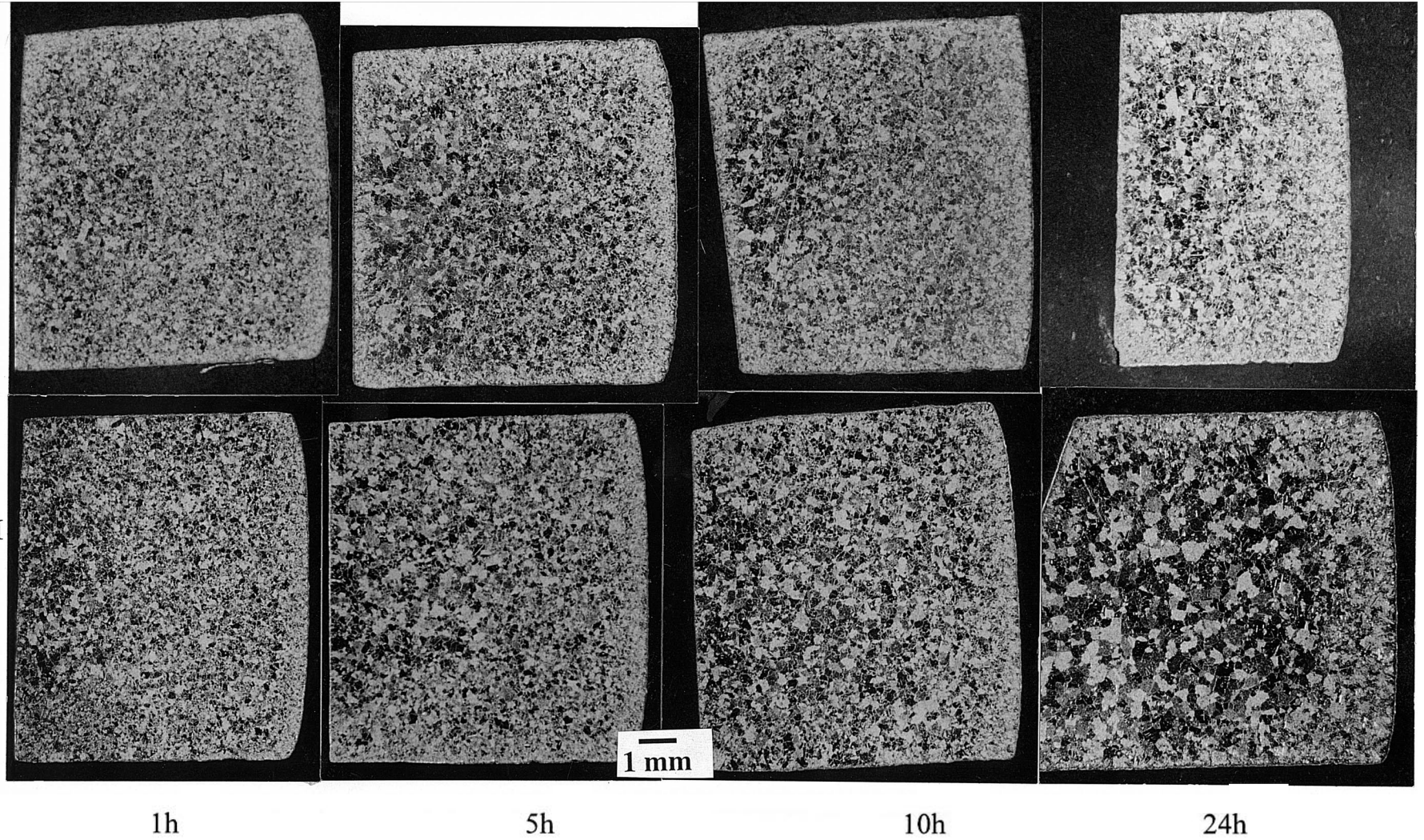


Fig. 14. Comparison of macrostructures observed in RCC specimens after forging at 2050F/0.0003 s⁻¹ strain rate.

PA

23

DH

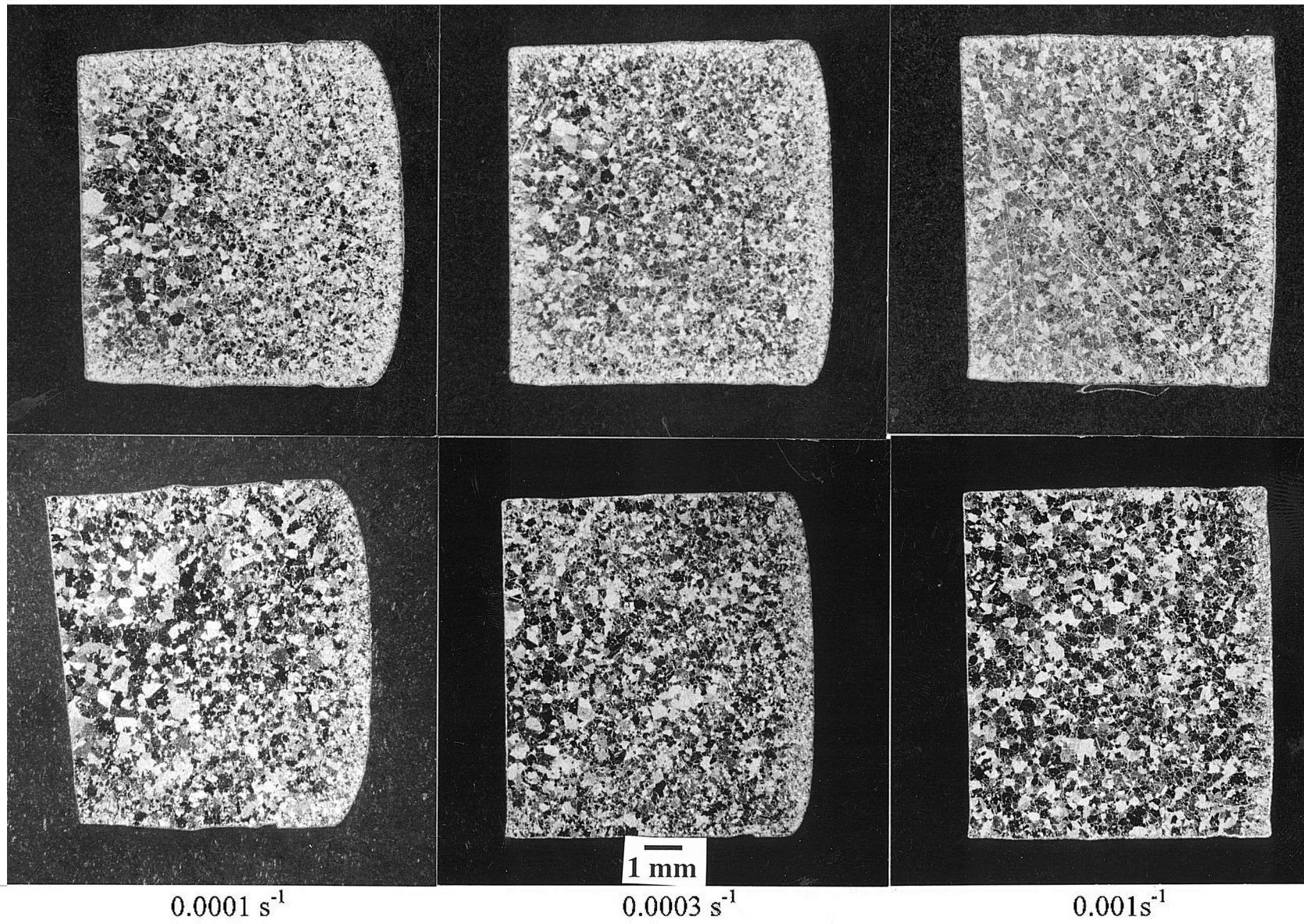


Fig. 15. Comparison of macrostructures observed in RCC specimens after forging at 2075F/1h presoak..

PA

DH

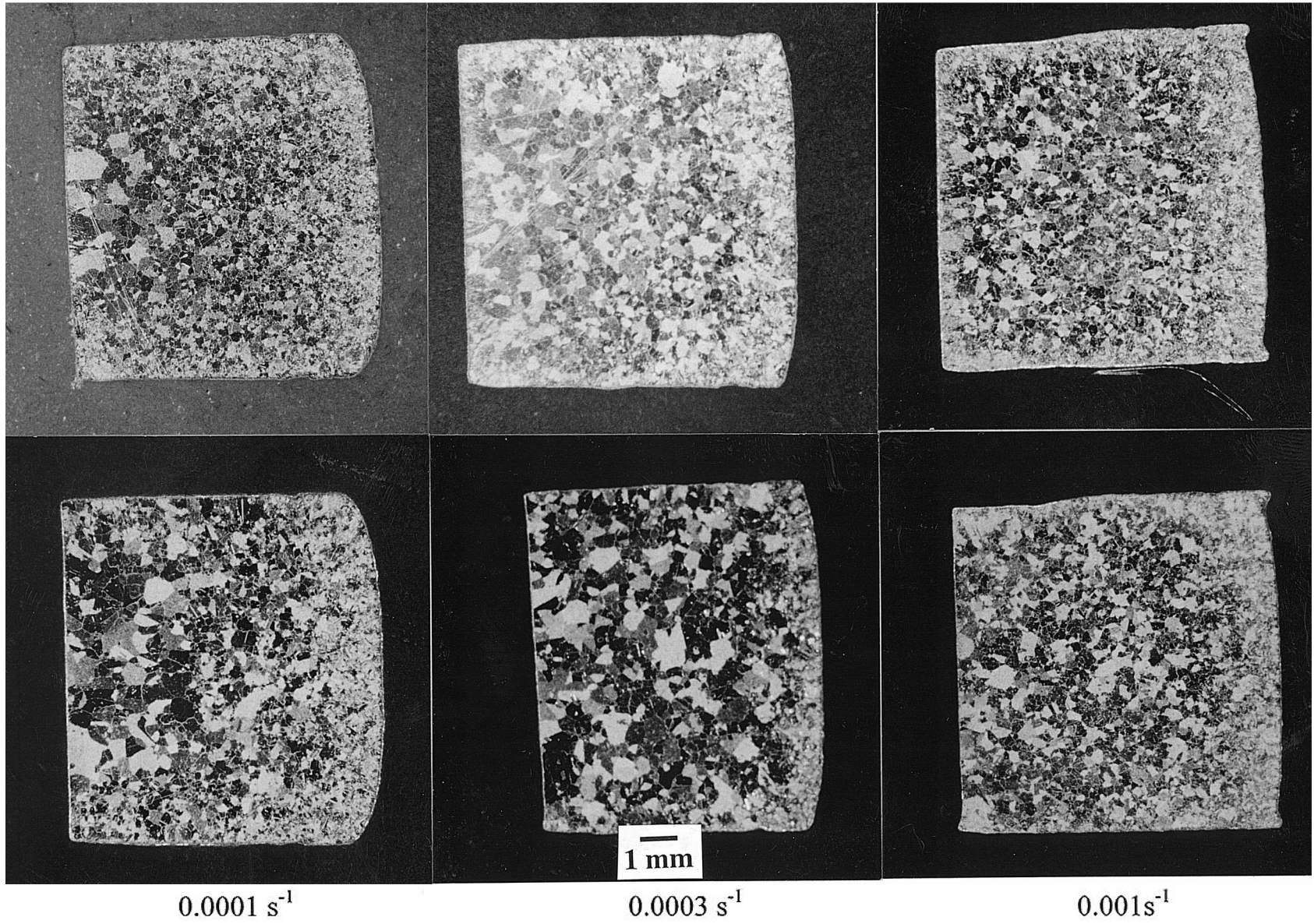


Fig. 16. Comparison of macrostructures observed in RCC specimens after forging at 2075F/10h presoak.

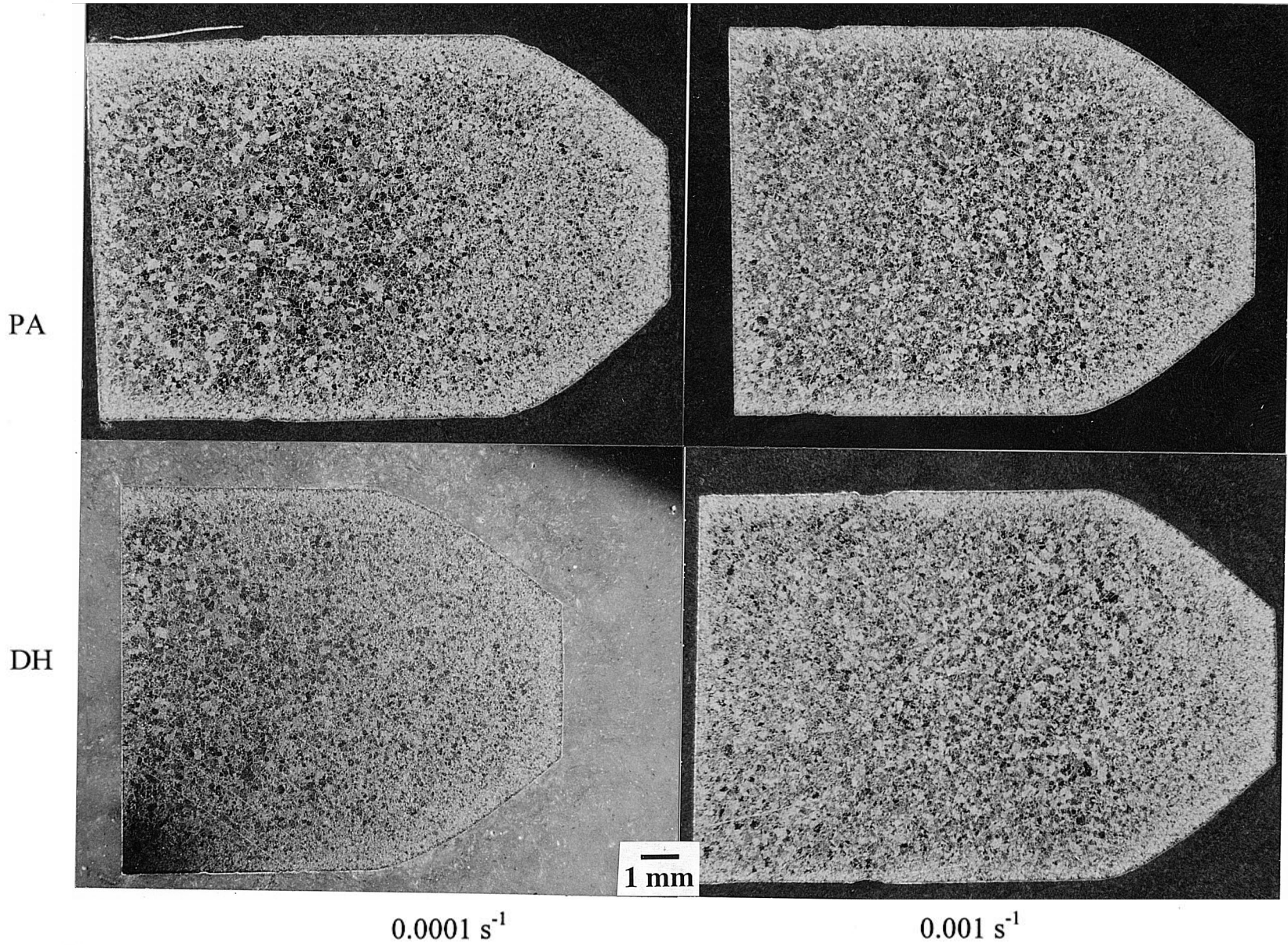


Fig. 17. Comparison of macrostructures observed in DC specimens after forging at 2025F/10h presoak.

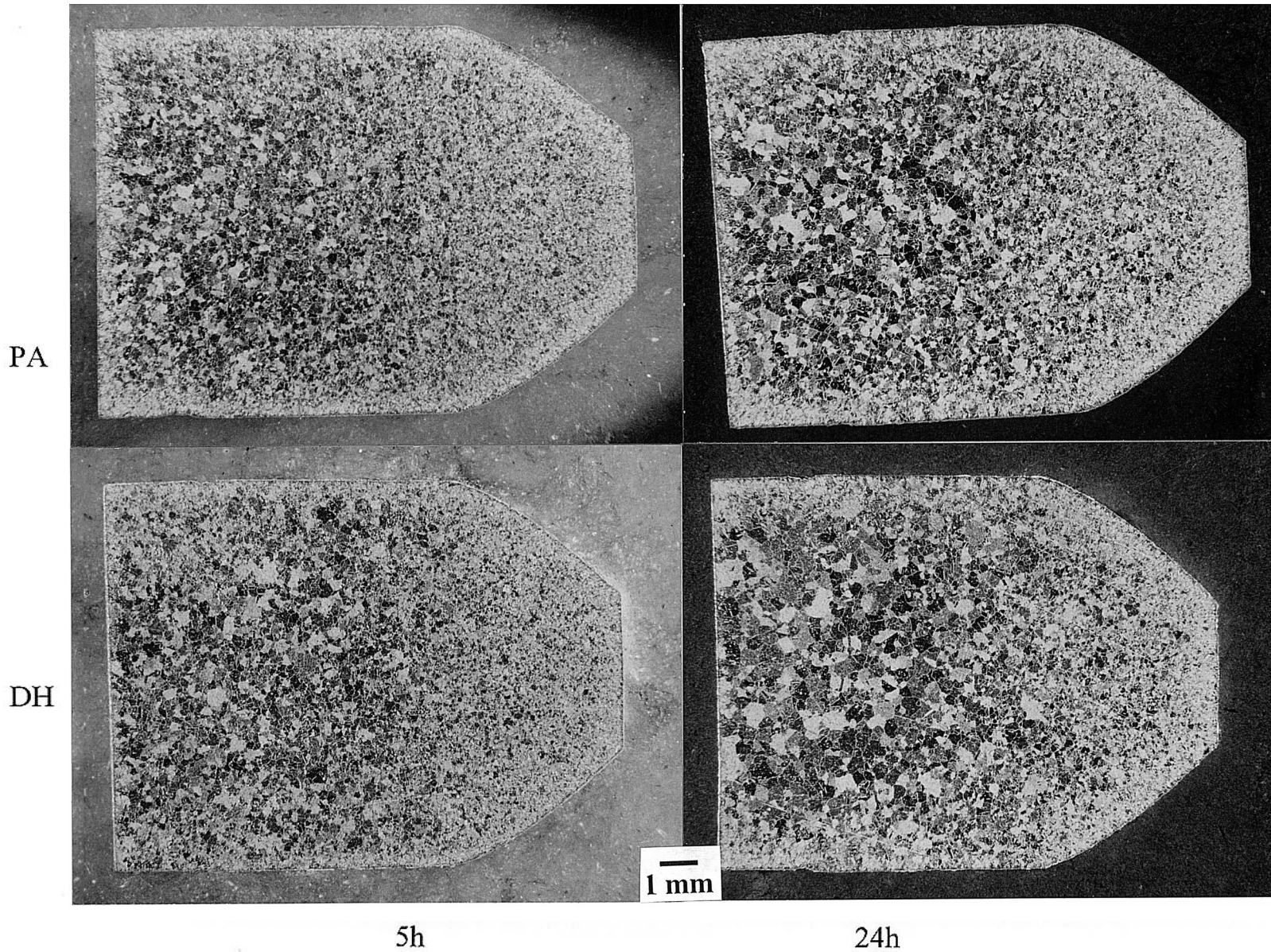


Fig. 18. Comparison of macrostructures observed in DC specimens after forging at 2050F/0.0003 s⁻¹ approximate strain rate.

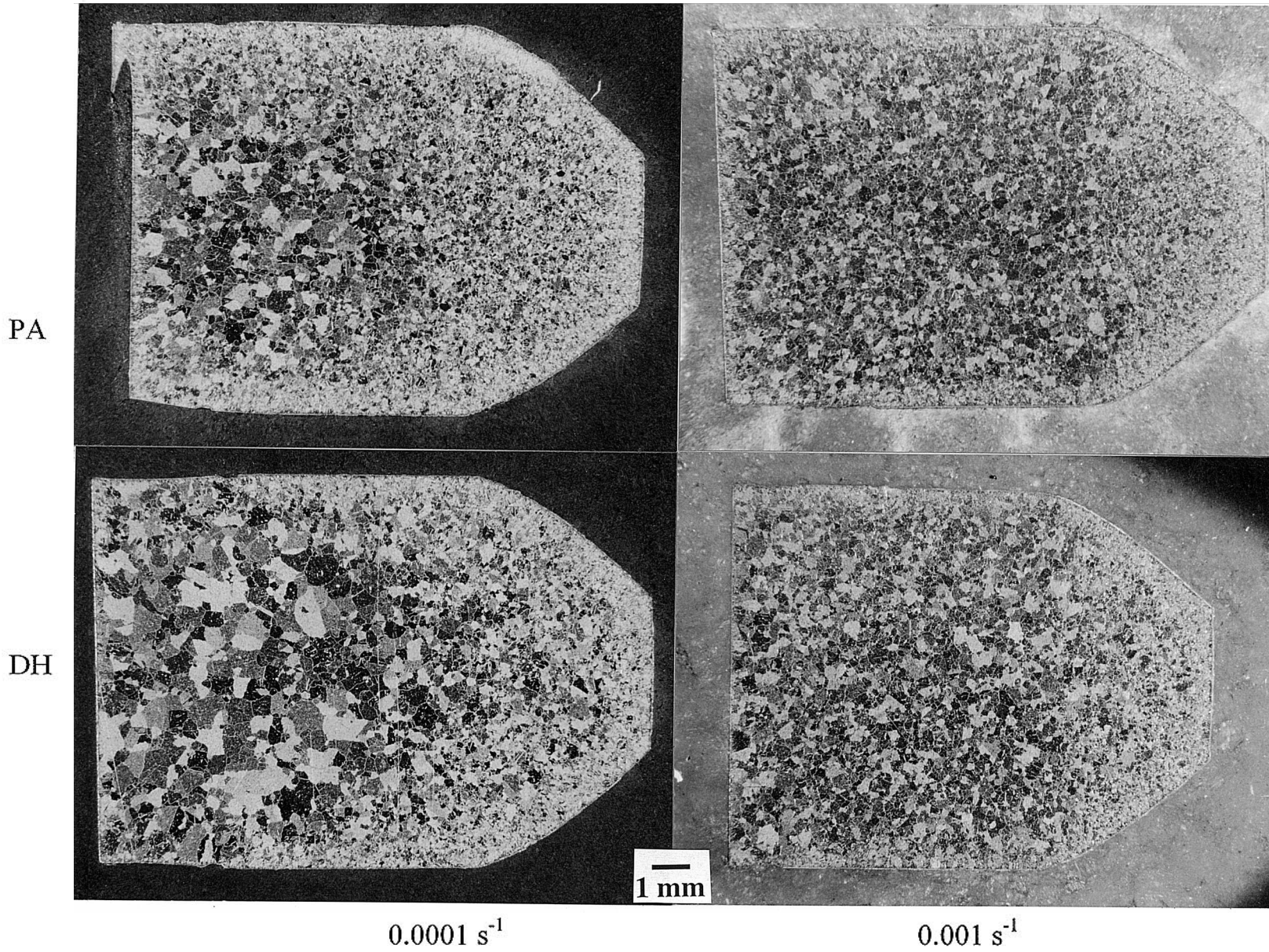


Fig. 19. Comparison of macrostructures observed in DC specimens after forging at 2075F/10h presoak.

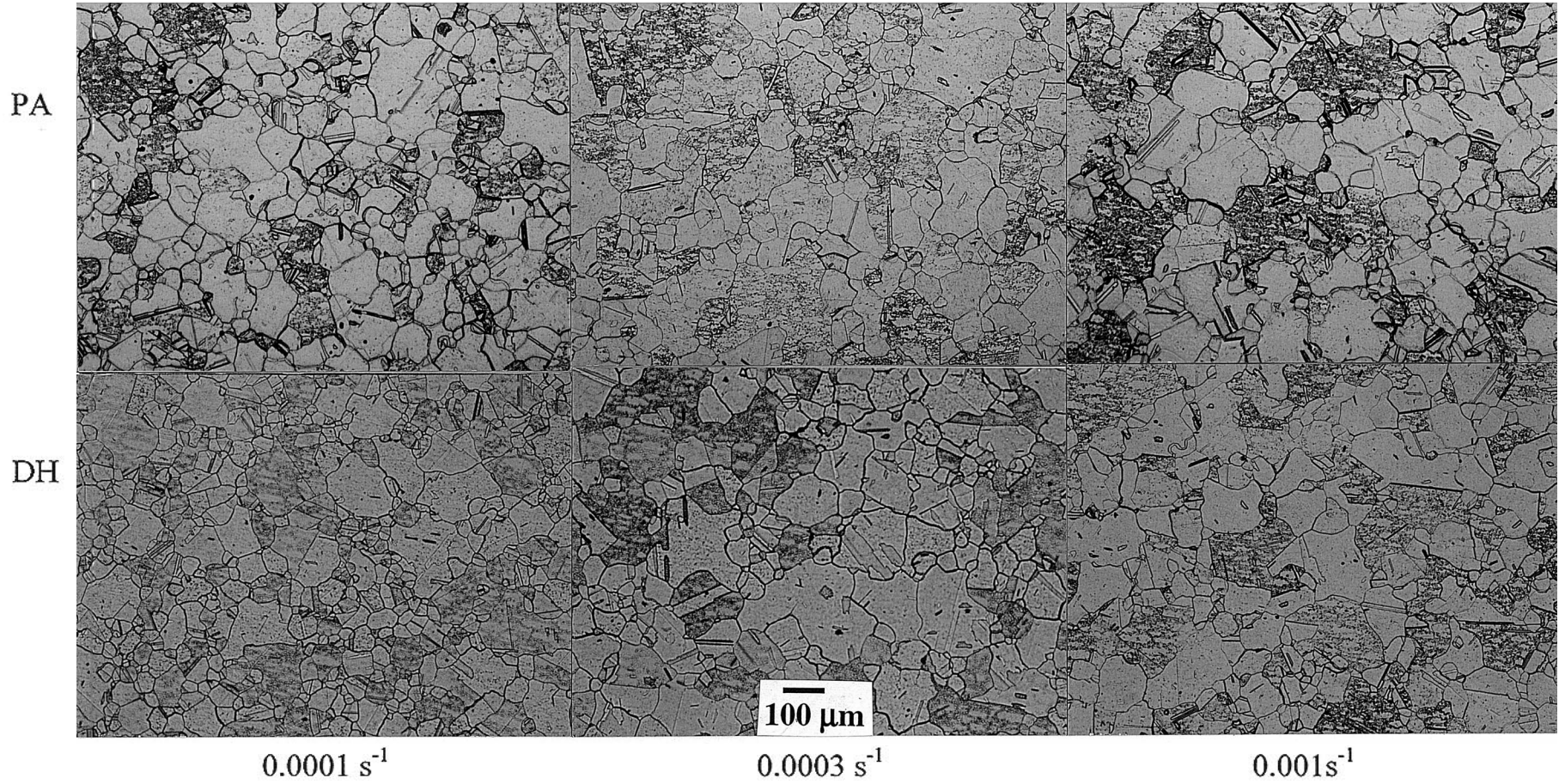


Fig. 20. Comparison of microstructures observed in RCC specimens after forging at 2025F/1h presoak.

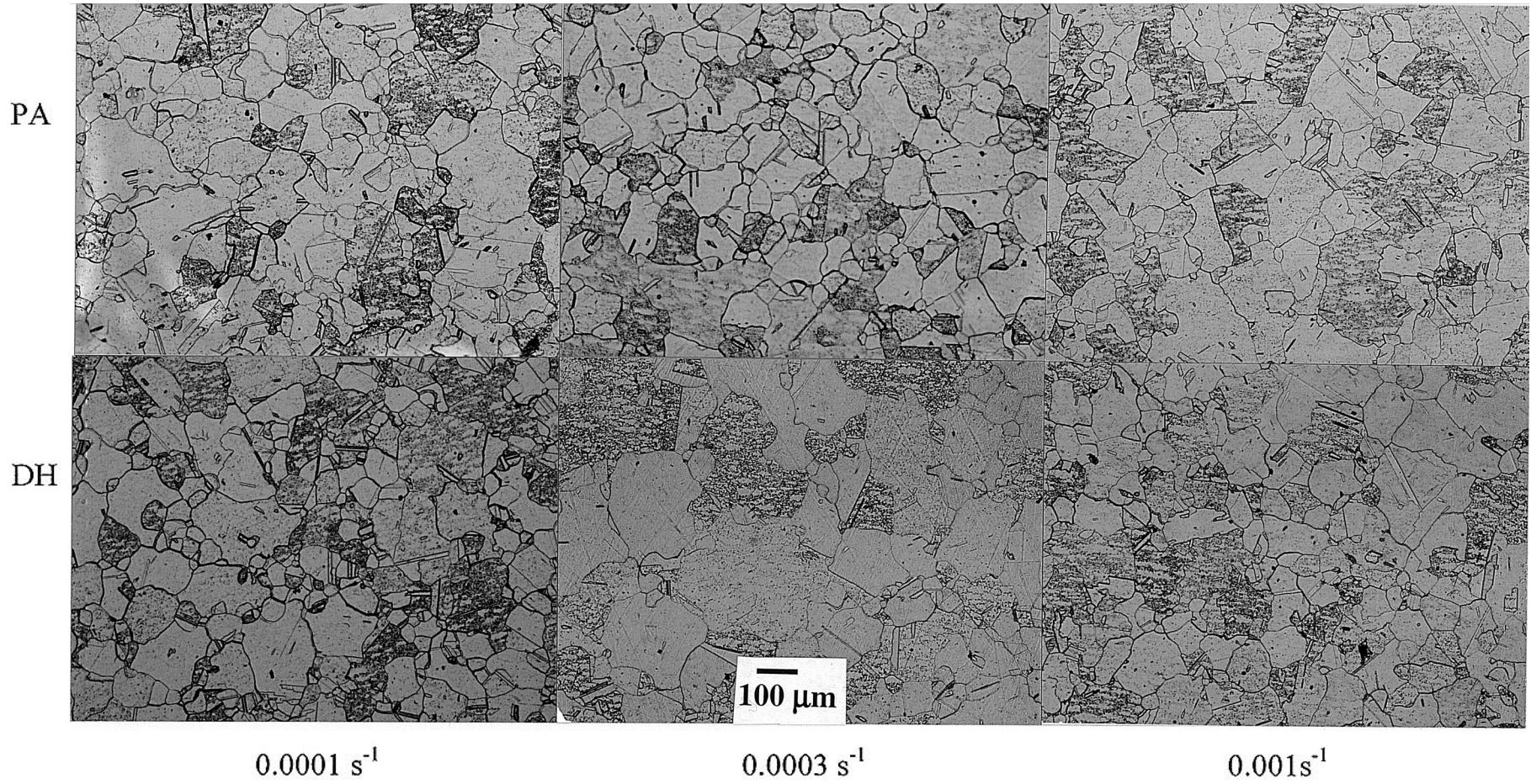


Fig. 21. Comparison of microstructures observed in RCC specimens after forging at 2025F/10h presoak.

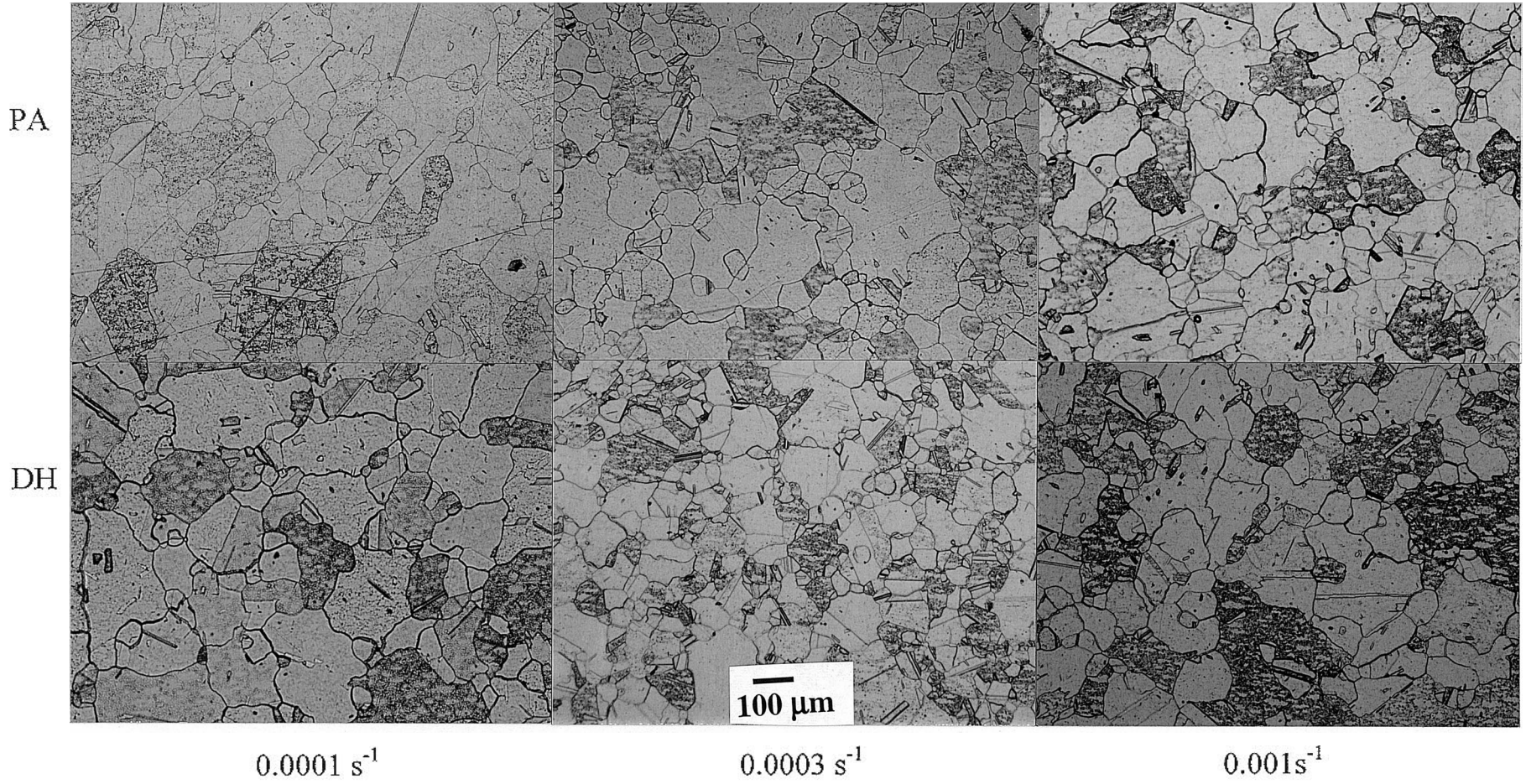


Fig. 22. Comparison of microstructures observed in RCC specimens after forging at 2050F/1h presoak.

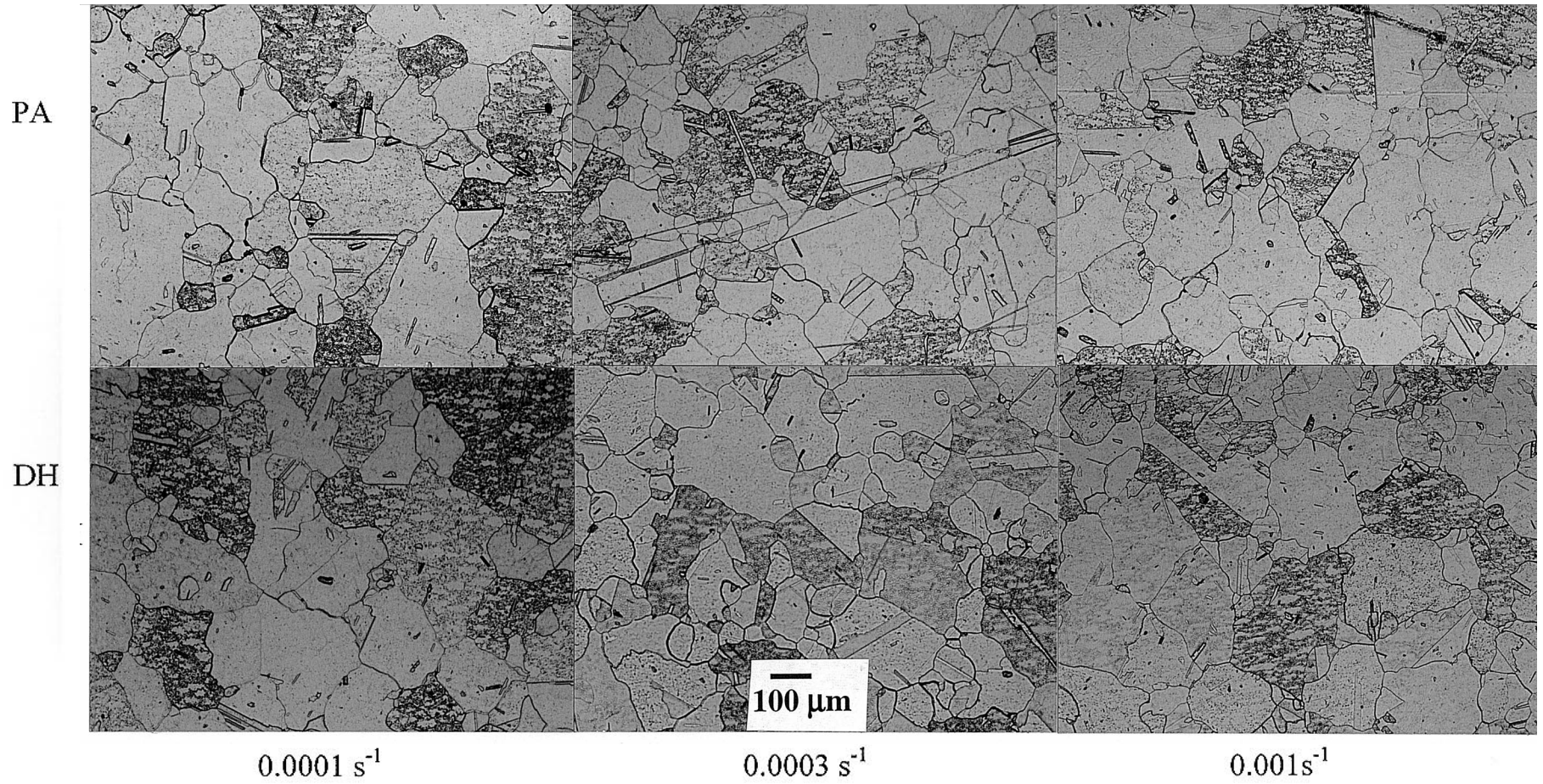


Fig. 23. Comparison of microstructures observed in RCC specimens after forging at 2050F/10h presoak.

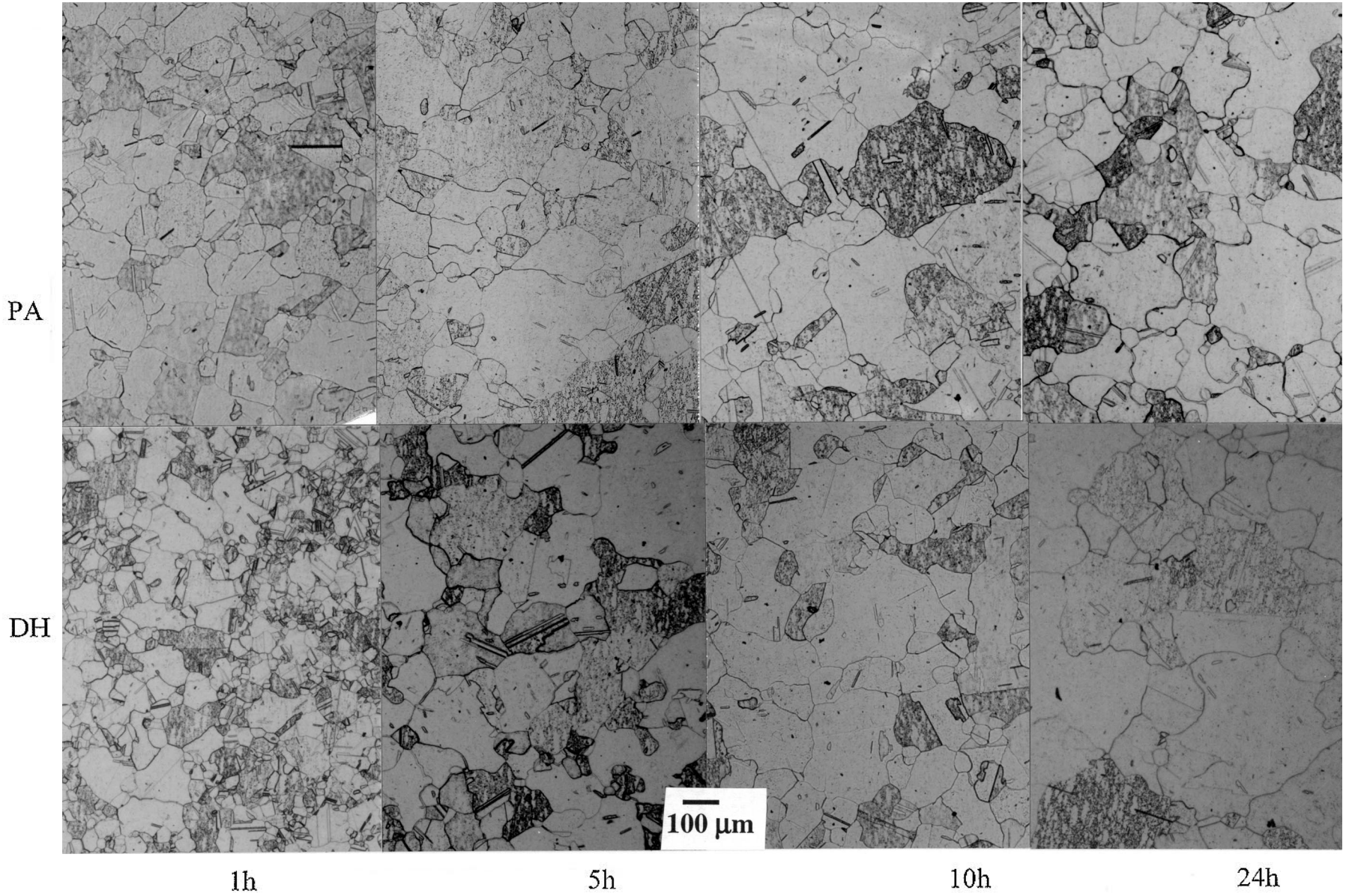


Fig. 24. Comparison of microstructures observed in RCC specimens after forging at 2050F/0.0003 s⁻¹ strain rate.

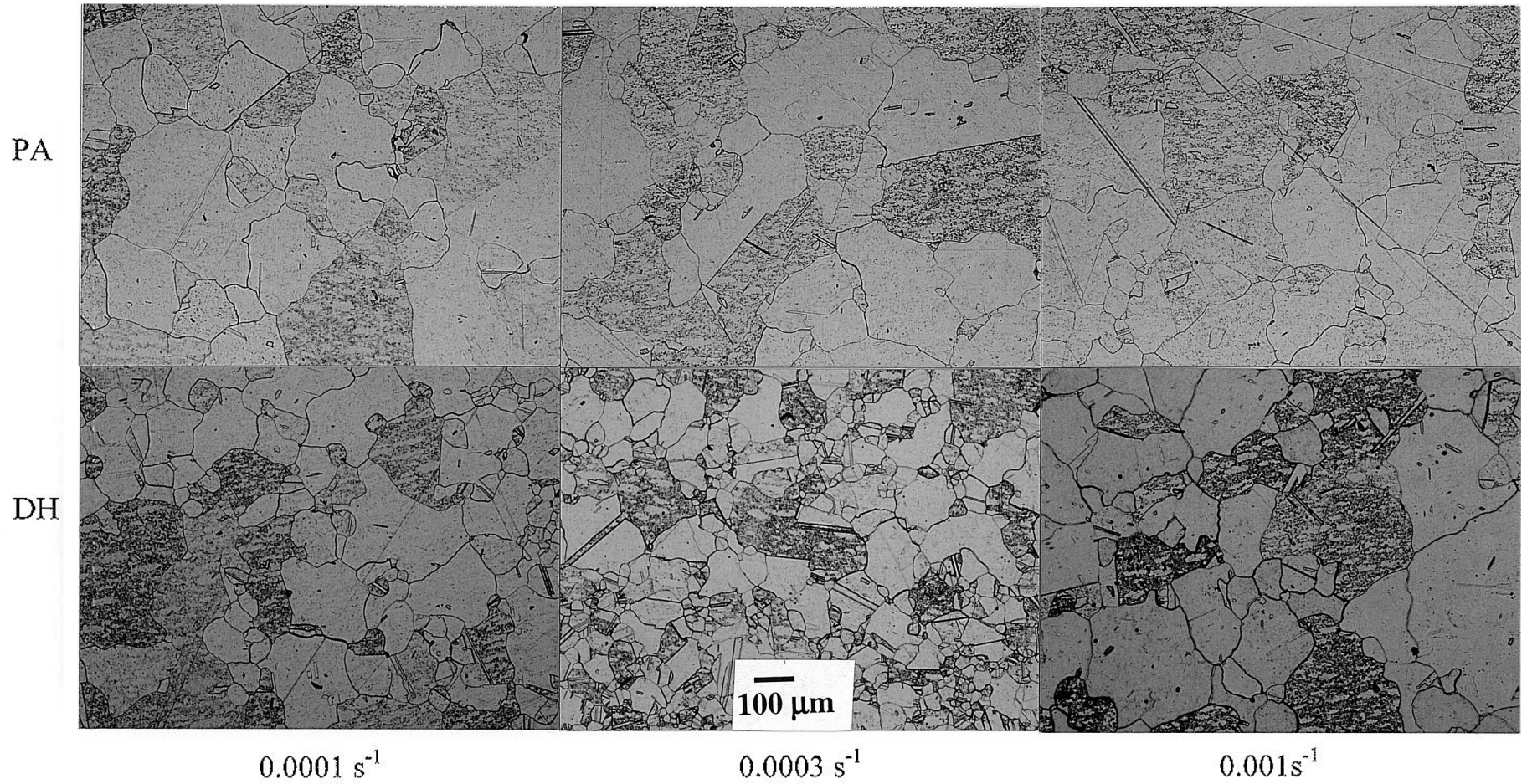


Fig. 25. Comparison of microstructures observed in RCC specimens after forging at 2075F/1h presoak.

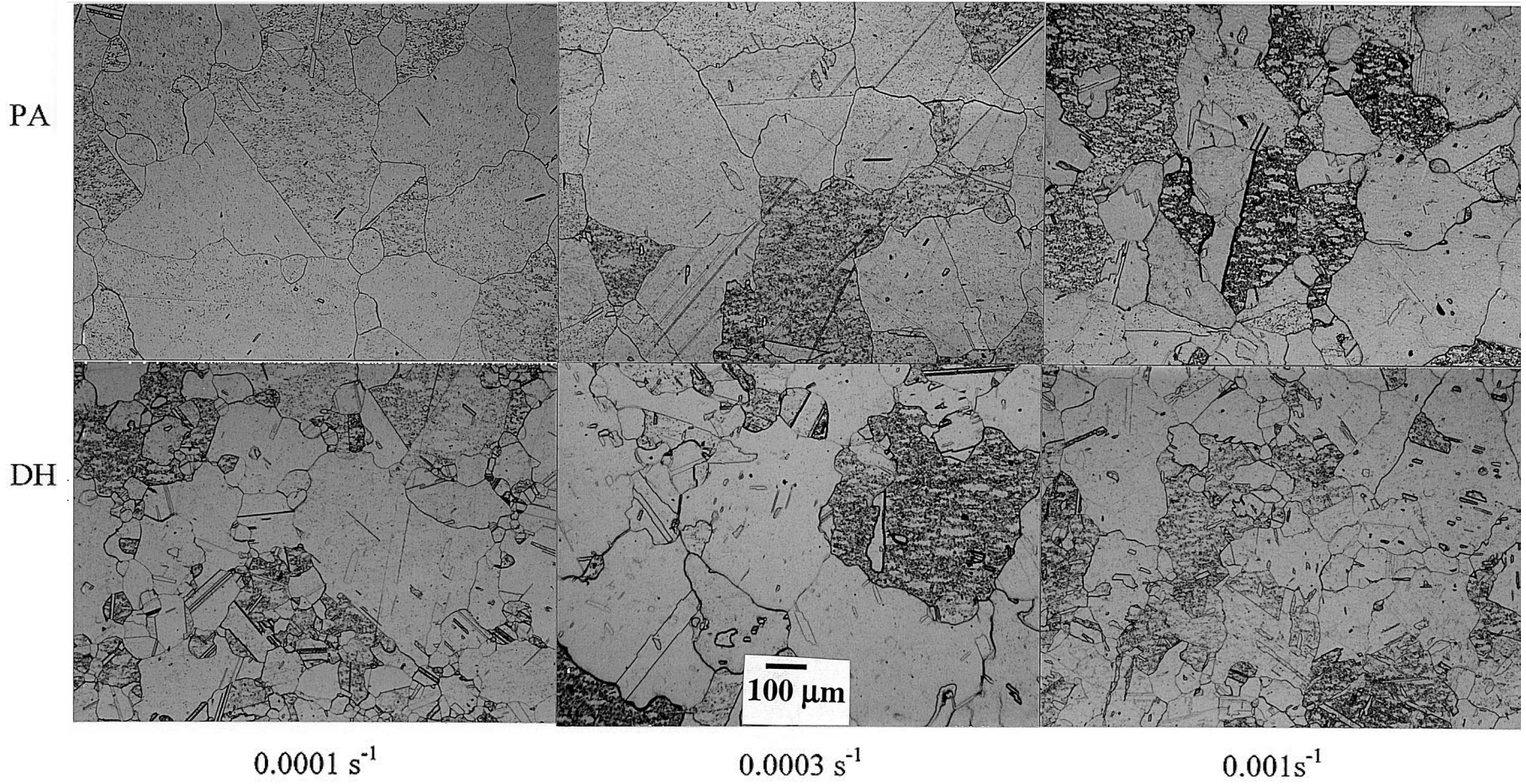


Fig. 26. Comparison of microstructures observed in RCC specimens after forging at 2075F/10h presoak.

PA

DH

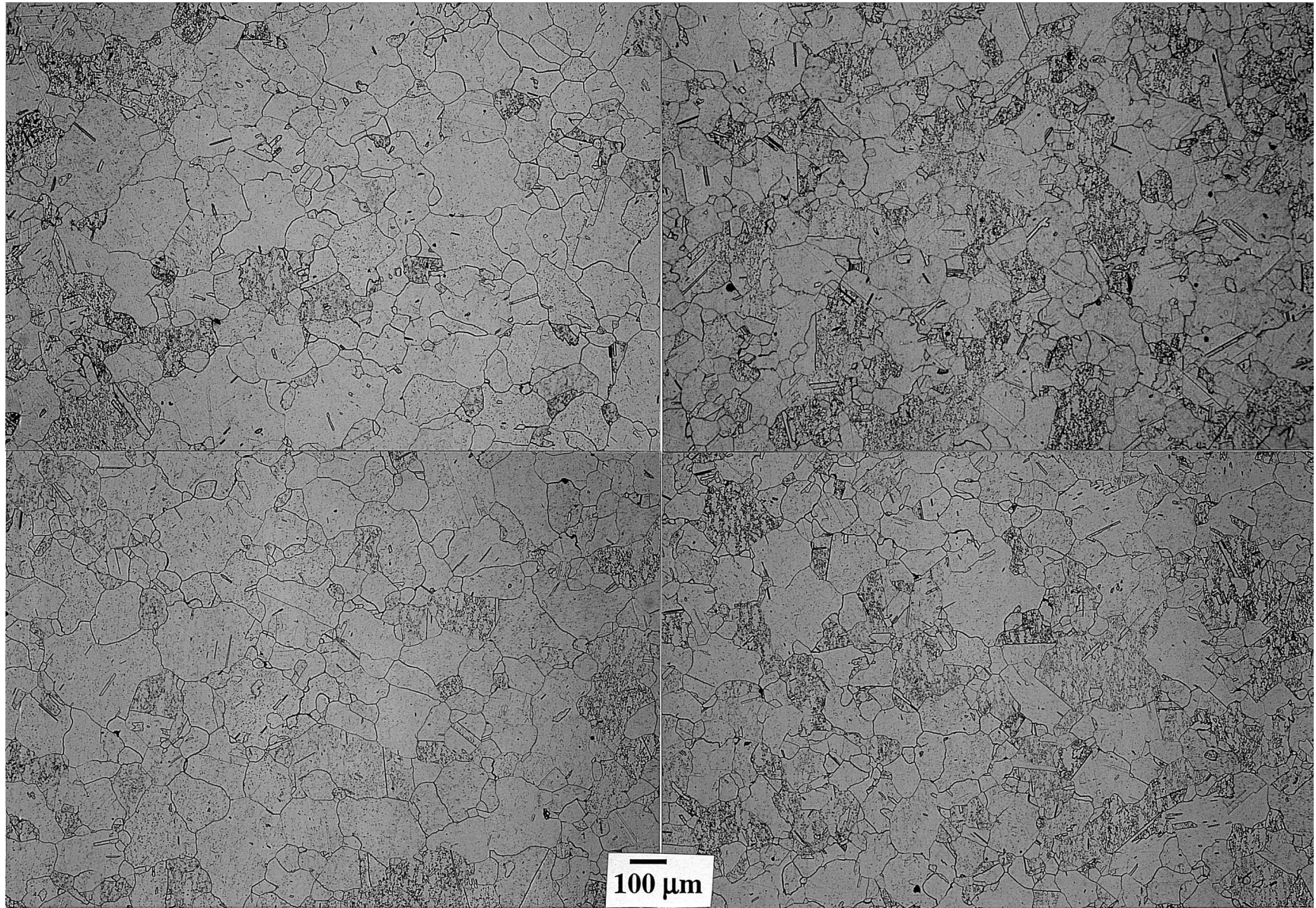


Fig. 27. Comparison of microstructures observed in DC specimens after forging at 2025F/10h presoak.

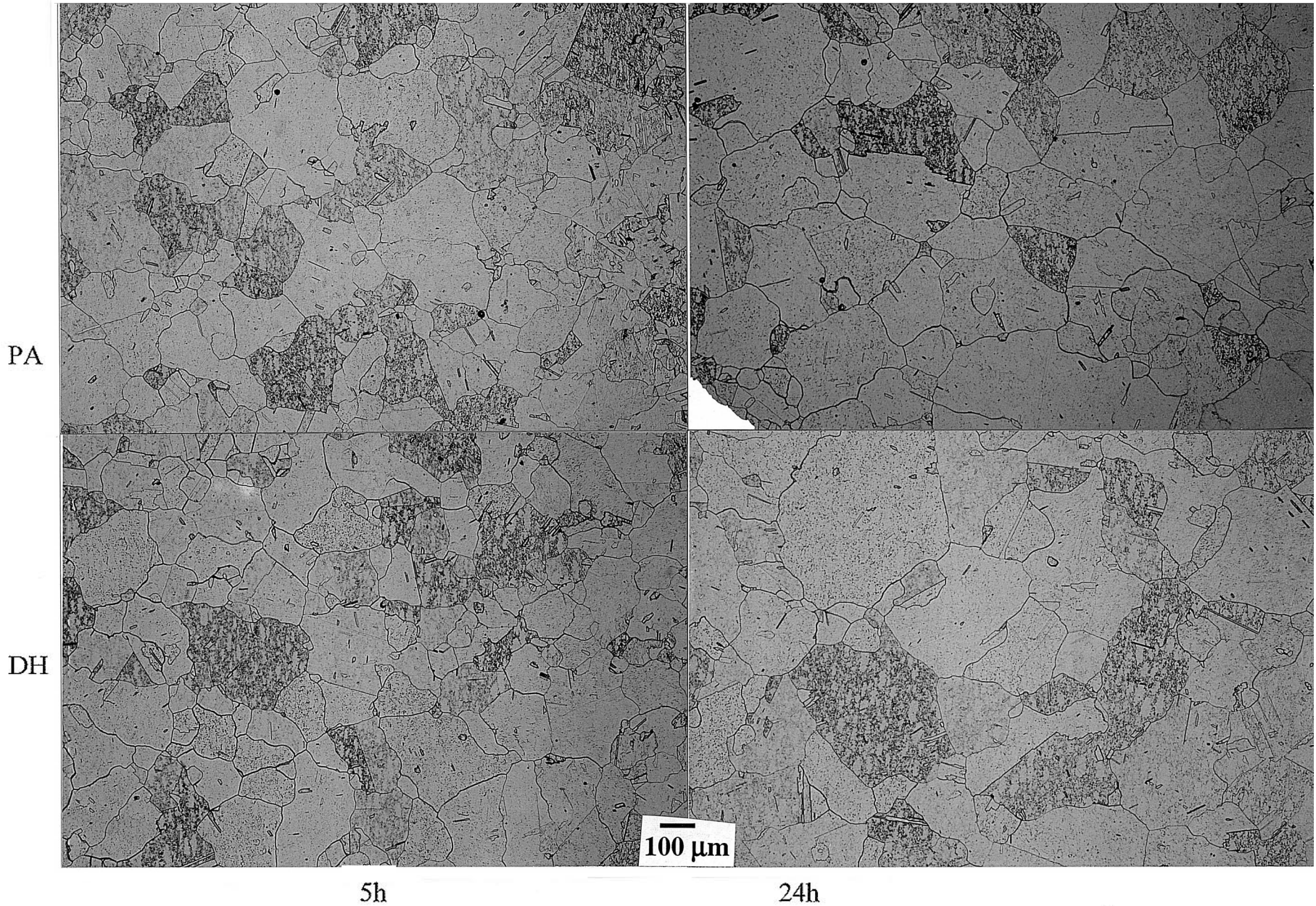


Fig. 28. Comparison of microstructures observed in DC specimens after forging at 2050F/0.0003 s⁻¹ approximate strain rate.

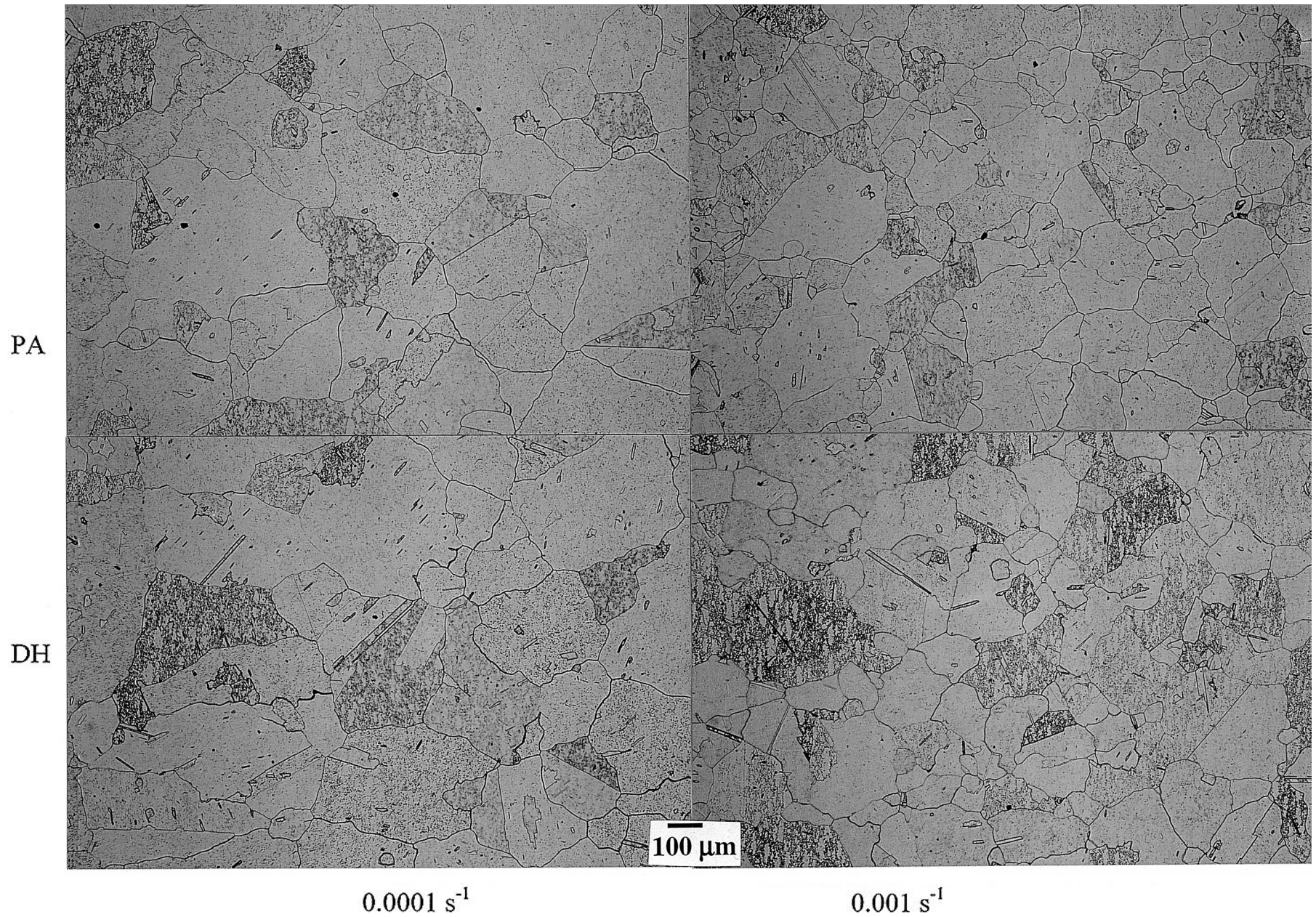


Fig. 29. Comparison of microstructures observed in DC specimens after forging at 2075F/10h presoak.

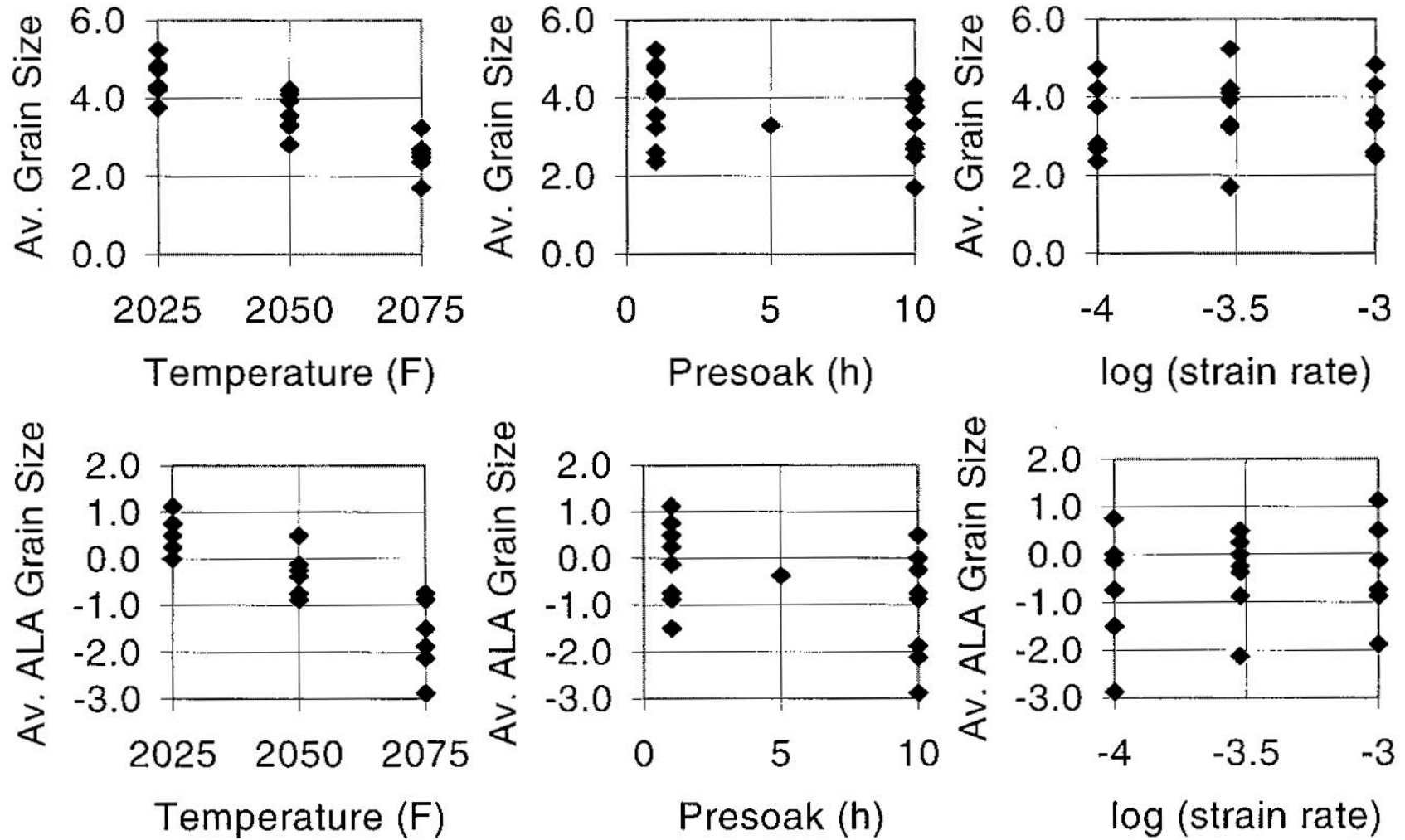


Fig. 30 Scatter plots of average and ALA grain size versus temperature, presoak time, and strain rate.

Appendix A-1

Least Squares Coefficients, Response LS, Model DESIGN_AUTO_LS

0 Term	1 Coeff.	2 Std. Error	3 T-value	4 Signif.	5 Transformed Term
1 1	0.240553	0.007880			
2 ~T	0.041239	0.009913	4.16	0.0008	((T-2.05e+03)/2.5e+01)
3 ~P	0.082134	0.008091	10.15	0.0001	((P-5.5)/4.5)
4 ~LSR	0.277051	0.009909	27.96	0.0001	((LSR+3.5)/5e-01)

No. cases = 19 R-sq. = 0.9836 RMS Error = 0.03434
 Resid. df = 15 R-sq-adj. = 0.9804 Cond. No. = 1.022
 ~ indicates factors are transformed.

Least Squares Summary ANOVA, Response LS Model DESIGN_AUTO_LS

0 Source	1 df	2 Sum Sq.	3 Mean Sq.	4 F-Ratio	5 Signif.
1 Total(Corr.)	18	1.081545			
2 Regression	3	1.063857	0.354619	300.70	0.0000
3 Residual	15	0.017689	0.001179		

R-sq. = 0.9836
 R-sq-adj. = 0.9804

Model obeys hierarchy. The sum of squares for each term is computed assuming higher order terms are first removed.

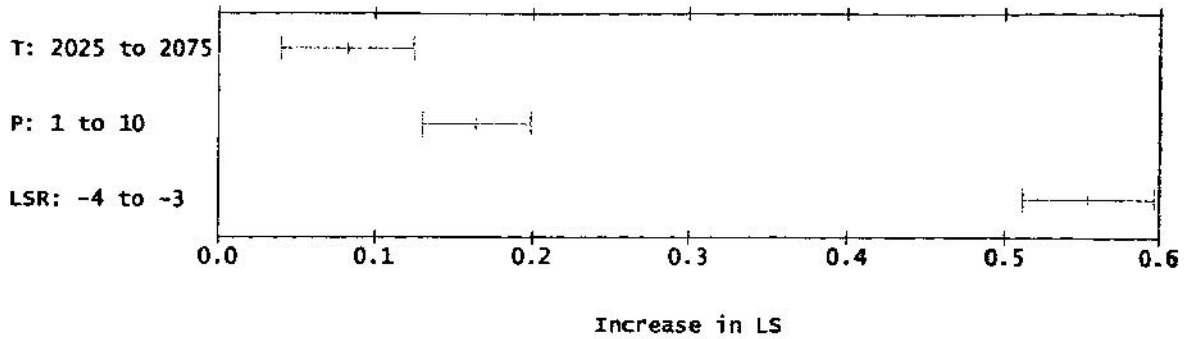
Least Squares Components ANOVA, Response LS Model DESIGN_AUTO_LS

0 Source	1 df	2 Sum Sq.	3 Mean Sq.	4 F-Ratio	5 Signif.	6 Transformed Term
1 Constant	1	1.052870				
2 ~T	1	0.020408	0.020408	17.31	0.0008	((T-2.05e+03)/2.5e+01)
3 ~P	1	0.121505	0.121505	103.00	0.0000	((P-5.5)/4.5)
4 ~LSR	1	0.921797	0.921797	781.70	0.0000	((LSR+3.5)/5e-01)
5 Residual	15	0.017689	0.001179			

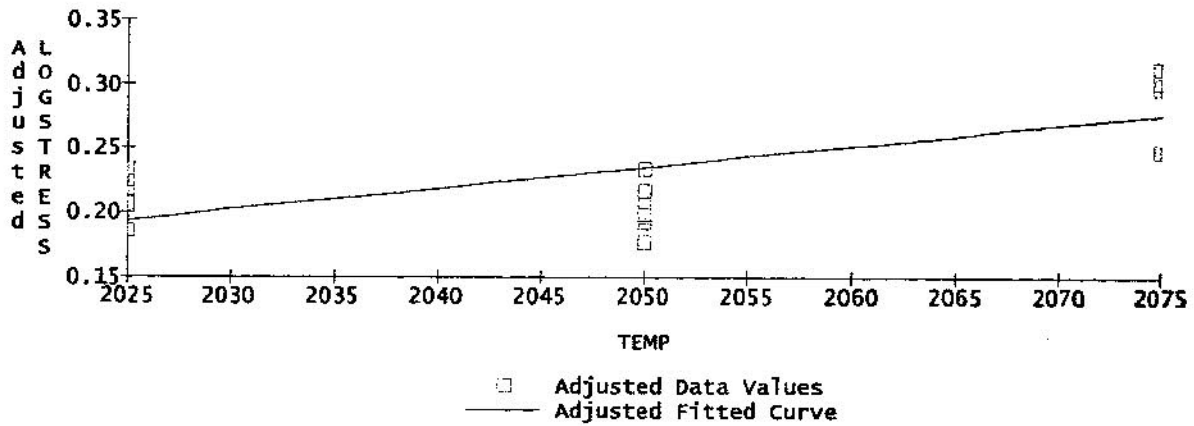
~ indicates factors are transformed. R-sq. = 0.9836
 R-sq-adj. = 0.9804
 Default sum of squares.
 Model obeys hierarchy. The sum of squares for each term is computed assuming higher order terms are first removed.

Appendix A-1 (cont.)

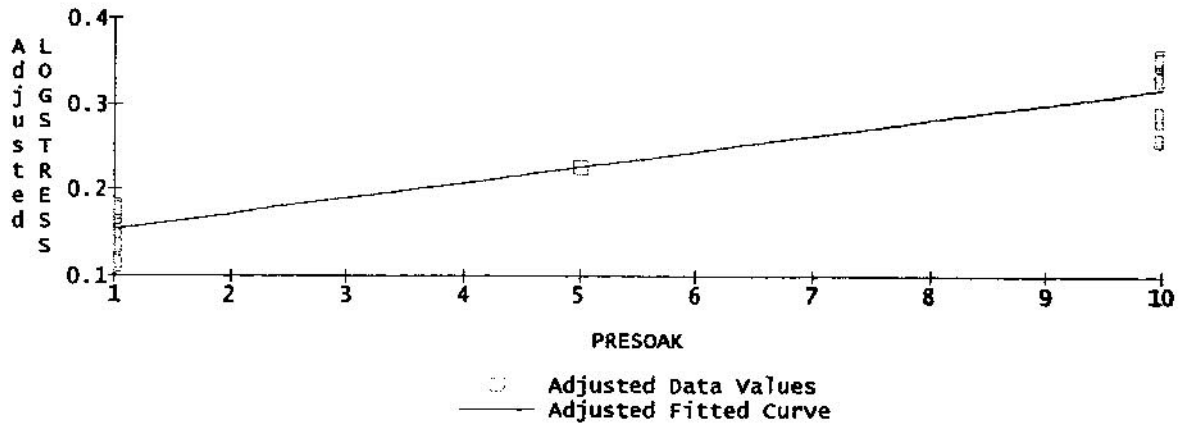
Mulreg @EXPTMP@MULREG, Model DESIGN_AUTO_LS
 Main Effects on Response LOGSTRESS
 (with 95% Confidence Intervals)



LOGSTRESS vs TEMP, Adjusted for Remaining Predictors
 Using Mulreg @EXPTMP@MULREG, Model DESIGN_AUTO_LS

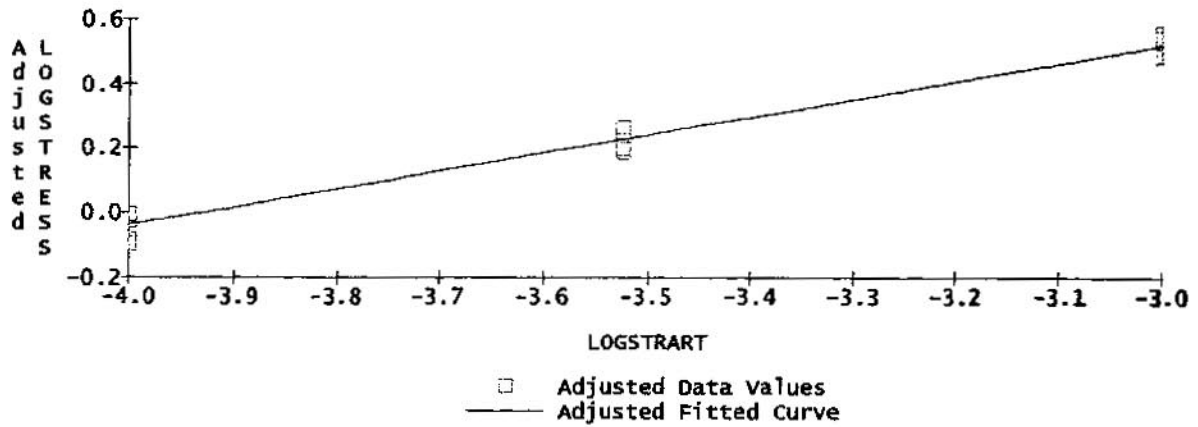


LOGSTRESS vs PRESOAK, Adjusted for Remaining Predictors
 Using Mulreg @EXPTMP@MULREG, Model DESIGN_AUTO_LS

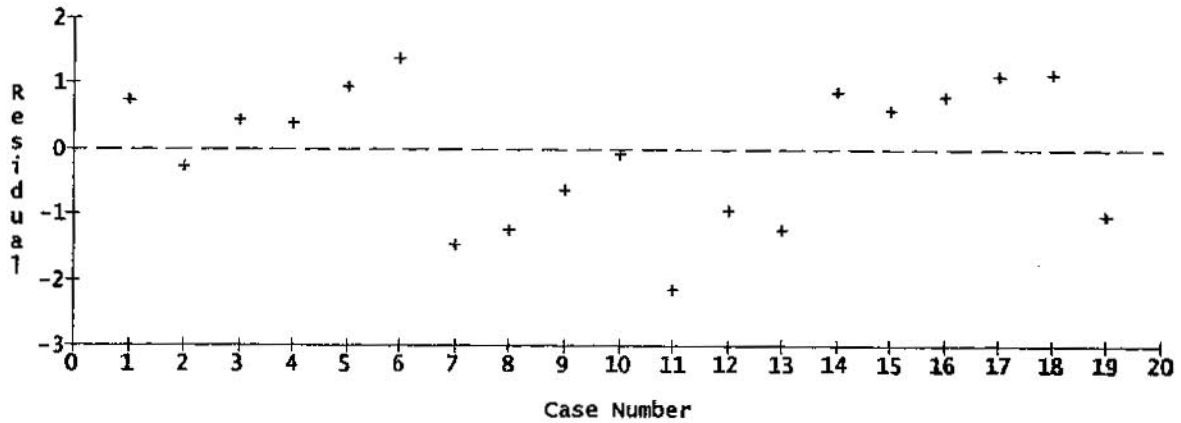


Appendix A-1 (cont.)

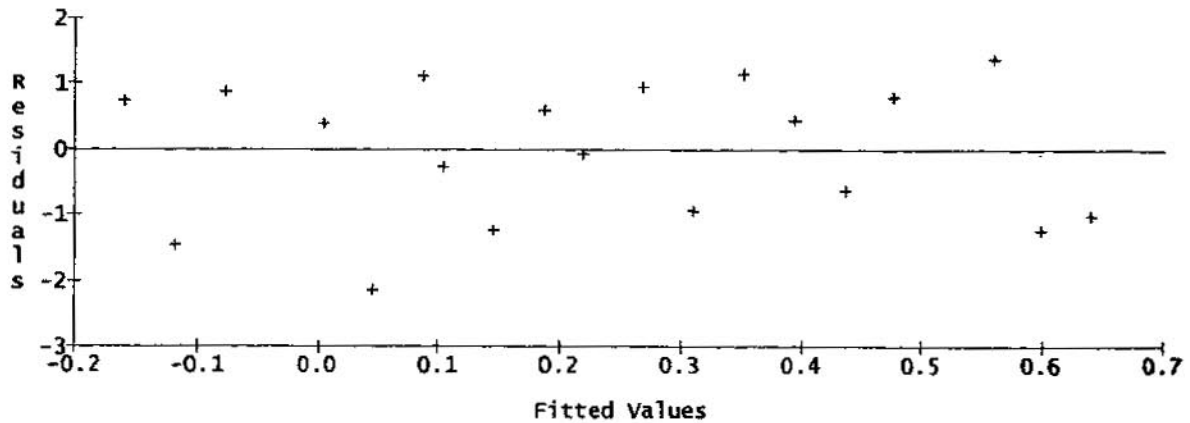
LOGSTRESS vs LOGSTART, Adjusted for Remaining Predictors
Using Mulreg @EXPTMP@MULREG, Model DESIGN_AUTO_LS



Case Order Graph of Residuals of LS
Using Studentized Residuals in Model DESIGN_AUTO_LS

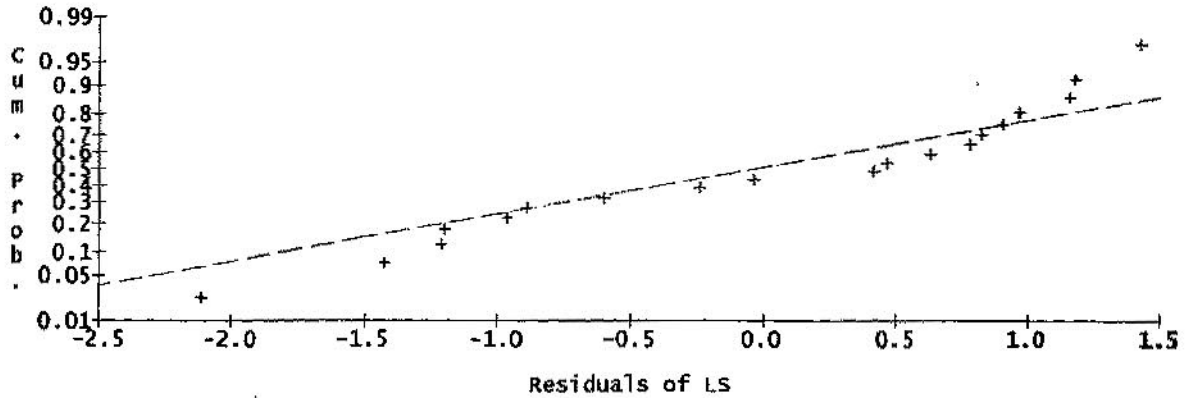


Residuals of LS vs Fitted Values
Using Studentized Residuals in Model DESIGN_AUTO_LS

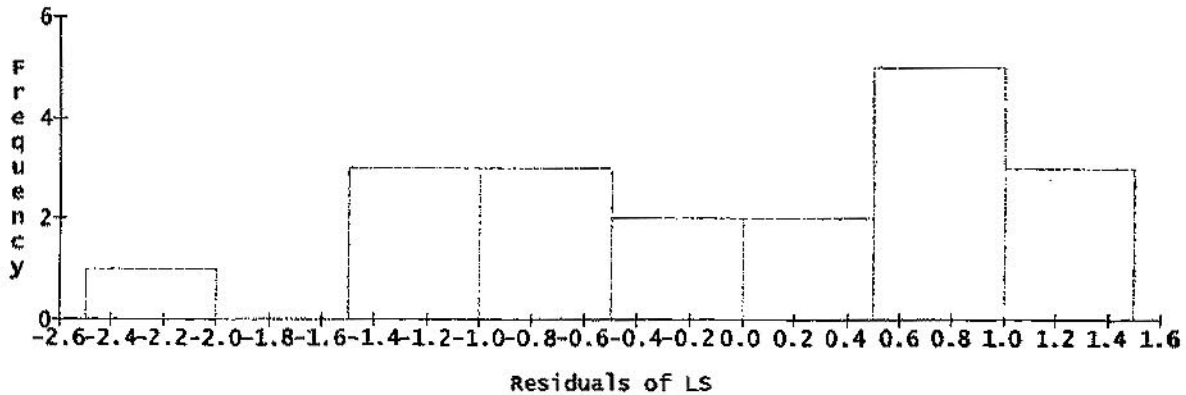


Appendix A-1 (cont.)

Normal Probability Plot of Residuals of LS
Using Studentized Residuals in Model DESIGN_AUTO_LS
(Sample size = 19)



Histogram of Residuals of LS
Using Studentized Residuals in Model DESIGN_AUTO_LS
(Sample size = 19)

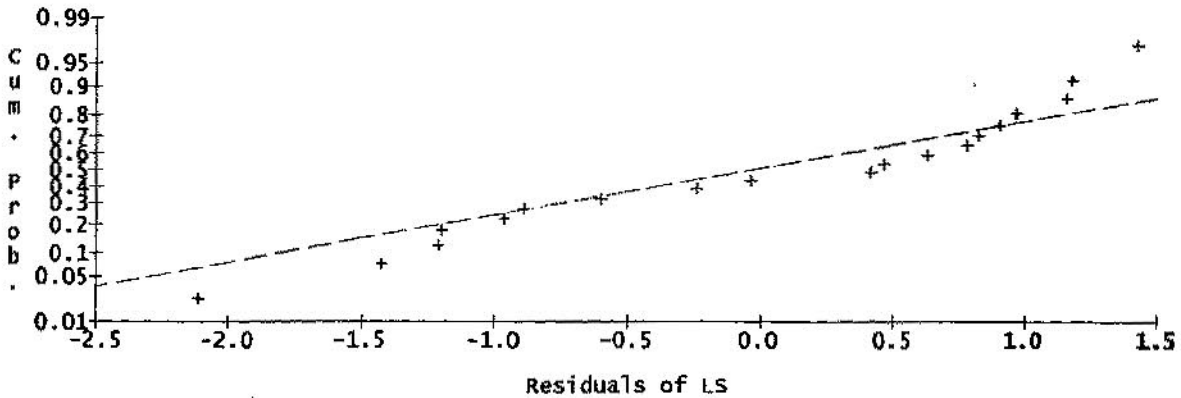


0 Factor, Response or Formula	1 Range	2 Initial Setting	3 Optimal Value
1 Factors			
2 TEMP	2025 to 2075	2050	2025
3 PRESOAK	1 to 10	5.5	1.0004
4 LOGSTRART	-4 to -3	-3.5	-3.9974
5 Responses			
6 LOGSTRESS	MIN		-0.15841

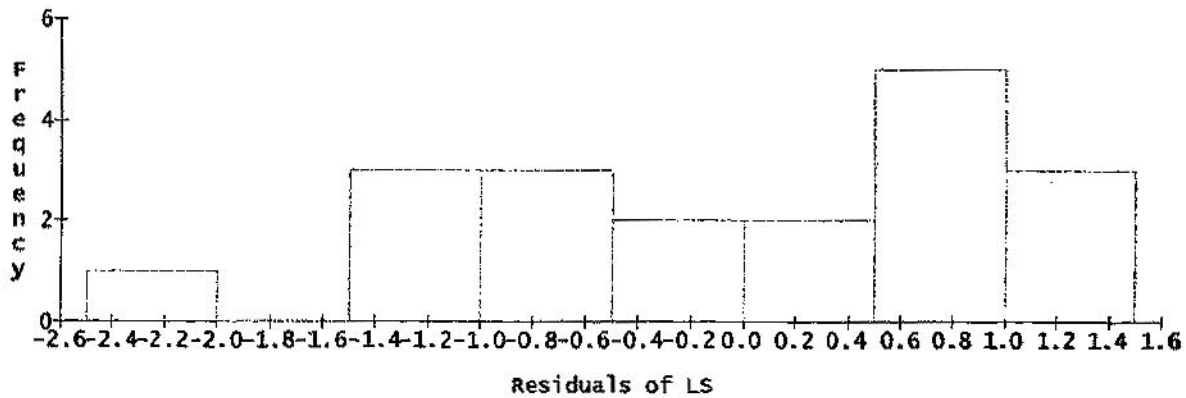
Converged to a tolerance of 0.000077 after 109 steps.

Appendix A-1 (cont.)

Normal Probability Plot of Residuals of LS
Using Studentized Residuals in Model DESIGN_AUTO_LS
(Sample size = 19)



Histogram of Residuals of LS
Using Studentized Residuals in Model DESIGN_AUTO_LS
(Sample size = 19)



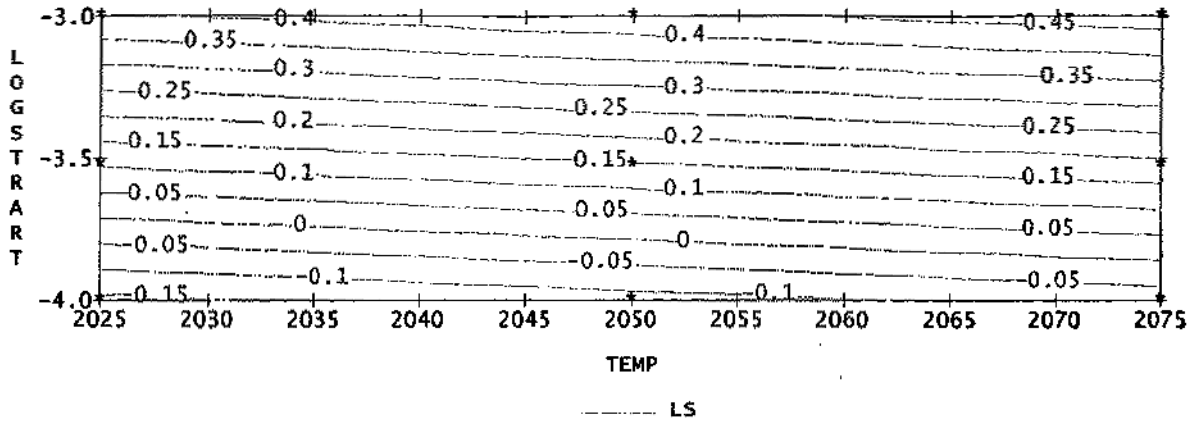
0 Factor, Response or Formula	1 Range	2 Initial Setting	3 Optimal Value

1 Factors			
2 TEMP	2025 to 2075	2050	2025
3 PRESOAK	1 to 10	5.5	1.0004
4 LOGSTRART	-4 to -3	-3.5	-3.9974
5			
6 Responses			
7 LOGSTRESS	MIN		-0.15841

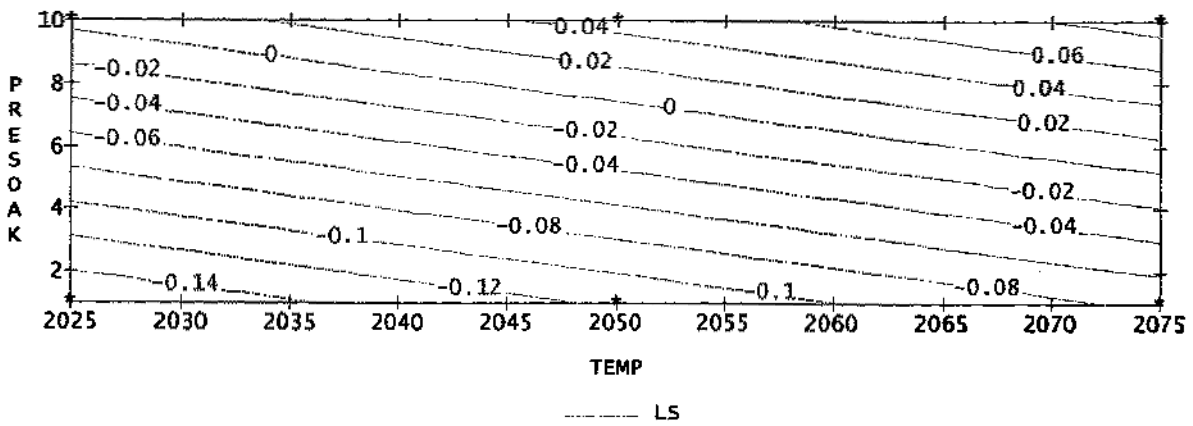
Converged to a tolerance of 0.000077 after 109 steps.

Appendix A-1 (cont.)

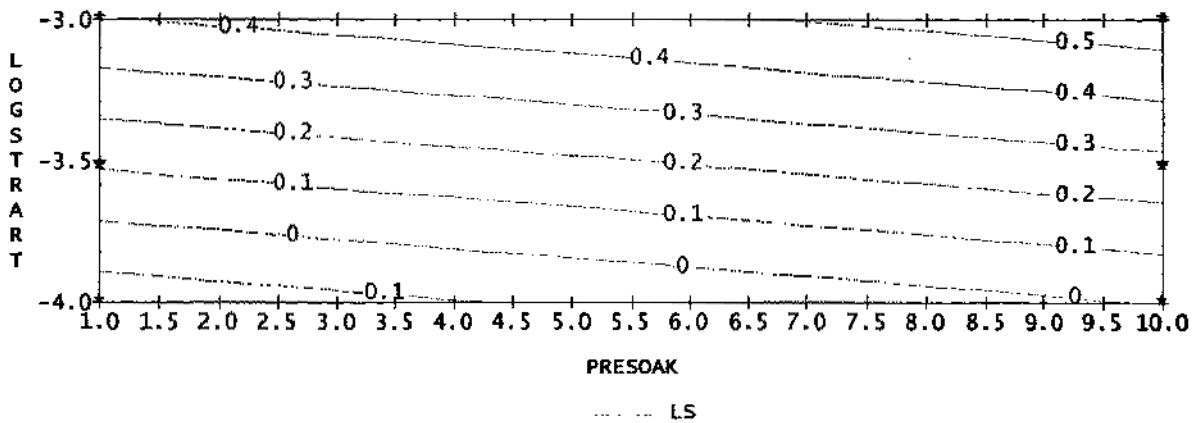
LOGSTRESS
PRESOAK = 1.0004



LOGSTRESS
LOGSTART = -3.9974



LOGSTRESS
TEMP = 2025



Appendix A-2

Bisquare Coefficients, Response LS, Model DESIGN_AUTO_LS

0 Term	1 Coeff.	2 Std. Error	3 T-value	4 Signif.	5 Transformed Term
1 1	0.207982	0.007335			
2 ~T	0.046337	0.005602			((T-2.05e+03)/2.5e+01)
3 ~P	0.085639	0.004572	18.73	0.0001	((P-5.5)/4.5)
4 ~LSR	0.281954	0.005600	50.35	0.0001	((LSR+3.5)/5e-01)
5 ~T**2	0.056926	0.009229	6.17	0.0001	((T-2.05e+03)/2.5e+01)**

No. cases = 19 R-sq. = 0.9953 RMS Error = 0.0194
 Resid. df = 14 R-sq-adj. = 0.9940 Cond. No. = 2.958
 ~ indicates factors are transformed.

Bisquare Summary ANOVA, Response LS Model DESIGN_AUTO_LS

0 Source	1 df	2 Sum Sq.	3 Mean Sq.	4 F-Ratio	5 Signif.
1 Total(Corr.)	18	1.133631			
2 Regression	4	1.128359	0.282090	749.20	0.0000
3 Linear	3	1.114033	0.371344	986.20	0.0000
4 Non-linear	1	0.014326	0.014326	38.04	0.0000
5 Residual	14	0.005272	0.000377		

R-sq. = 0.9953
 R-sq-adj. = 0.9940

Model obeys hierarchy. The sum of squares for each term is computed assuming higher order terms are first removed.

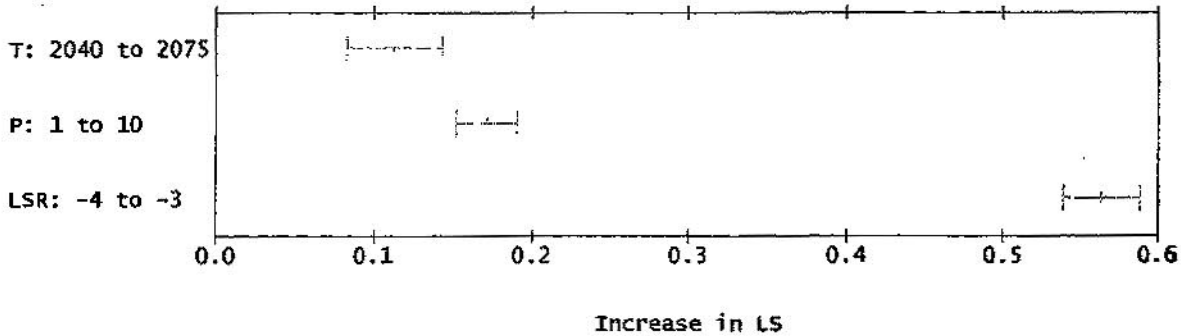
Bisquare Components ANOVA, Response LS Model DESIGN_AUTO_LS

0 Source	1 df	2 Sum Sq.	3 Mean Sq.	4 F-Ratio	5 Signif.	6 Transformed Term
1 Constant	1	1.082406				
2 ~T	1	0.025765	0.025765	68.43	0.0000	((T-2.05e+03)/2.5e+01)
3 ~P	1	0.132090	0.132090	350.80	0.0000	((P-5.5)/4.5)
4 ~LSR	1	0.954705	0.954705	2535.00	0.0000	((LSR+3.5)/5e-01)
5 ~T**2	1	0.014326	0.014326	38.04	0.0000	((T-2.05e+03)/2.5e+01)**
6 Residual	14	0.005272	0.000377			

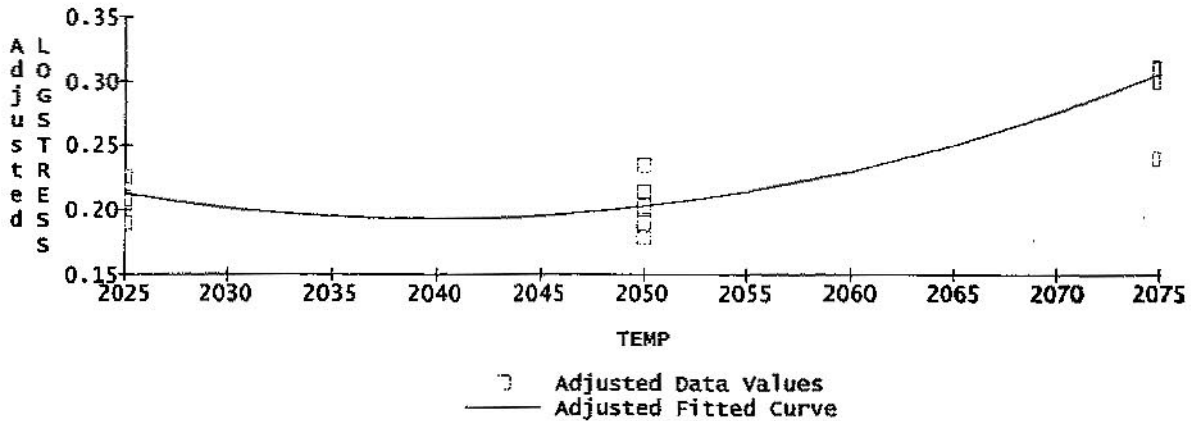
~ indicates factors R-sq. = 0.9953
 are transformed. R-sq-adj. = 0.9940
 Default sum of squares.
 Model obeys hierarchy. The sum of squares for each term is computed assuming higher order terms are first removed.

Appendix A-2 (cont.)

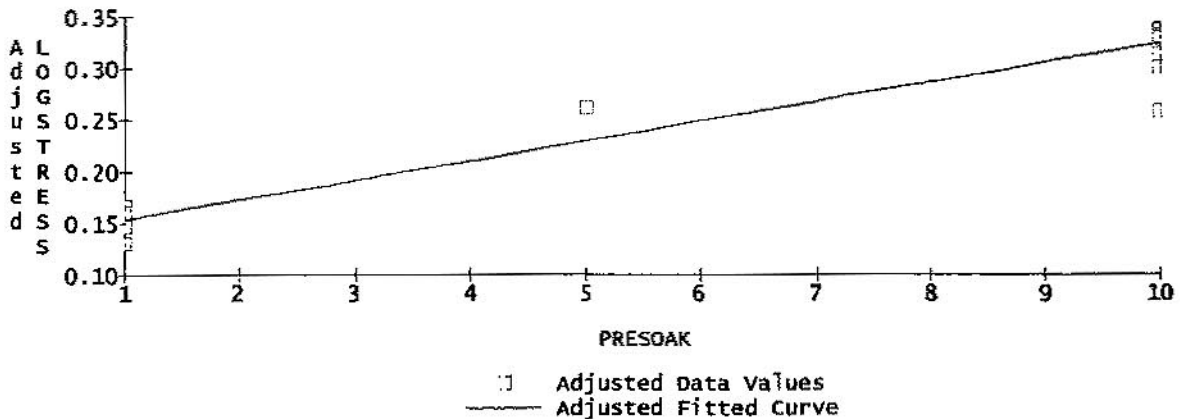
Mulreg @EXPTMP@MULREG, Model DESIGN_AUTO_LS
Main Effects on Response LOGSTRESS
(with 95% Confidence Intervals)



LOGSTRESS vs TEMP, Adjusted for Remaining Predictors
Using Mulreg @EXPTMP@MULREG, Model DESIGN_AUTO_LS

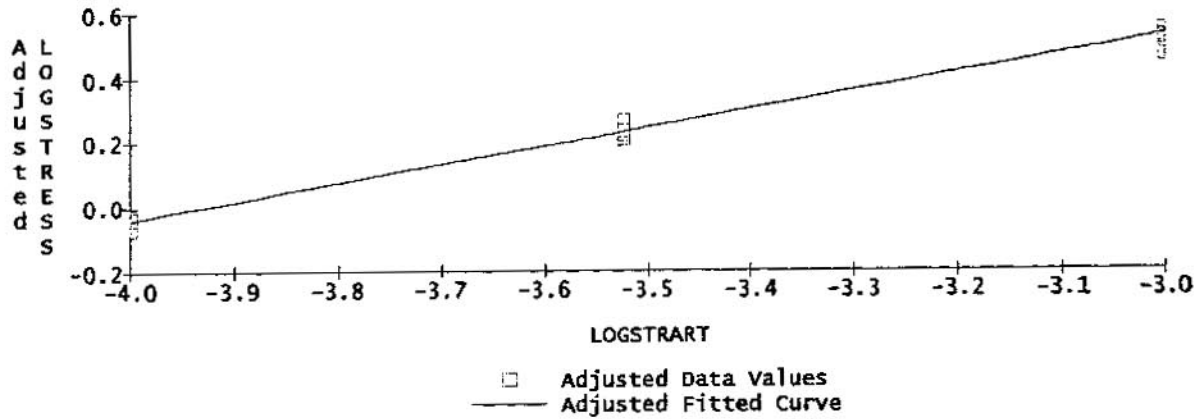


LOGSTRESS vs PRESOAK, Adjusted for Remaining Predictors
Using Mulreg @EXPTMP@MULREG, Model DESIGN_AUTO_LS

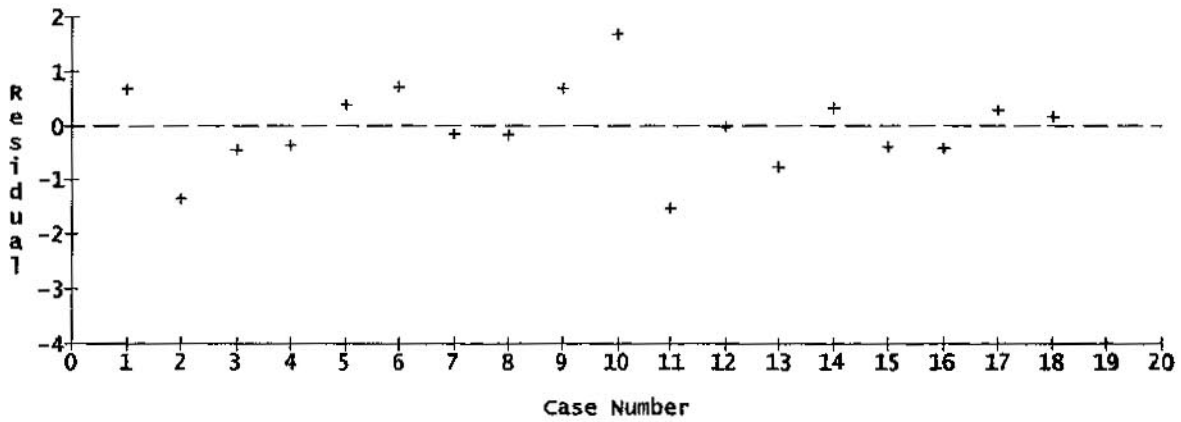


Appendix A-2 (cont.)

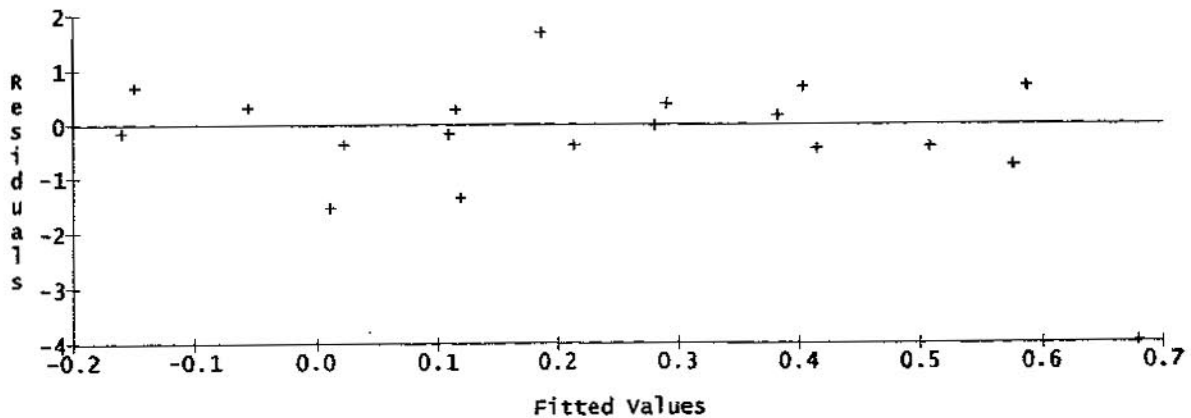
LOGSTRESS vs LOGSTRART, Adjusted for Remaining Predictors
Using Mulreg @EXPTMP@MULREG, Model DESIGN_AUTO_LS



Case Order Graph of Residuals of LS
Using Studentized Residuals in Model DESIGN_AUTO_LS

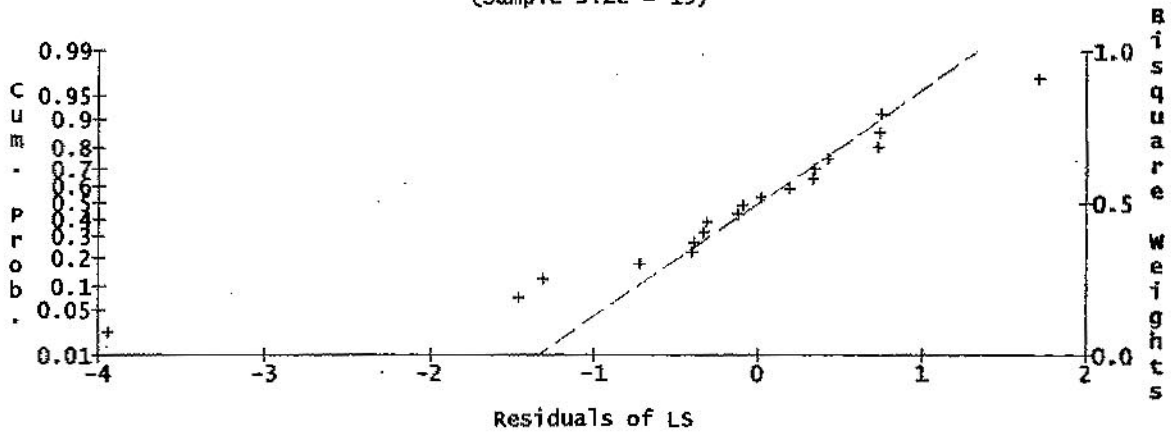


Residuals of LS vs Fitted Values
Using studentized Residuals in Model DESIGN_AUTO_LS

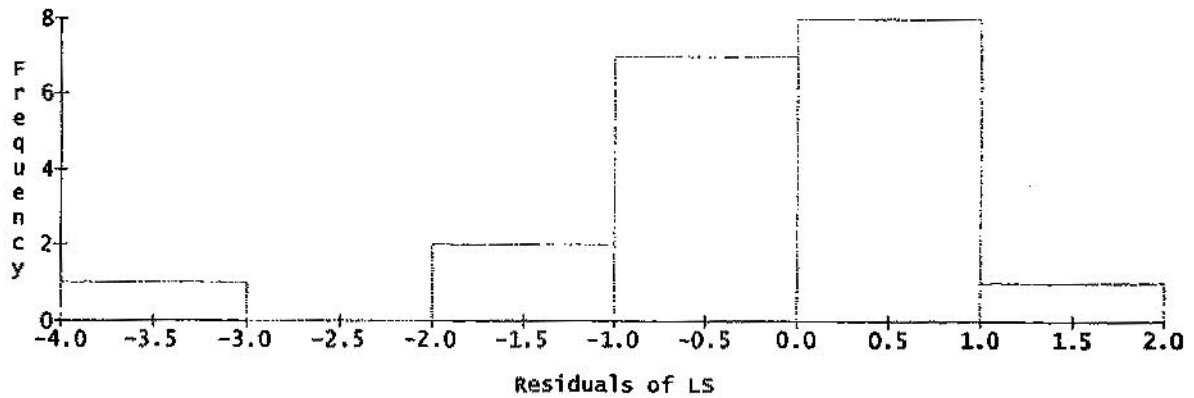


Appendix A-2 (cont.)

Normal Probability Plot of Residuals of LS
Using Studentized Residuals in Model DESIGN_AUTO_LS
(Sample size = 19)



Histogram of Residuals of LS
Using Studentized Residuals in Model DESIGN_AUTO_LS
(Sample size = 19)



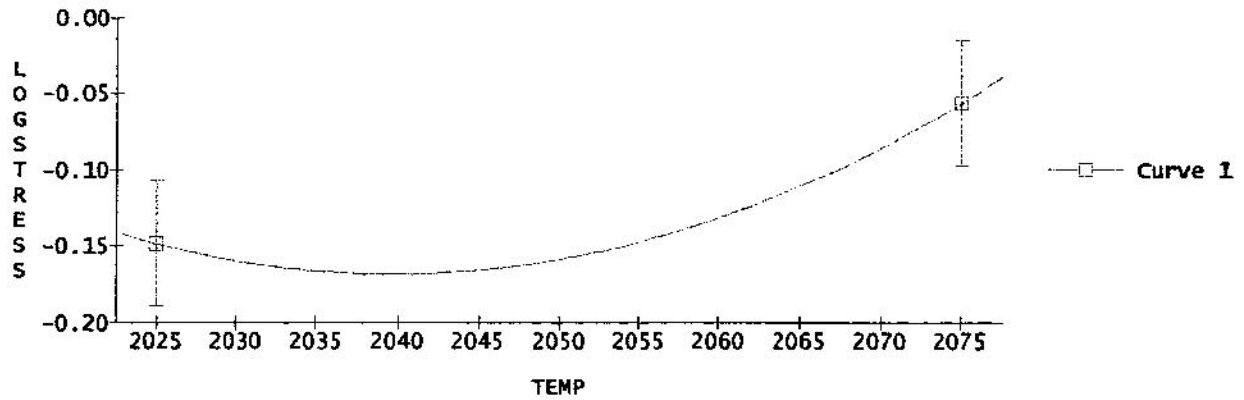
0 Factor, Response or Formula	1 Range	2 Initial Setting	3 Optimal Value

1 Factors			
2 TEMP	2025 to 2075	2050	2039.3
3 PRESOAK	1 to 10	5.5	1.0512
4 LOGSTART	-4 to -3	-3.5	-3.9999
5			
6 Responses			
7 LOGSTRESS	MIN		-0.16798

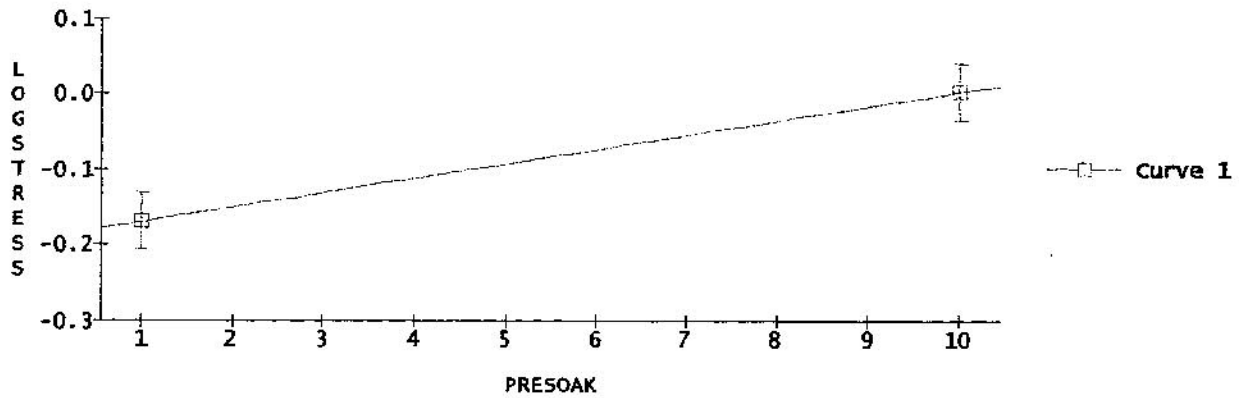
Converged to a tolerance of 0.000077 after 71 steps.

Appendix A-2 (cont.)

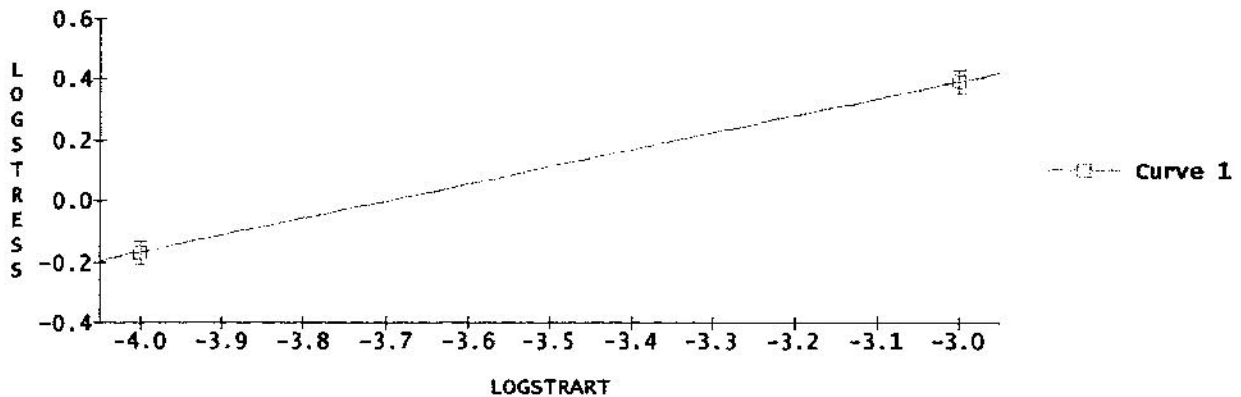
Predictions and 95% simultaneous confidence intervals
for mean responses of LOGSTRESS using model DESIGN_AUTO_LS
P = 1.0512, LSR = -3.9999



Predictions and 95% simultaneous confidence intervals
for mean responses of LOGSTRESS using model DESIGN_AUTO_LS
LSR = -3.9999, T = 2039.3

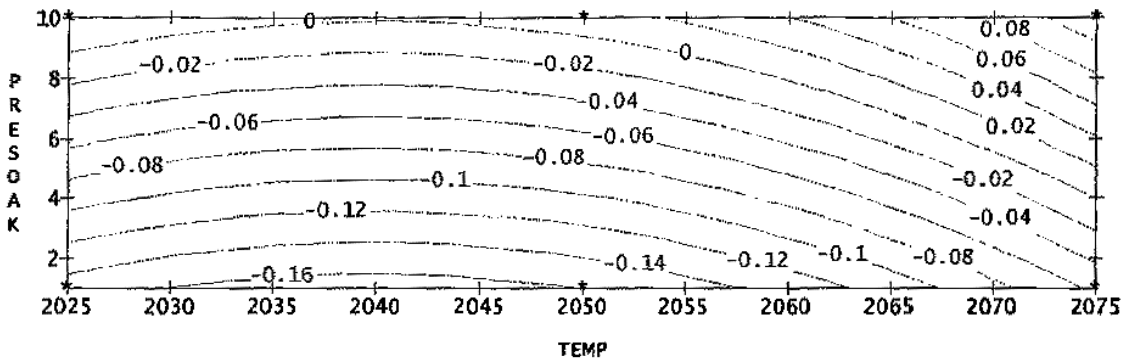


Predictions and 95% simultaneous confidence intervals
for mean responses of LOGSTRESS using model DESIGN_AUTO_LS
T = 2039.3, P = 1.0512



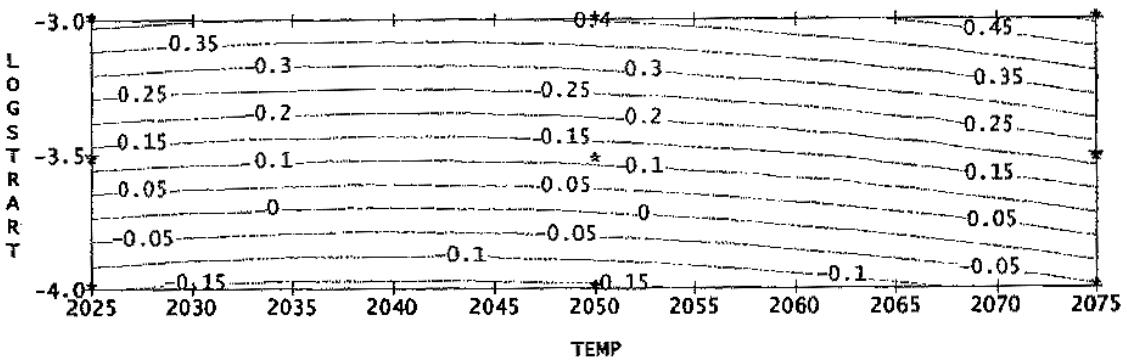
Appendix A-2 (cont.)

LOGSTRESS
LOGSTRART = -3.9999



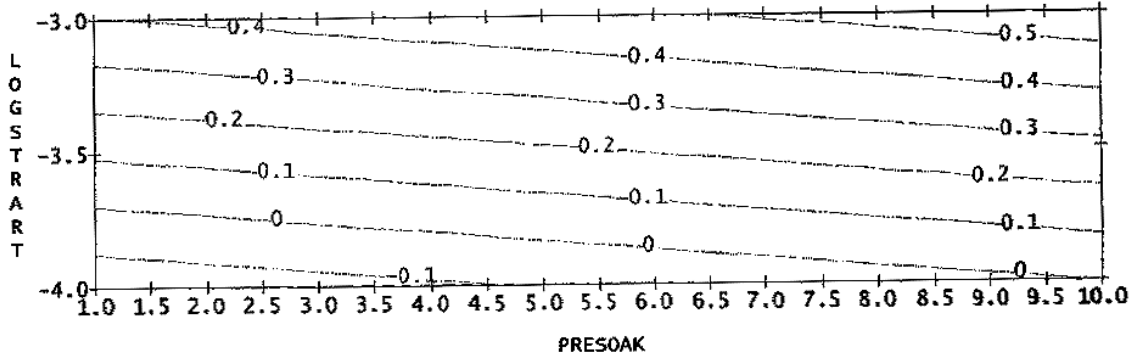
----- LS

LOGSTRESS
PRESOAK = 1.0512



----- LS

LOGSTRESS
TEMP = 2039.3



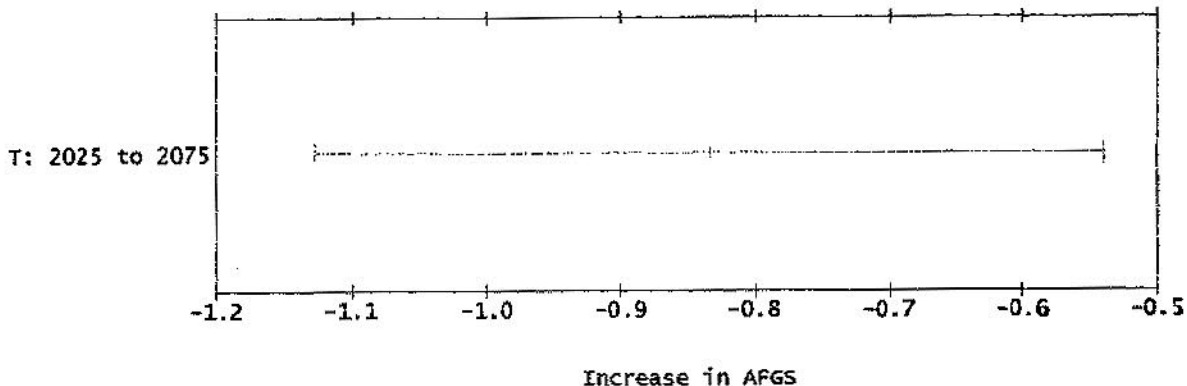
----- LS

Predictions and 95% simultaneous confidence intervals
for mean responses of LOGSTRESS using model DESIGN_AUTO_LS
LSR = -3

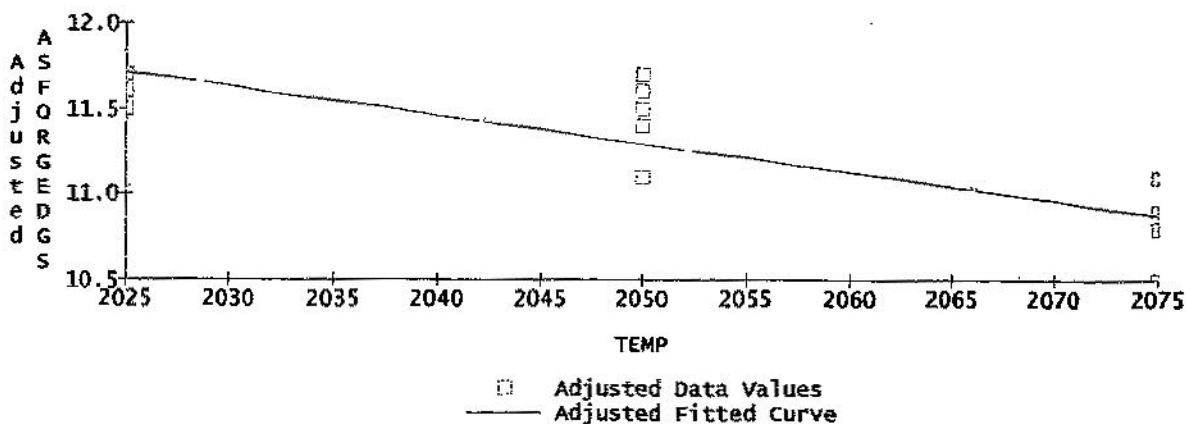
P	T=2025
5	Lower 0.453458
	Predicted 0.491009
	Upper 0.528560

Appendix A-3C (cont.)

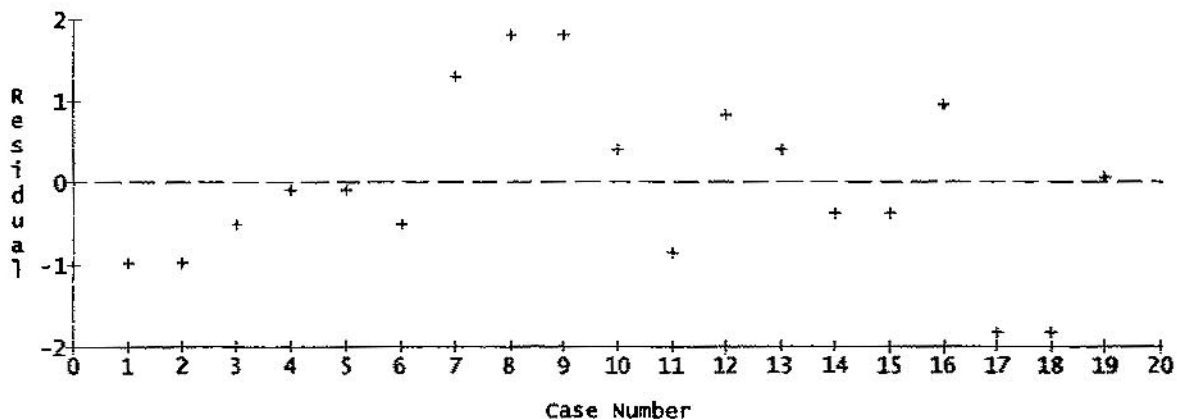
Mulreg @EXPT@MULREG, Model DESIGN_AUTO_AFGS
 Main Effects on Response ASFORGEDGS
 (with 95% Confidence Intervals)



ASFORGEDGS vs TEMP, Adjusted for Remaining Predictors
 Using Mulreg @EXPT@MULREG, Model DESIGN_AUTO_AFGS

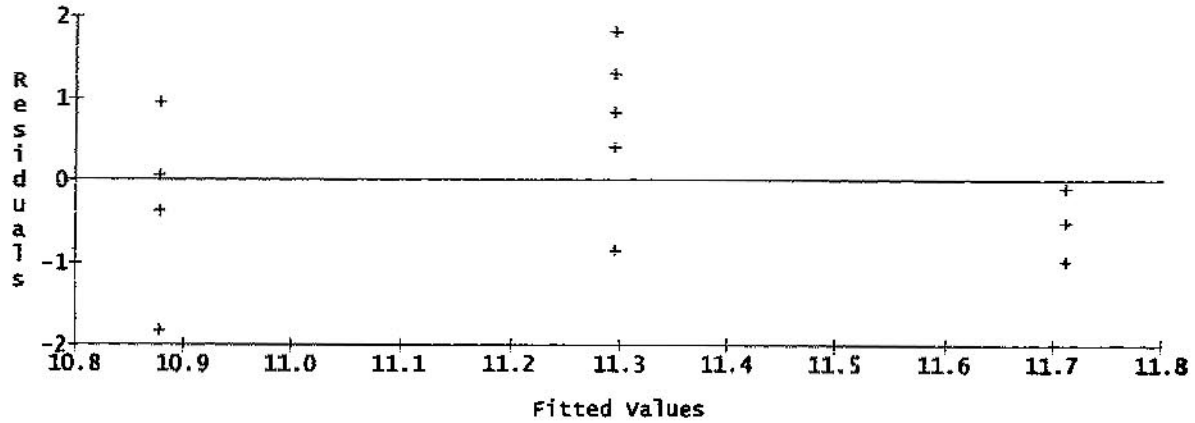


Case Order Graph of Residuals of AFGS
 Using Studentized Residuals in Model DESIGN_AUTO_AFGS

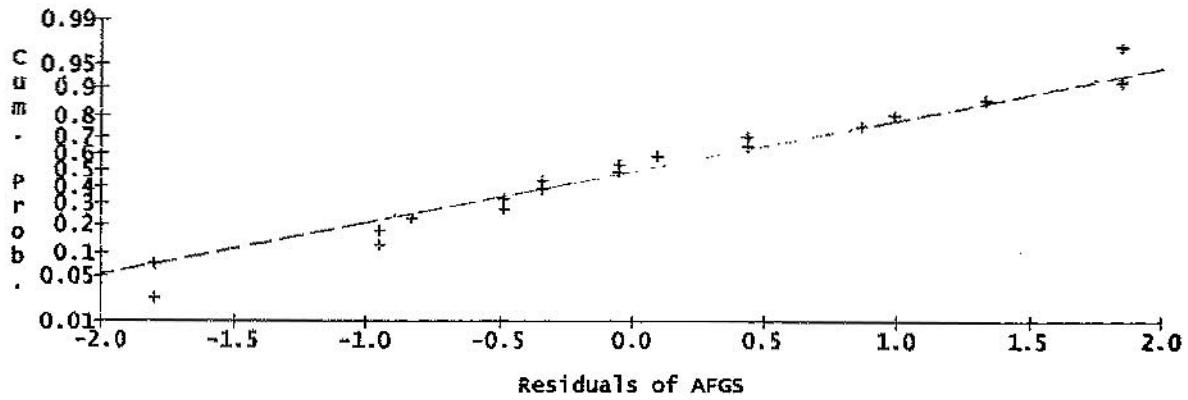


Appendix A-3C (cont.)

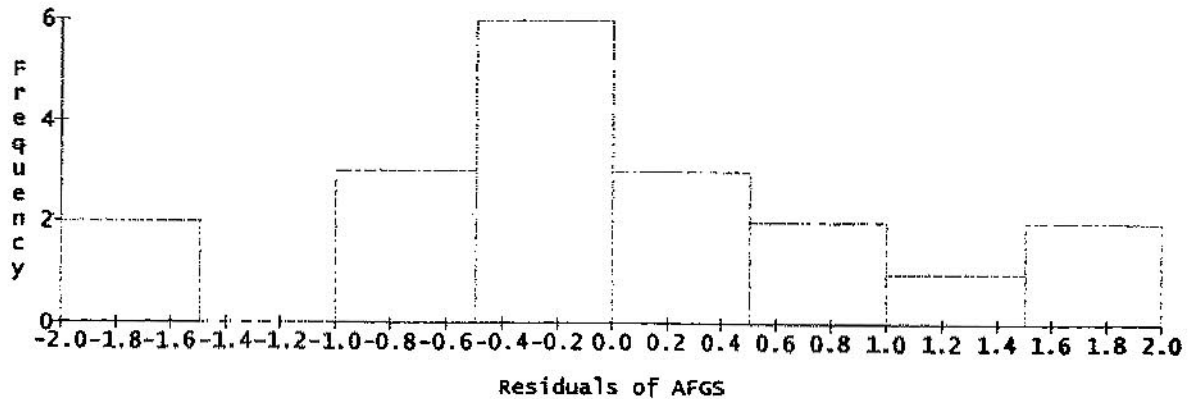
Residuals of AFGS vs Fitted Values
Using Studentized Residuals in Model DESIGN_AUTO_AFGS



Normal Probability Plot of Residuals of AFGS
Using Studentized Residuals in Model DESIGN_AUTO_AFGS
(Sample size = 19)



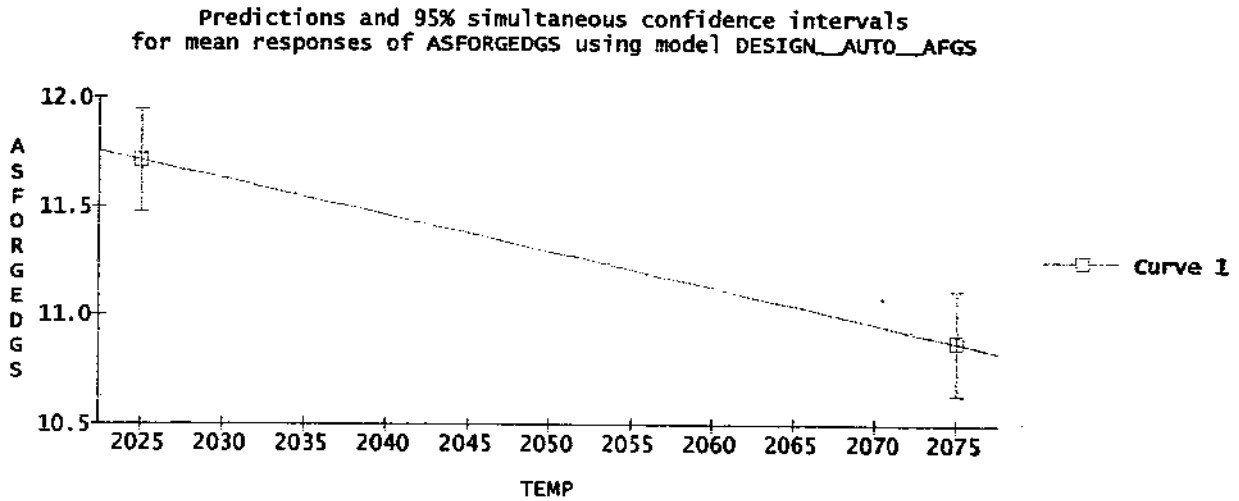
Histogram of Residuals of AFGS
Using Studentized Residuals in Model DESIGN_AUTO_AFGS
(Sample size = 19)



Appendix A-3C (cont.)

0 Factor, Response or Formula	1 Range	2 Initial Setting	3 Optimal Value
1 Factors			
2 TEMP	2025 TO 2075	2050	2025
3 PRESOAK	1 TO 10	5.5	7.75
4			
5 Responses			
6 ASFORGEDGS	MAX		11.711
7 AVGS_ALA			3.9699

Converged to a tolerance of 0.00012 after 46 steps.



Appendix A-3U

Least squares Coefficients, Response AFGS, Model DESIGN_AUTO_AFGS

0 Term	1 Coeff.	2 Std. Error	3 T-value	4 Signif.	5 Transformed Term
1 1	11.486292	0.047556			
2 ~T	-0.415313	0.036322			((T-2.05e+03)/2.5e+01)
3 ~P	-0.077218	0.029643			((P-5.5)/4.5)
4 ~LSR	0.091960	0.036302			((LSR+3.5)/5e-01)
5 ~T*P	-0.100000	0.036315	-2.75	0.0175	((T-2.05e+03)/2.5e+01)*((P-5.5)/4.5)
6 ~T*LSR	0.088773	0.044462	2.00	0.0691	((T-2.05e+03)/2.5e+01)*((LSR+3.5)/5e-01)
7 ~T**2	-0.301556	0.059832	-5.04	0.0003	((T-2.05e+03)/2.5e+01)**2

No. cases = 19 R-sq. = 0.9381 RMS Error = 0.1258
 Resid. df = 12 R-sq-adj. = 0.9072 Cond. No. = 2.958
 ~ indicates factors are transformed.

Least Squares Summary ANOVA, Response AFGS Model DESIGN_AUTO_AFGS

0 Source	1 df	2 Sum Sq.	3 Mean Sq.	4 F-Ratio	5 Signif.
1 Total(Corr.)	18	3.069474			
2 Regression	6	2.879564	0.479927	30.33	0.0000
3 Linear	3	2.294470	0.764823	48.33	0.0000
4 Non-linear	3	0.585094	0.195031	12.32	0.0006
5 Residual	12	0.189909	0.015826		

R-sq. = 0.9381
 R-sq-adj. = 0.9072

Model obeys hierarchy. The sum of squares for each term is computed assuming higher order terms are first removed.

Least Squares Components ANOVA, Response AFGS Model DESIGN_AUTO_AFGS

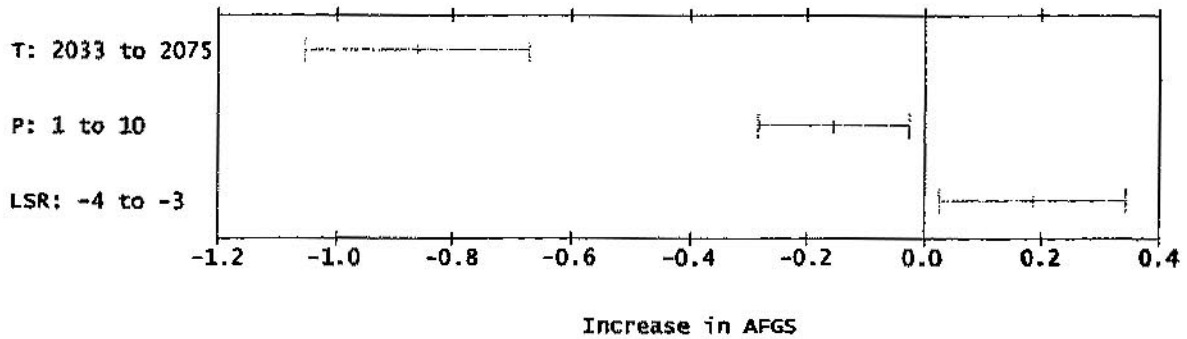
0 Source	1 df	2 Sum Sq.	3 Mean Sq.	4 F-Ratio	5 Signif.	6 Transformed Term
1 Constant	1	2424				
2 ~T	1	2.083333	2.083333	131.60	0.0000	((T-2.05e+03)/2.5e+01)
3 ~P	1	0.107391	0.107391	6.79	0.0230	((P-5.5)/4.5)
4 ~LSR	1	0.101557	0.101557	6.42	0.0263	((LSR+3.5)/5e-01)
5 ~T*P	1	0.120000	0.120000	7.58	0.0175	((T-2.05e+03)/2.5e+01)*((P-5.5)/4.5)
6 ~T*LSR	1	0.063089	0.063089	3.99	0.0691	((T-2.05e+03)/2.5e+01)*((LSR+3.5)/5e-01)
7 ~T**2	1	0.402005	0.402005	25.40	0.0003	((T-2.05e+03)/2.5e+01)**2
8 Residual	12	0.189909	0.015826			

~ indicates factors are transformed. R-sq. = 0.9381
 R-sq-adj. = 0.9072

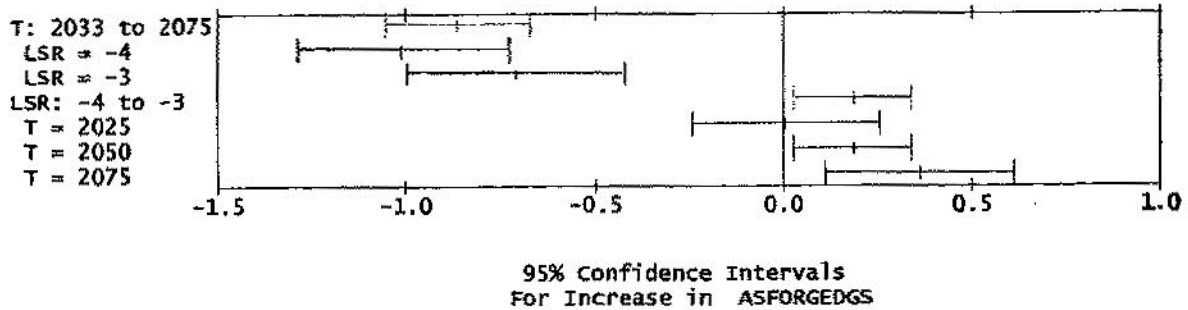
Default sum of squares.
 Model obeys hierarchy. The sum of squares for each term is computed assuming higher order terms are first removed.

Appendix A-3U (cont.)

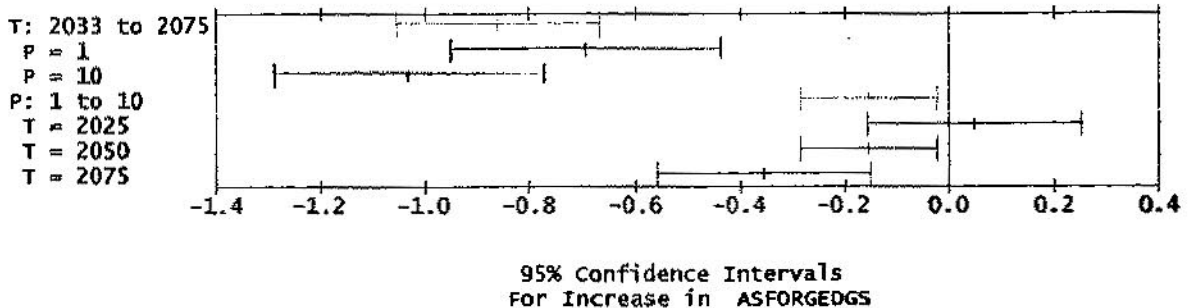
Mulreg @EXPT@MULREG, Model DESIGN_AUTO_AFGS
Main Effects on Response ASFORGEDGS
(with 95% Confidence Intervals)



Mulreg @EXPT@MULREG, Model DESIGN_AUTO_AFGS
Interaction Effects of TEMP with LOGSTART
On Response ASFORGEDGS

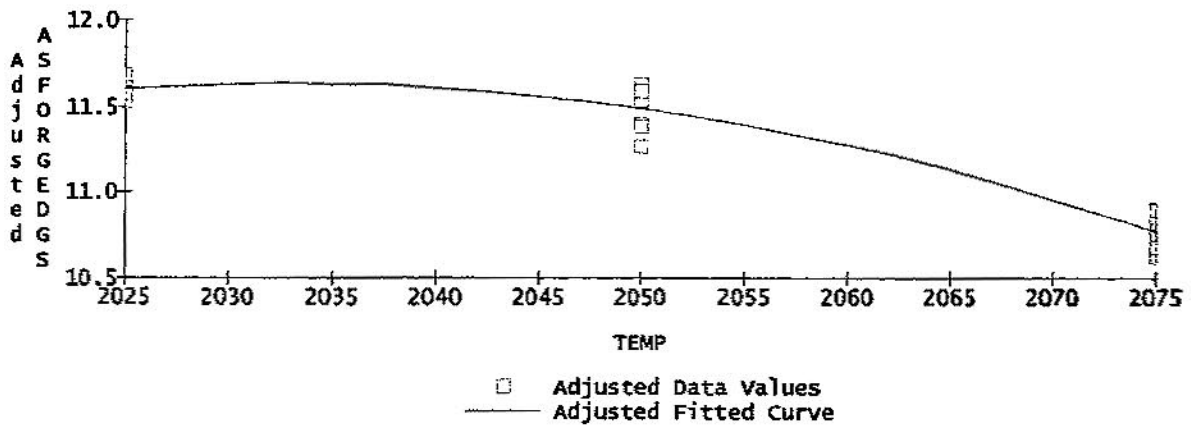


Mulreg @EXPT@MULREG, Model DESIGN_AUTO_AFGS
Interaction Effects of TEMP with PRESOAK
On Response ASFORGEDGS

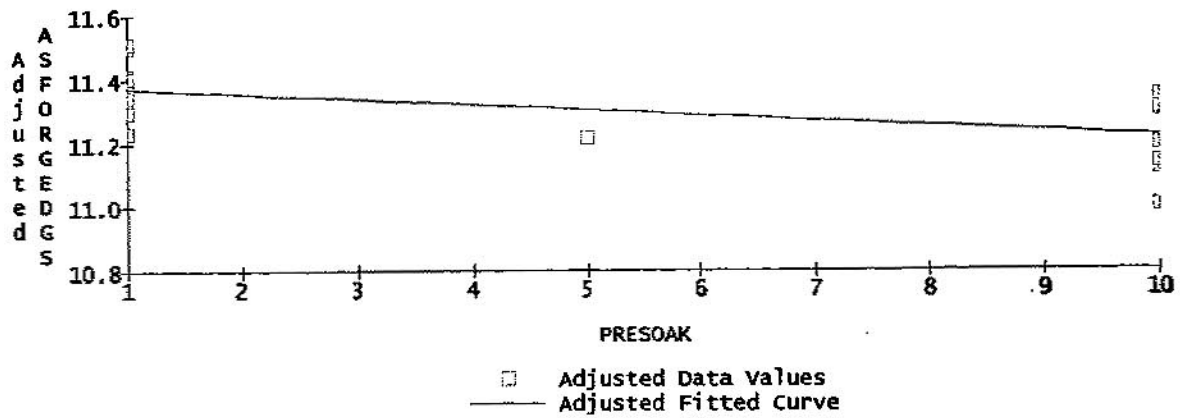


Appendix A-3U (cont.)

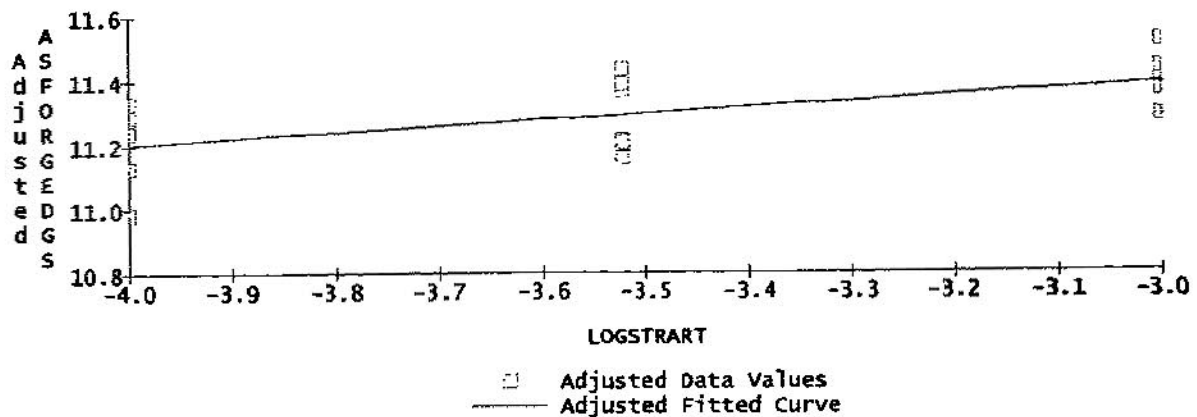
ASFORGEDGS vs TEMP, Adjusted for Remaining Predictors
Using Mulreg @EXPT@MULREG, Model DESIGN_AUTO_AFGS



ASFORGEDGS vs PRESOAK, Adjusted for Remaining Predictors
Using Mulreg @EXPT@MULREG, Model DESIGN_AUTO_AFGS

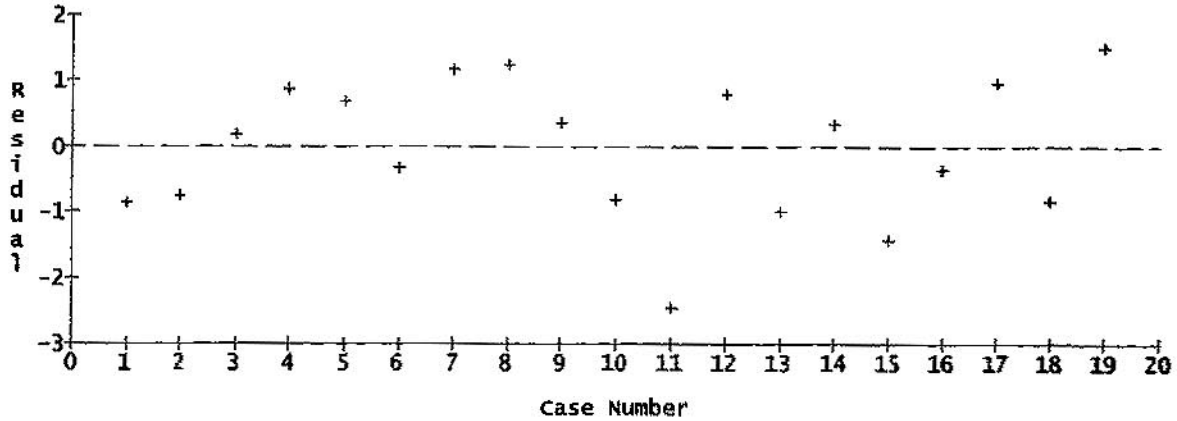


ASFORGEDGS vs LOGSTRART, Adjusted for Remaining Predictors
Using Mulreg @EXPT@MULREG, Model DESIGN_AUTO_AFGS

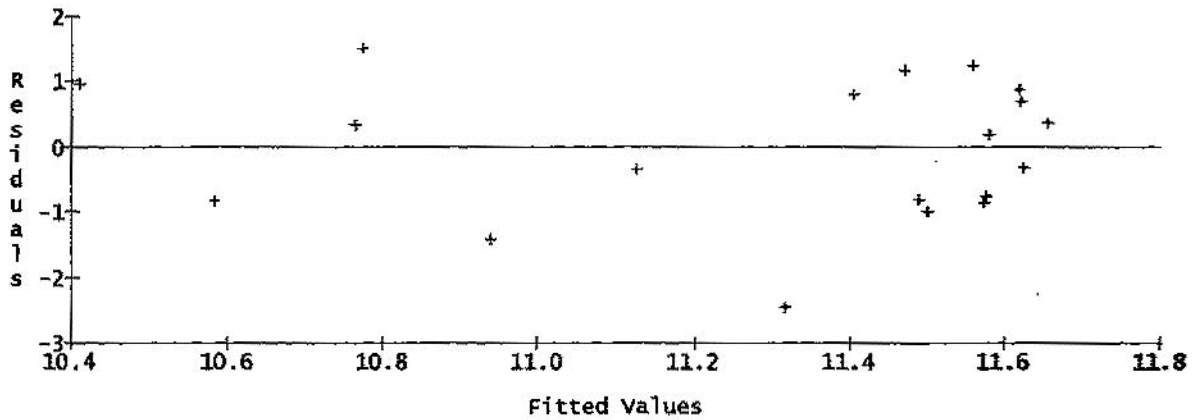


Appendix A-3U (cont.)

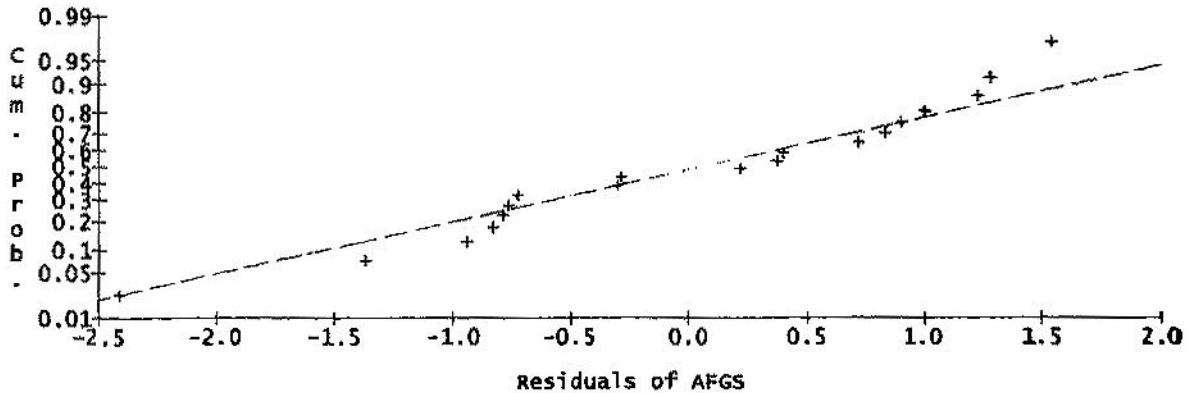
Case Order Graph of Residuals of AFGS
Using Studentized Residuals in Model DESIGN_AUTO_AFGS



Residuals of AFGS vs Fitted Values
Using Studentized Residuals in Model DESIGN_AUTO_AFGS

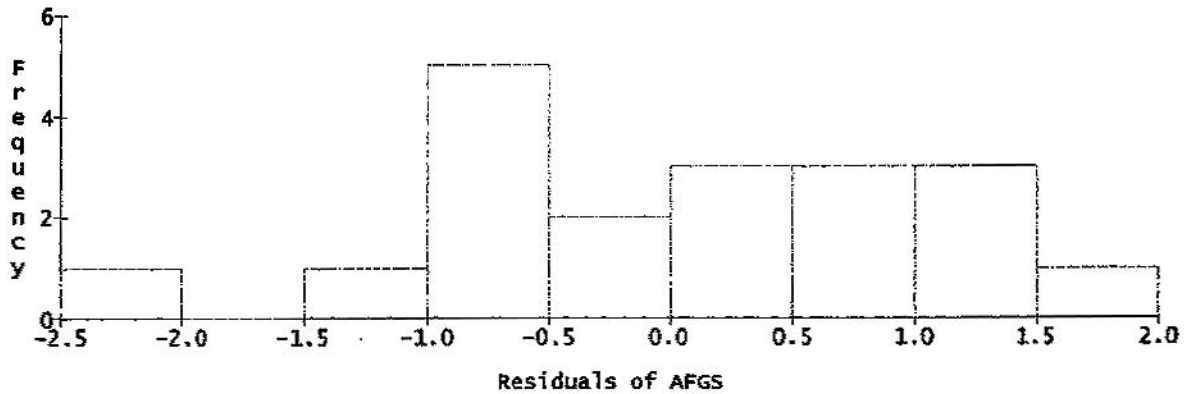


Normal Probability Plot of Residuals of AFGS
Using Studentized Residuals in Model DESIGN_AUTO_AFGS
(Sample size = 19)



Appendix A-3U (cont.)

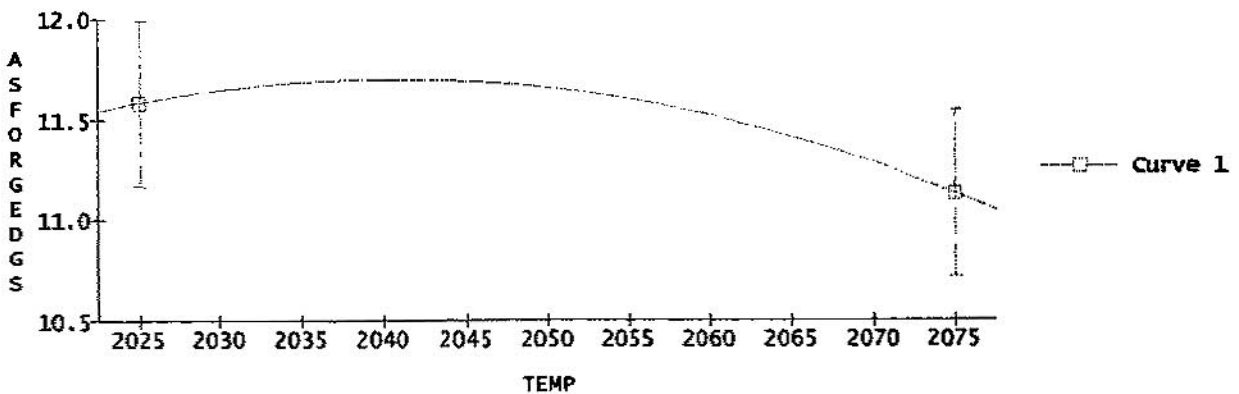
Histogram of Residuals of AFGS
Using Studentized Residuals in Model DESIGN_AUTO_AFGS
(Sample size = 19)



0 Factor, Response or Formula	1 Range	2 Initial Setting	3 Optimal Value
1 Factors			
2 TEMP	2025 to 2075	2050	2040.3
3 PRESOAK	1 to 10	5.5	1.002
4 LOGSTART	-4 to -3	-3.5	-3.001
5			
6 Responses			
7 ASFORGEDGS	MAX		11.698
8 LOGSTRESS			0.39439

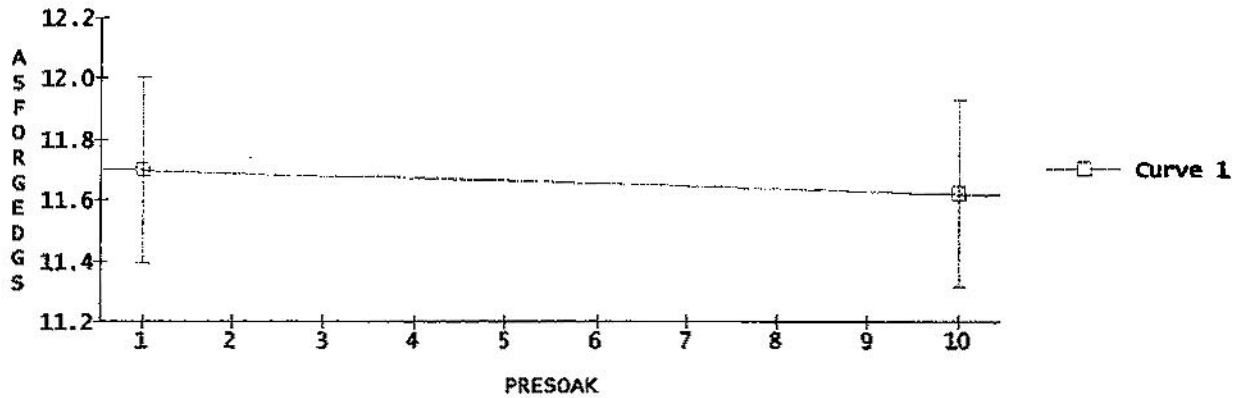
converged to a tolerance of 0.00012 after 45 steps.

Predictions and 95% simultaneous confidence intervals
for mean responses of ASFORGEDGS using model DESIGN_AUTO_AFGS
 $P = 1.002$, $LSR = -3.001$

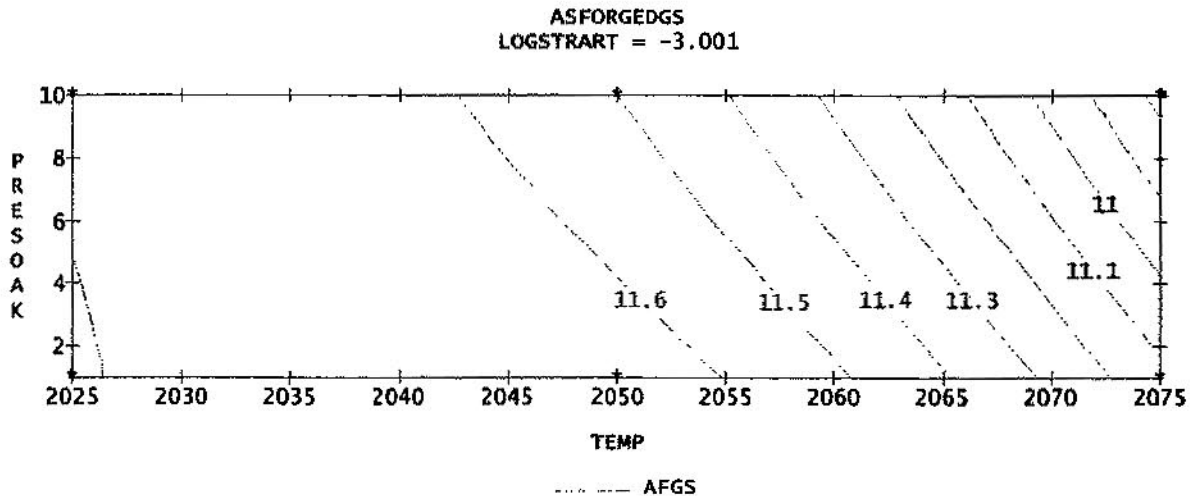
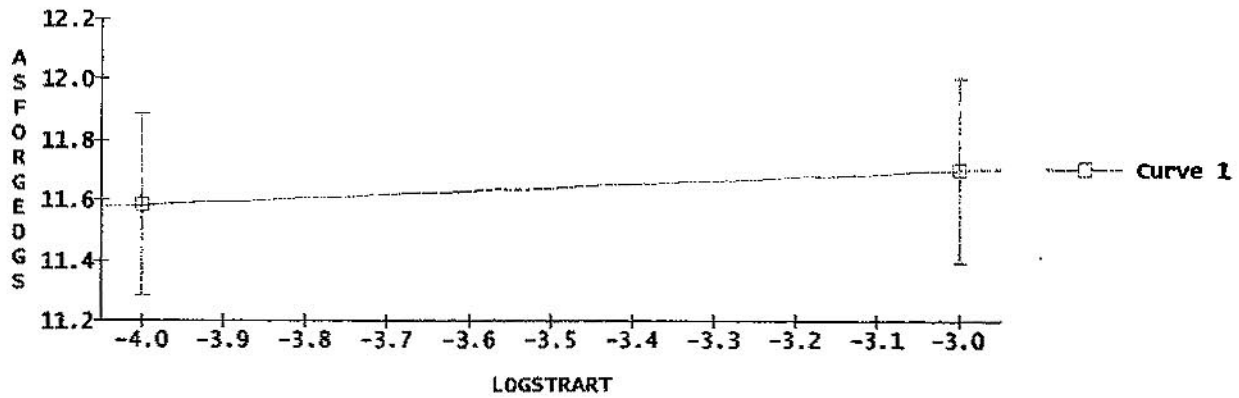


Appendix A-3U (cont.)

Predictions and 95% simultaneous confidence intervals
for mean responses of ASFORGEDGS using model DESIGN_AUTO_AFGS
LSR = -3.001, T = 2040.3

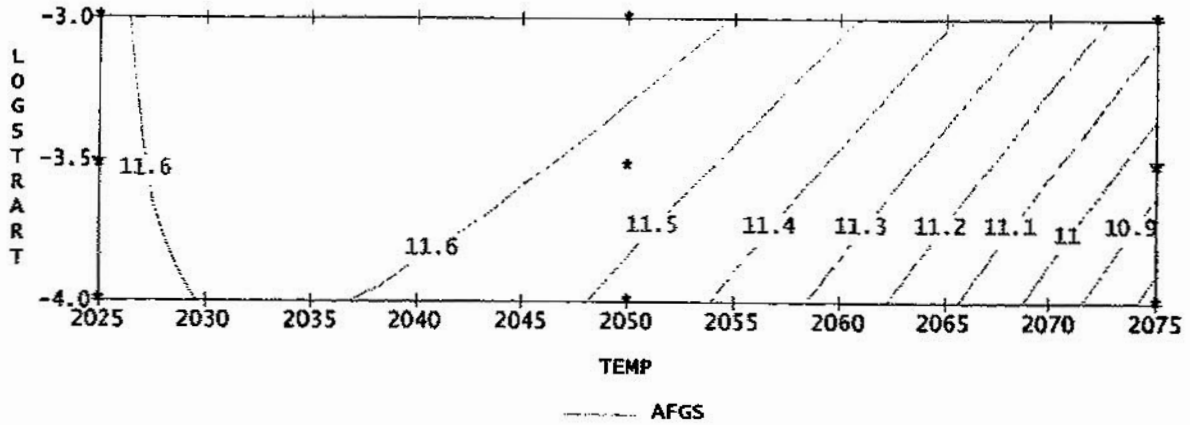


Predictions and 95% simultaneous confidence intervals
for mean responses of ASFORGEDGS using model DESIGN_AUTO_AFGS
T = 2040.3, P = 1.002

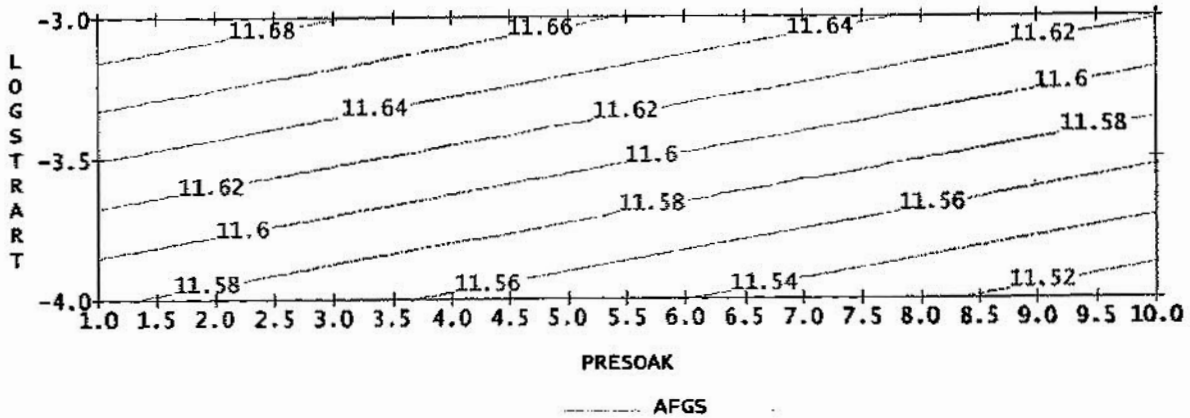


Appendix A-3U (cont.)

ASFORGEDGS
PRESOAK = 1.002



ASFORGEDGS
TEMP = 2040.3



Predictions and 95% simultaneous confidence intervals
for mean responses of ASFORGEDGS using model DESIGN_AUTO_AFGS
LSR = -3

P	T=2025
5	Lower 11.249138
	Predicted 11.600705
	Upper 11.952272

Appendix A-4C

Least Squares Coefficients, Response AVG, Model DESIGN__AUTO__AVG

0 Term	1 Coeff.	2 Std. Error	3 T-value	4 Signif.	5 Transformed Term
1 1	3.577042	0.092453			
2 ~T	-1.008333	0.116332	-8.67	0.0001	((T-2.05e+03)/2.5e+01)
3 ~P	-0.325844	0.094954	-3.43	0.0034	((P-5.5)/4.5)

No. cases = 19 R-sq. = 0.8445 RMS Error = 0.403
 Resid. df = 16 R-sq-adj. = 0.8251 Cond. No. = 1.006
 ~ indicates factors are transformed.

TABLE:49296 3R x 5C

16-SEP-2000 21:12 Page 1

Least Squares Summary ANOVA, Response AVG Model DESIGN__AUTO__AVG

0 Source	1 df	2 Sum Sq.	3 Mean Sq.	4 F-Ratio	5 Signif.
1 Total(Corr.)	18	16.71158			
2 Regression	2	14.11321	7.05661	43.45	0.0000
3 Residual	16	2.59836	0.16240		

R-sq. = 0.8445
 R-sq-adj. = 0.8251

Model obeys hierarchy. The sum of squares for each term is computed assuming higher order terms are first removed.

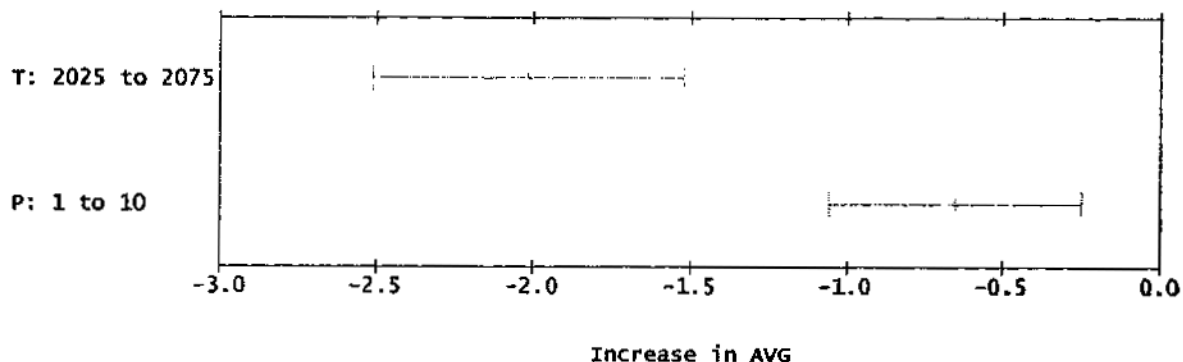
Least Squares Components ANOVA, Response AVG Model DESIGN__AUTO__AVG

0 Source	1 df	2 Sum Sq.	3 Mean Sq.	4 F-Ratio	5 Signif.	6 Transformed Term
1 Constant	1	243.36842				
2 ~T	1	12.20083	12.20083	75.13	0.0000	((T-2.05e+03)/2.5e+01)
3 ~P	1	1.91238	1.91238	11.78	0.0034	((P-5.5)/4.5)
4 Residual	16	2.59836	0.16240			

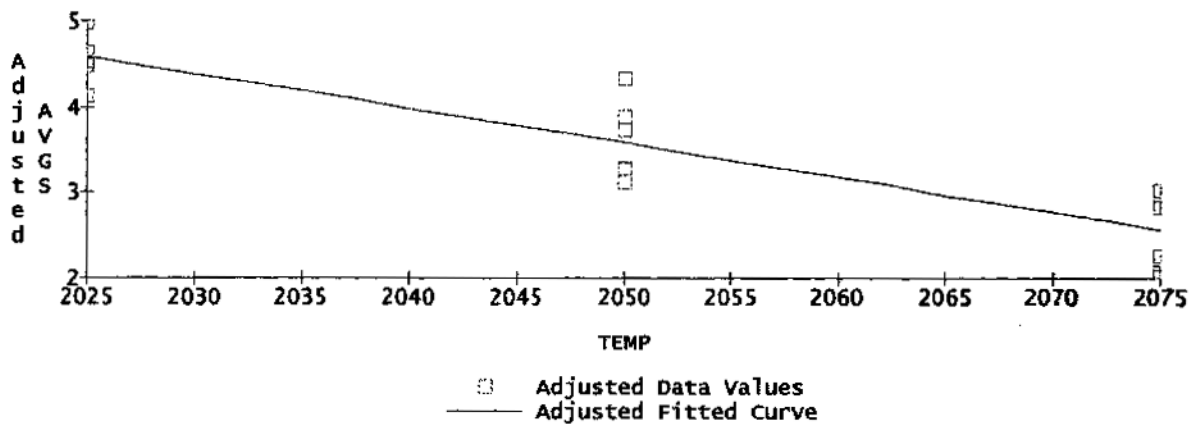
~ indicates factors are transformed. R-sq. = 0.8445
 R-sq-adj. = 0.8251
 Default sum of squares.
 Model obeys hierarchy. The sum of squares for each term is computed assuming higher order terms are first removed.

Appendix A-4C (cont.)

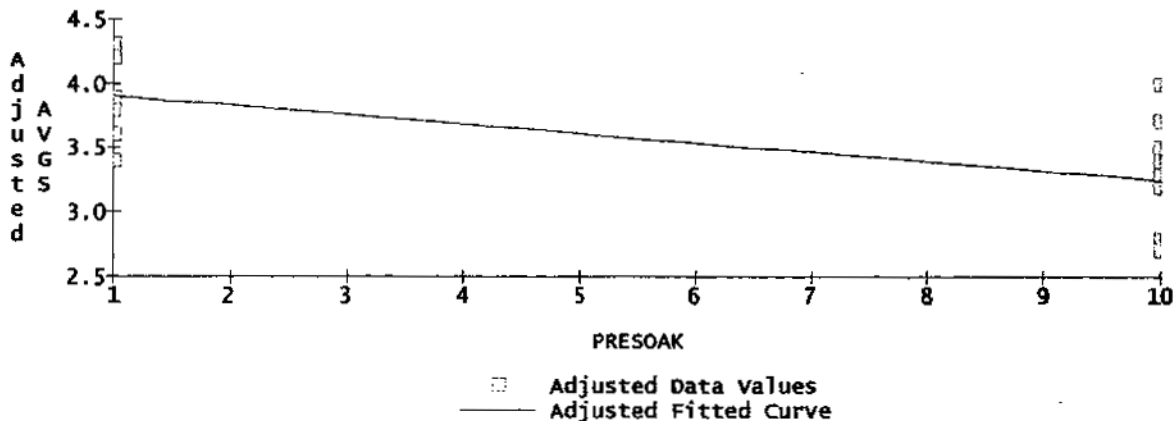
Mulreg @EXPT@MULREG, Model DESIGN_AUTO_AVG
 Main Effects on Response AVGS
 (with 95% confidence Intervals)



AVGS vs TEMP, Adjusted for Remaining Predictors
 Using Mulreg @EXPT@MULREG, Model DESIGN_AUTO_AVG

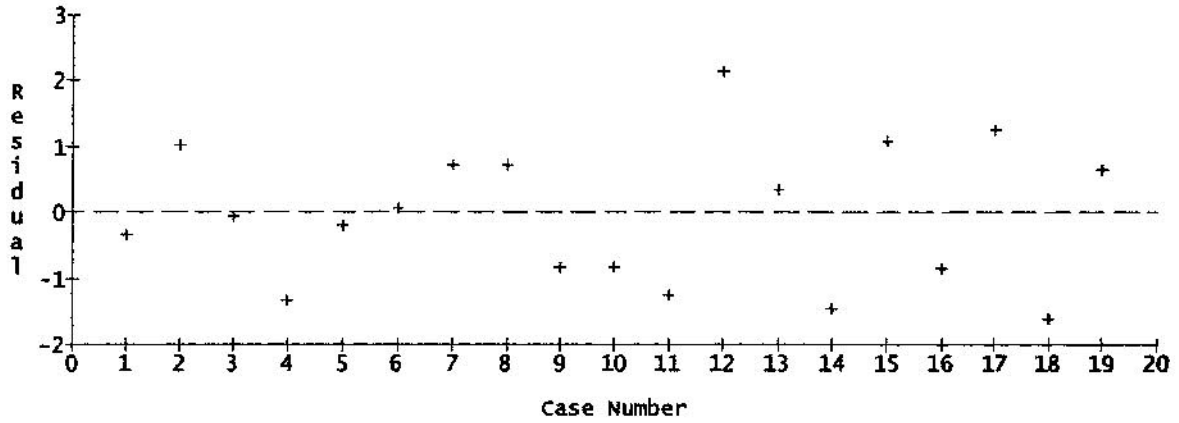


AVGS vs PRESOAK, Adjusted for Remaining Predictors
 Using Mulreg @EXPT@MULREG, Model DESIGN_AUTO_AVG

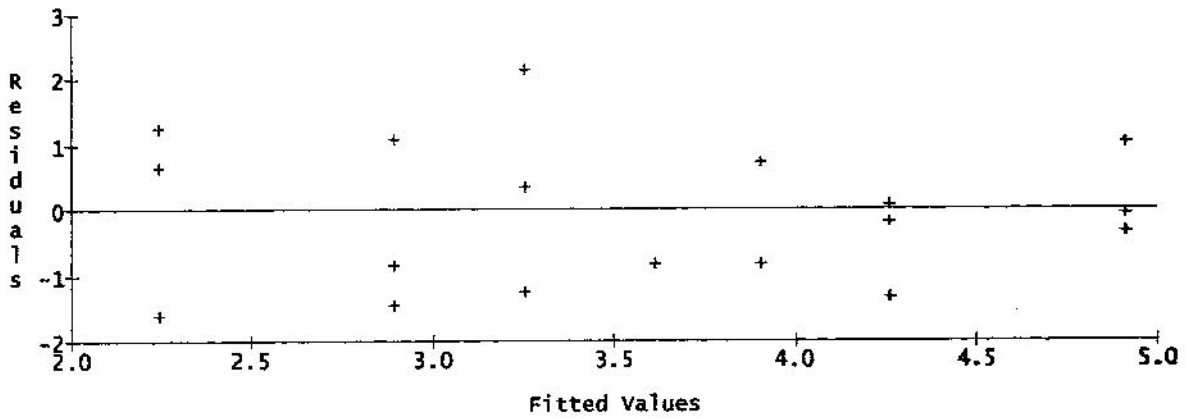


Appendix A-4C (cont.)

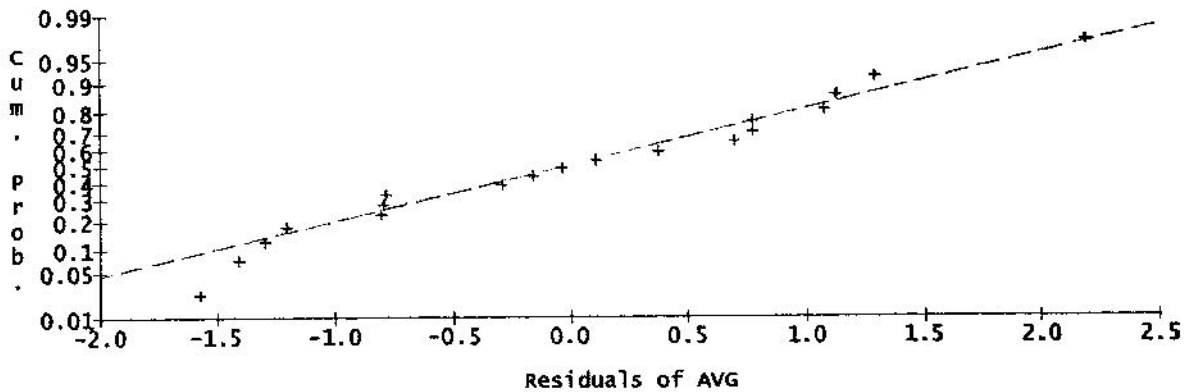
Case Order Graph of Residuals of AVG
Using Studentized Residuals in Model DESIGN_AUTO_AVG



Residuals of AVG vs Fitted Values
Using Studentized Residuals in Model DESIGN_AUTO_AVG

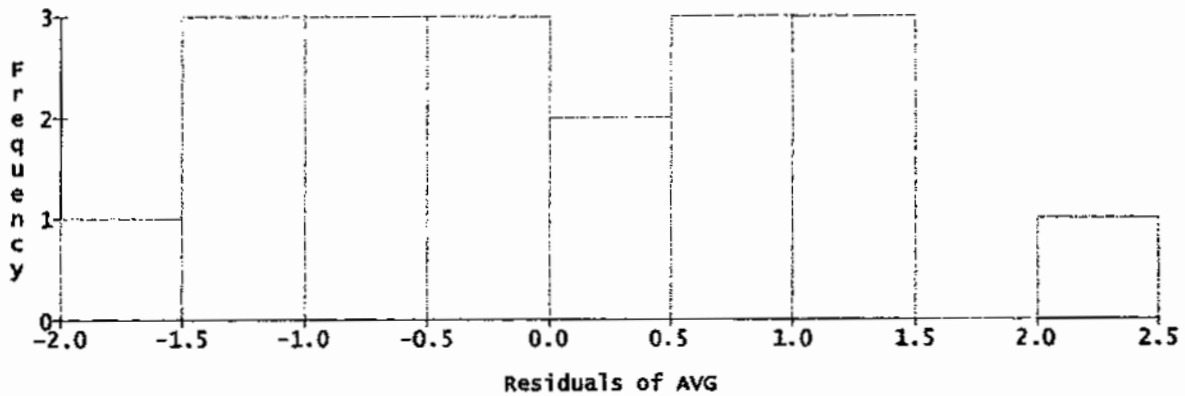


Normal Probability Plot of Residuals of AVG
Using Studentized Residuals in Model DESIGN_AUTO_AVG
(Sample size = 19)



Appendix A-4C (cont.)

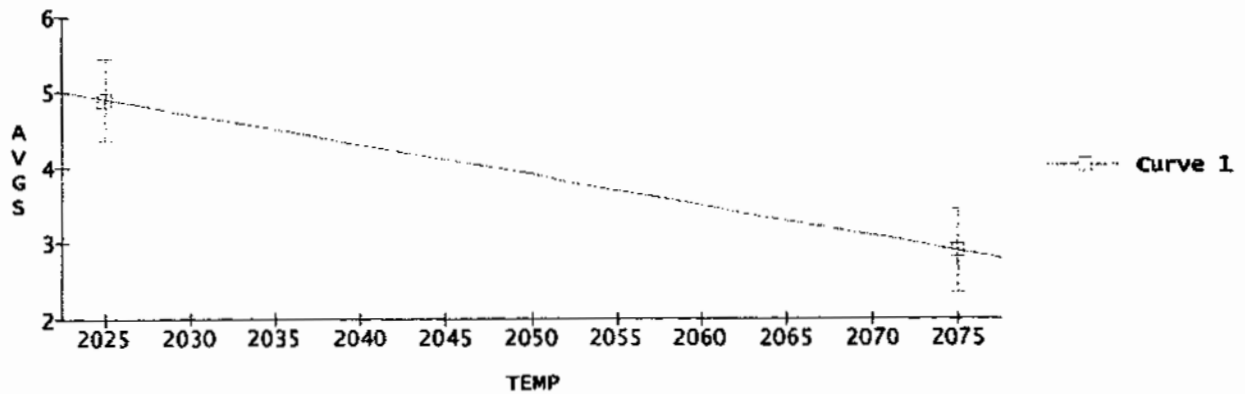
Histogram of Residuals of AVG
Using Studentized Residuals in Model DESIGN_AUTO_AVG
(Sample size = 19)



0 Factor, Response or Formula	1 Range	2 Initial Setting	3 optimal Value
1 Factors			
2 TEMP	2025 to 2075	2050	2025
3 PRESOAK	1 to 10	5.5	1.0065
4			
5 Responses			
6 AVGS	MAX		4.9106

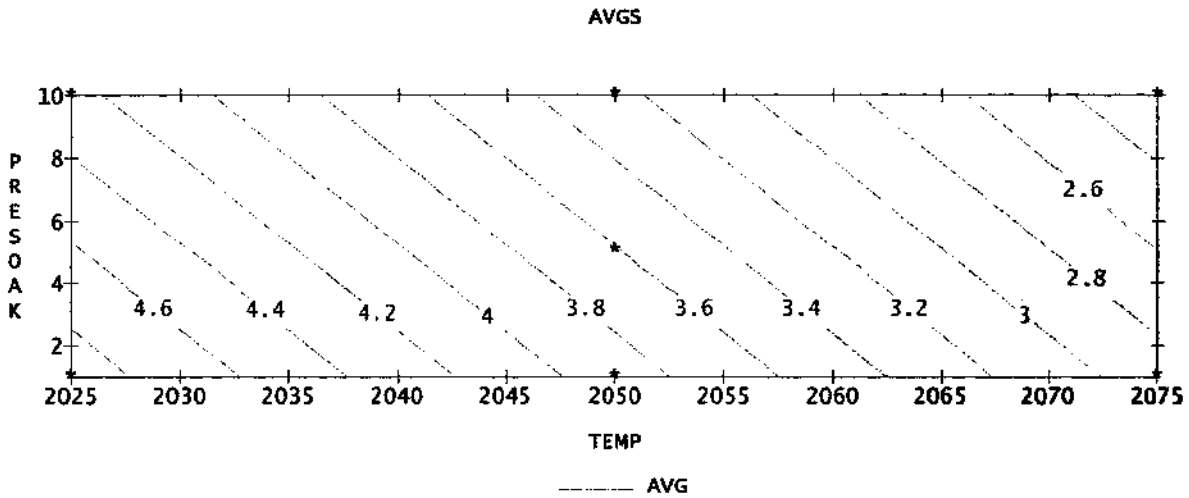
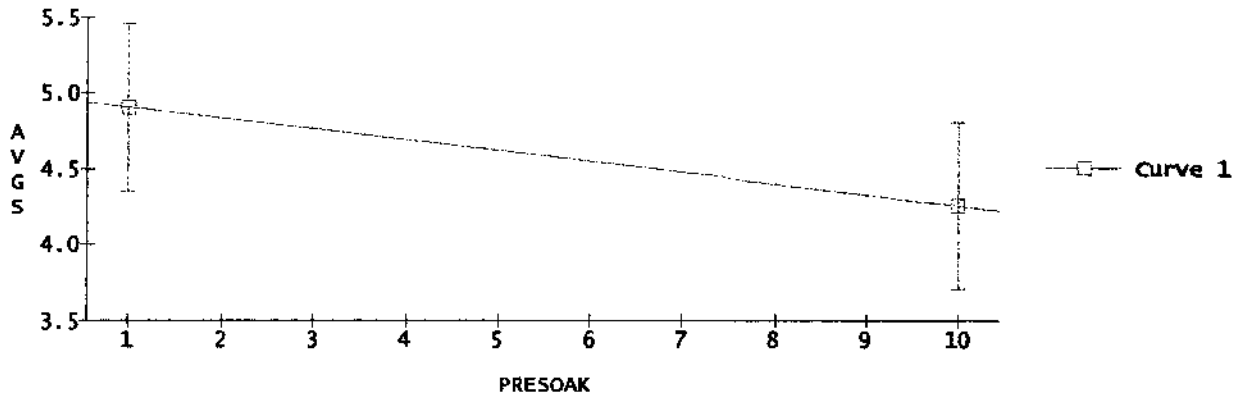
Converged to a tolerance of 0.00036 after 39 steps.

Predictions and 95% simultaneous confidence intervals
for mean responses of AVGS using model DESIGN_AUTO_AVG
P = 1.0065



Appendix A-4C (cont.)

Predictions and 95% simultaneous confidence intervals
for mean responses of AVGS using model DESIGN_AUTO_AVG
T = 2025

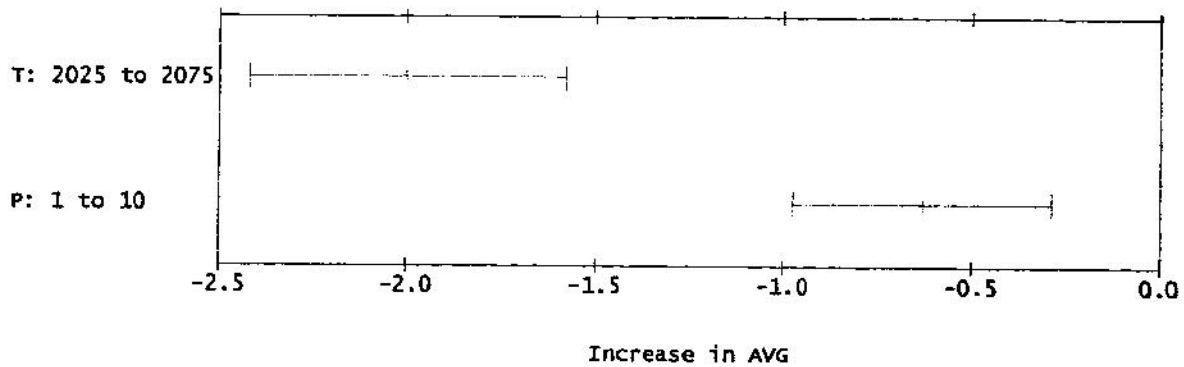


Predictions and 95% simultaneous confidence intervals
for mean responses of AVGS using model DESIGN_AUTO_AVG

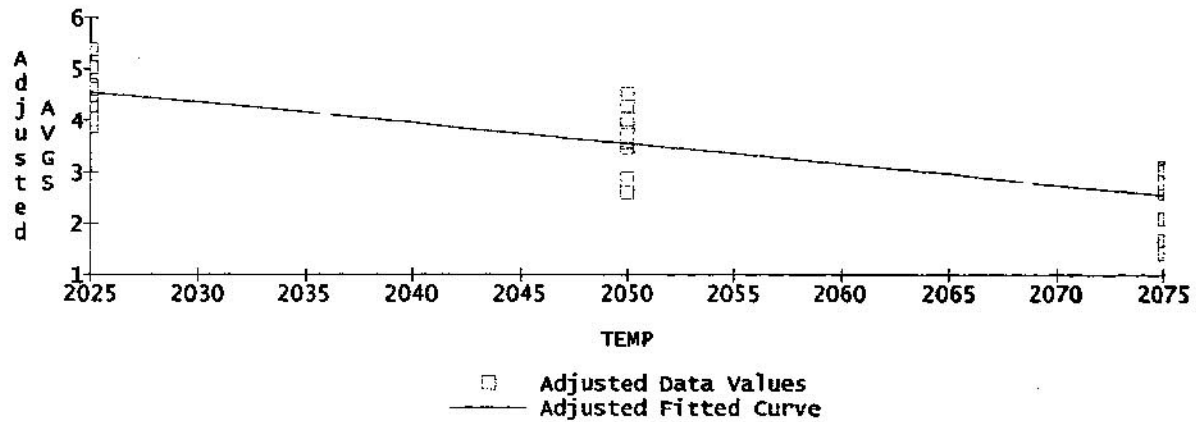
P	T=2025
5	Lower 4.157342 Predicted 4.621580 Upper 5.085819

Appendix A-4U (cont.)

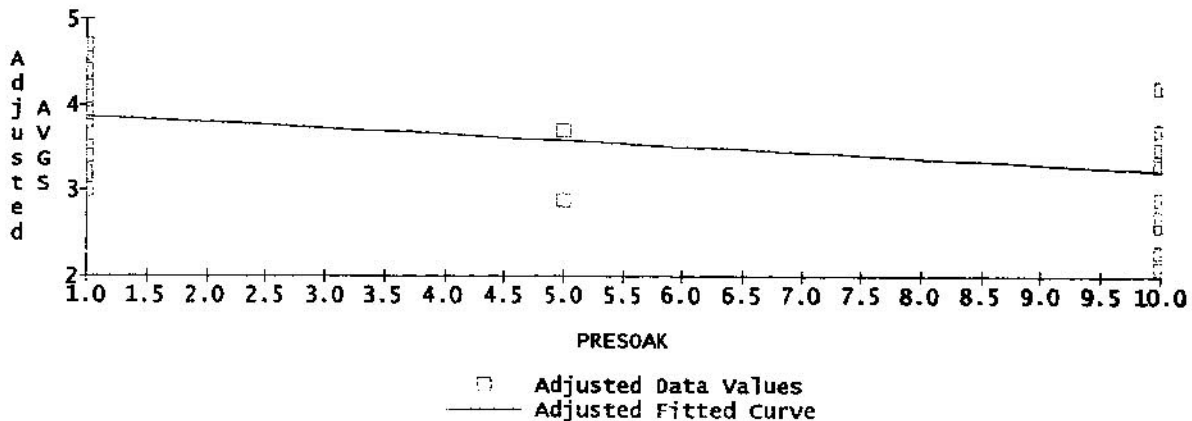
Mulreg @EXPT@MULREG, Model DESIGN_AUTO_AVG
 Main Effects on Response AVGS
 (with 95% Confidence Intervals)



AVGS vs TEMP, Adjusted for Remaining Predictors
 Using Mulreg @EXPT@MULREG, Model DESIGN_AUTO_AVG

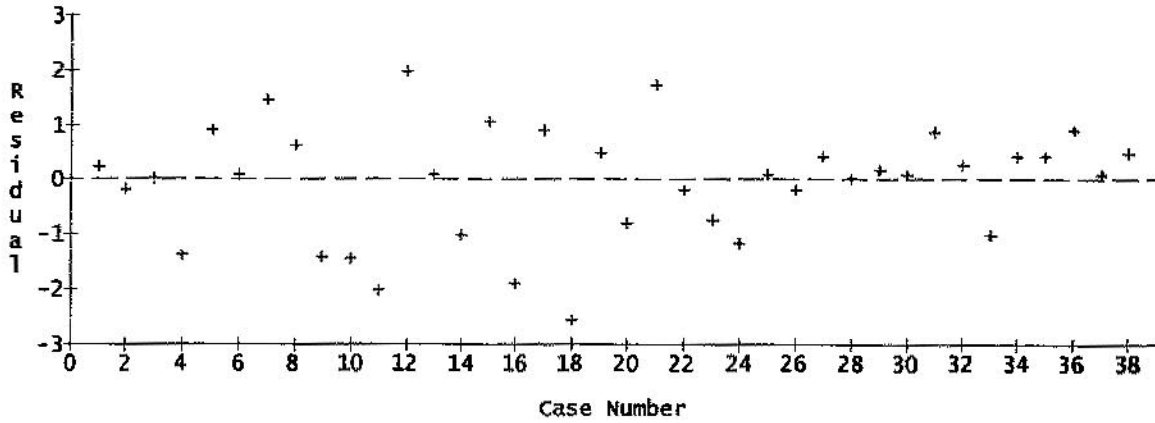


AVGS vs PRESOAK, Adjusted for Remaining Predictors
 Using Mulreg @EXPT@MULREG, Model DESIGN_AUTO_AVG

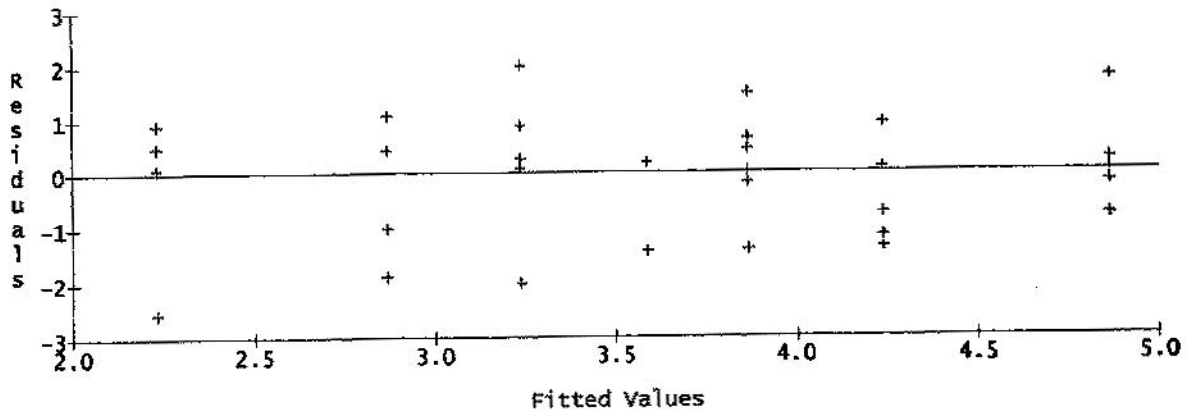


Appendix A-4U (cont.)

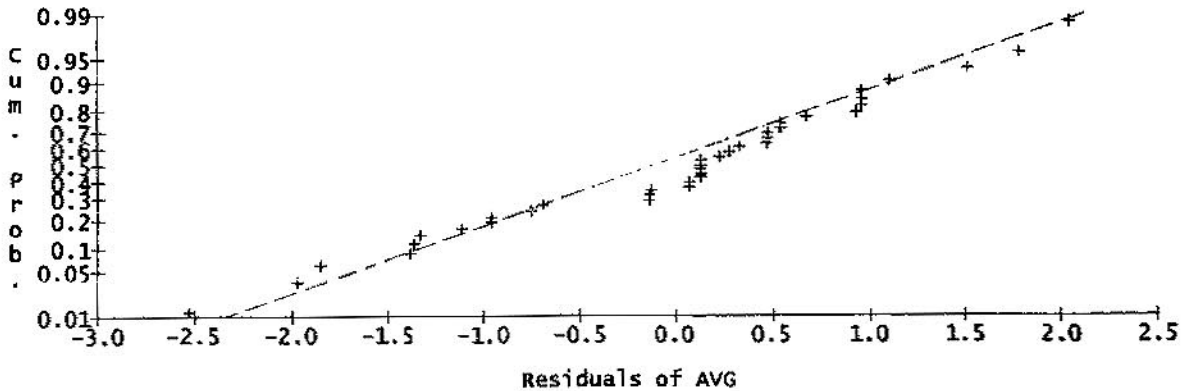
Case Order Graph of Residuals of AVG
Using Studentized Residuals in Model DESIGN_AUTO_AVG



Residuals of AVG vs Fitted Values
Using studentized Residuals in Model DESIGN_AUTO_AVG

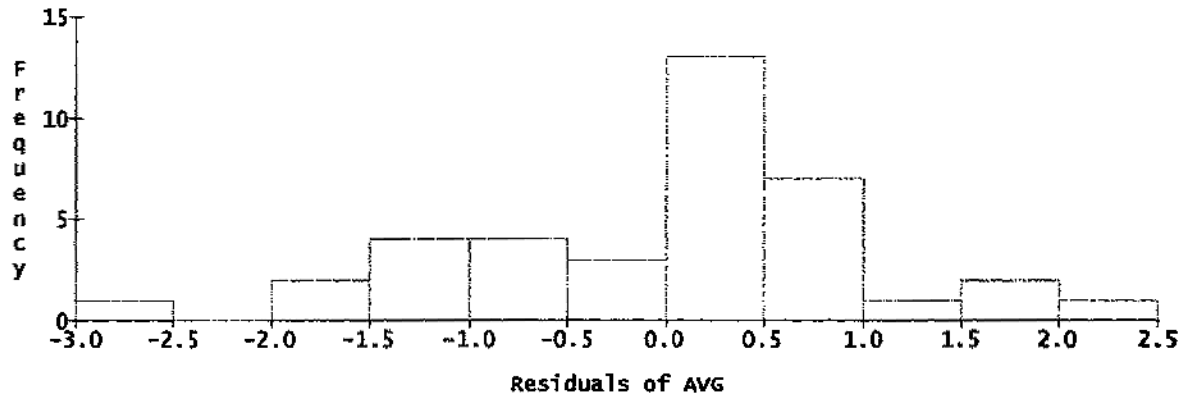


Normal Probability Plot of Residuals of AVG
Using Studentized Residuals in Model DESIGN_AUTO_AVG
(Sample size = 38)



Appendix A-4U (cont.)

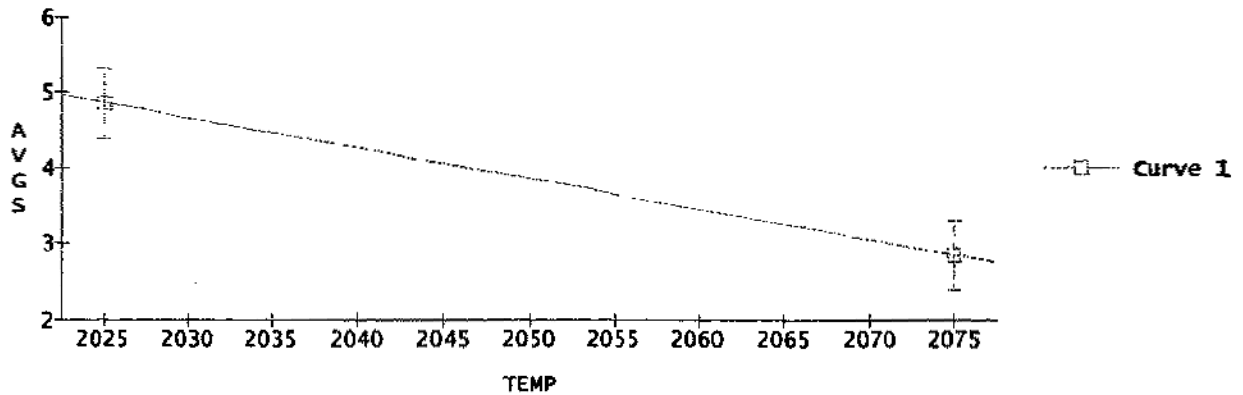
Histogram of Residuals of AVG
Using Studentized Residuals in Model DESIGN_AUTO_AVG
(Sample size = 38)



0 Factor, Response or Formula	1 Range	2 Initial Setting	3 Optimal Value
1 Factors			
2 TEMP	2025 to 2075	2050	2025.1
3 PRESOAK	1 to 10	5.5	1.0088
4			
5 Responses			
6 AVGS	MAX		4.8616

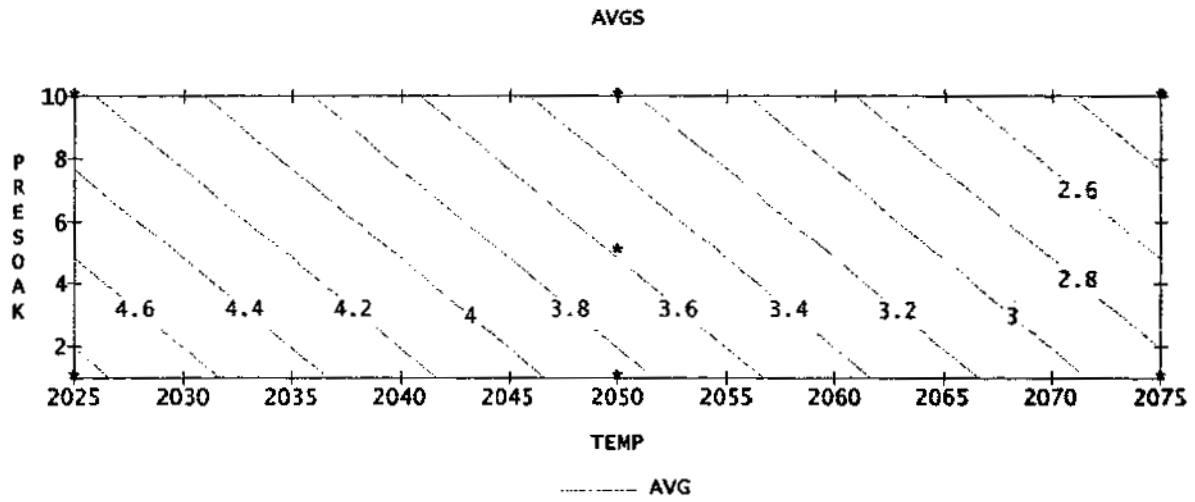
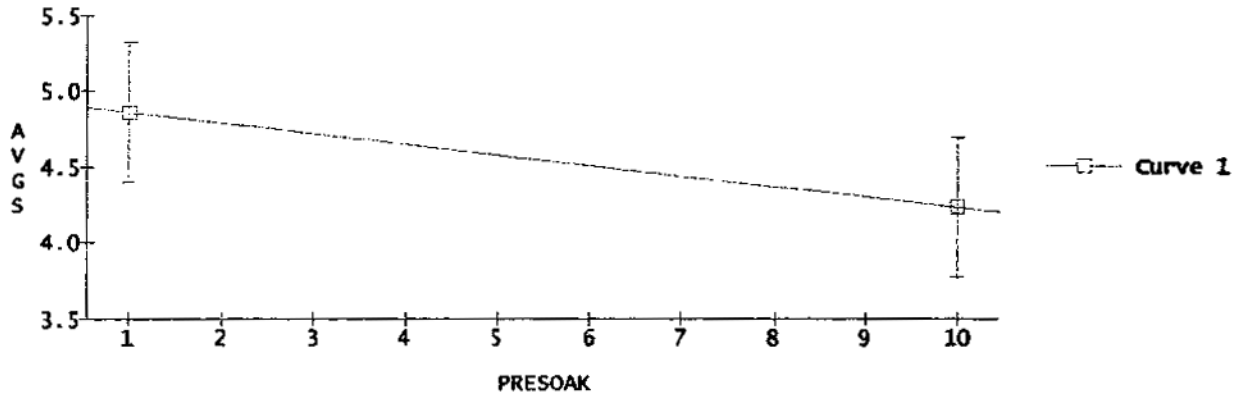
Converged to a tolerance of 0.00046 after 29 steps.

Predictions and 95% simultaneous confidence intervals
for mean responses of AVGS using model DESIGN_AUTO_AVG
P = 1.0088



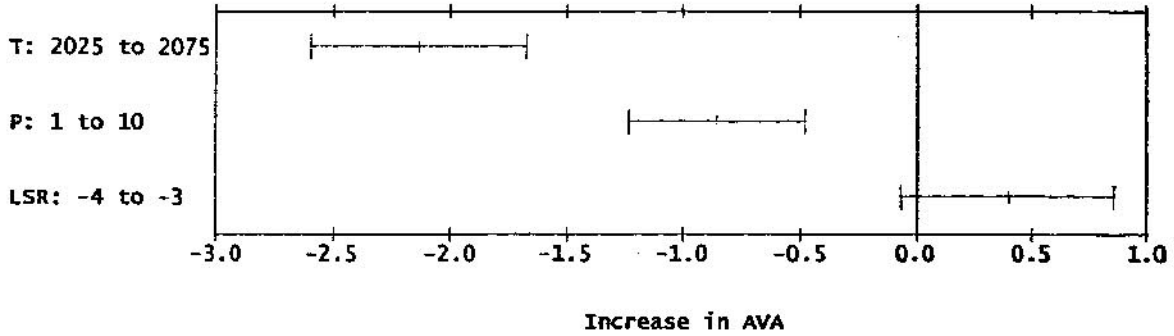
Appendix A-4U (cont.)

Predictions and 95% simultaneous confidence intervals
for mean responses of AVGS using model DESIGN_AUTO_AVG
T = 2025.1

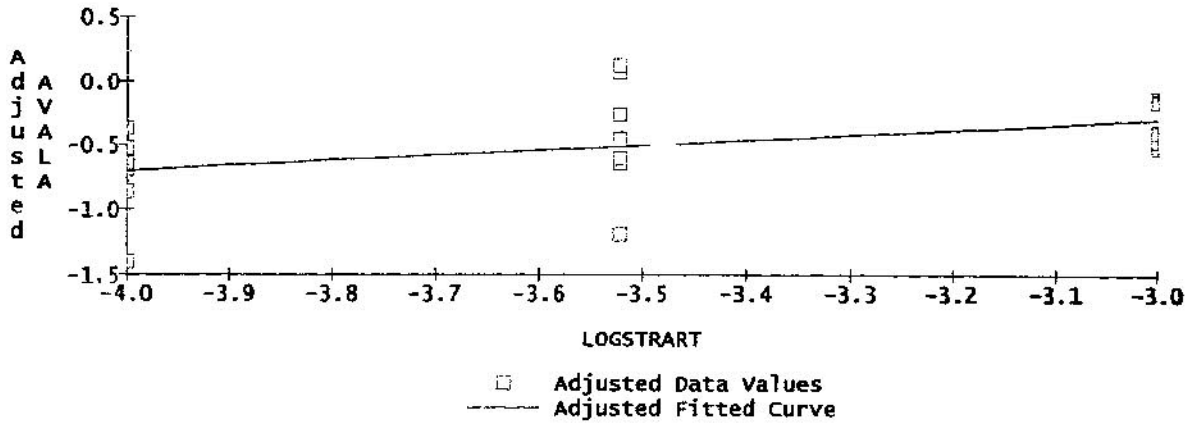


Appendix A-5C (cont.)

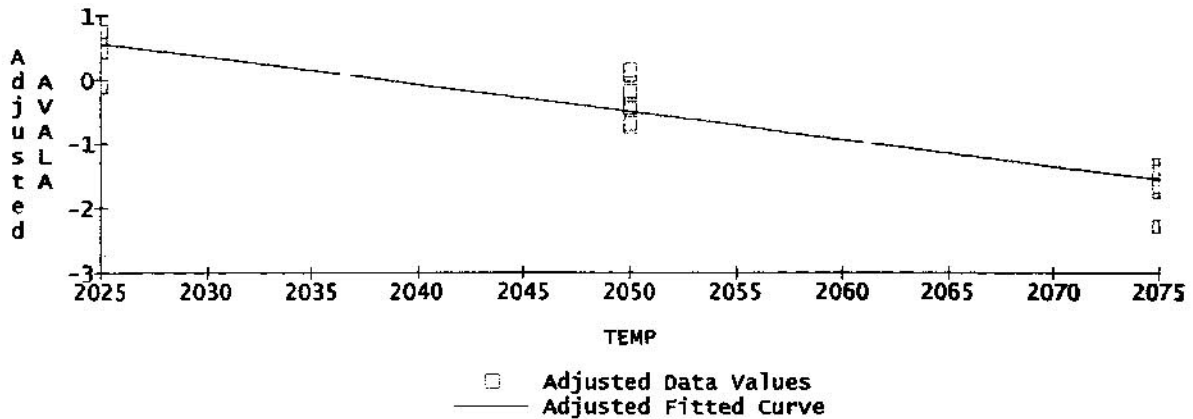
Mulreg @EXPT@MULREG, Model DESIGN_AUTO_AVA
 Main Effects on Response AVALA
 (with 95% Confidence Intervals)



AVALA vs LOGSTRART, Adjusted for Remaining Predictors
 Using Mulreg @EXPT@MULREG, Model DESIGN_AUTO_AVA

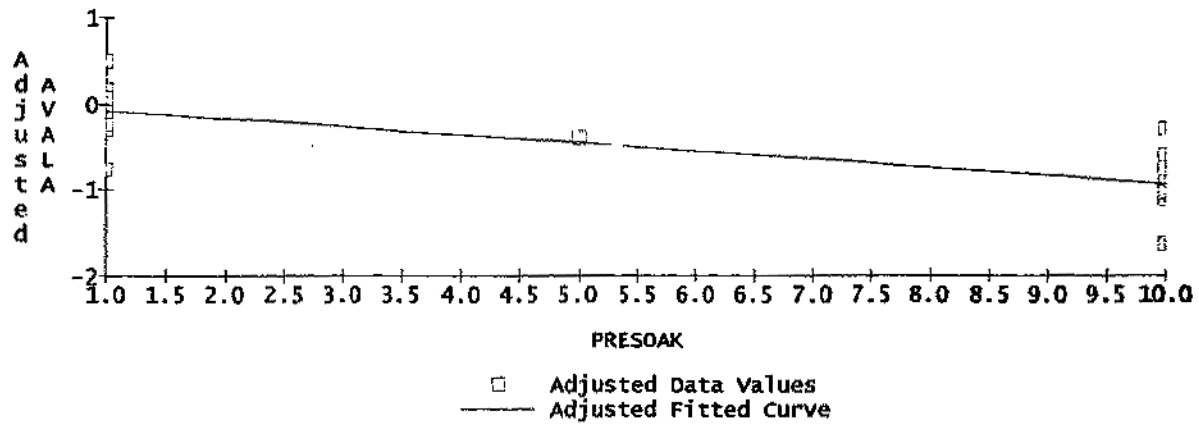


AVALA vs TEMP, Adjusted for Remaining Predictors
 Using Mulreg @EXPT@MULREG, Model DESIGN_AUTO_AVA

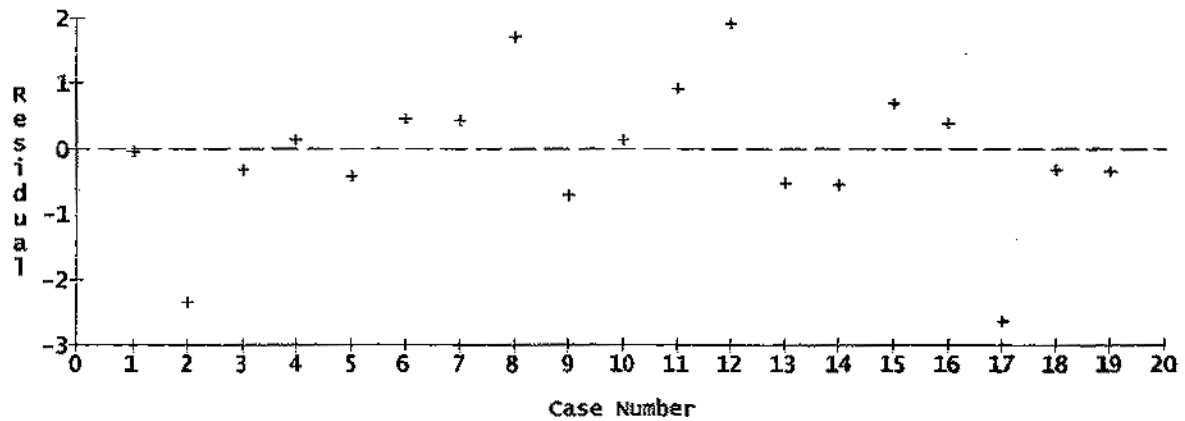


Appendix A-5C (cont.)

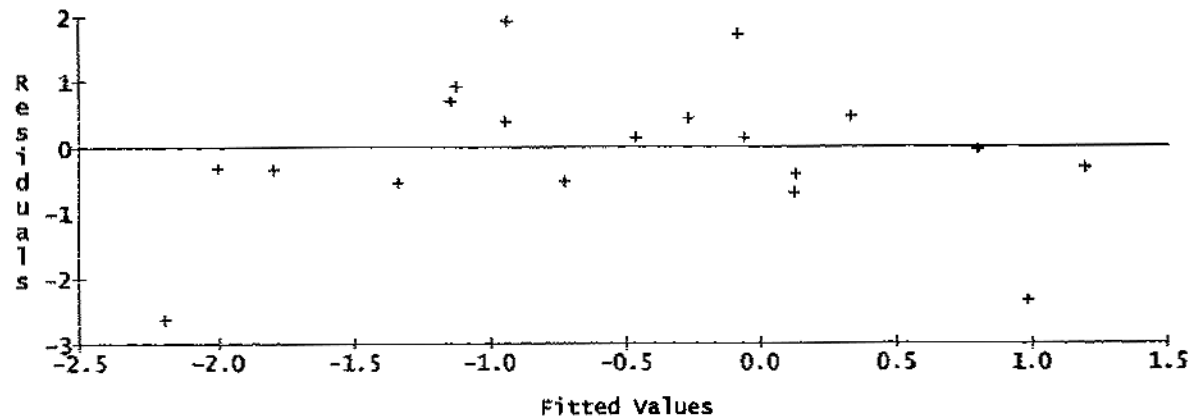
AVALA vs PRESOAK, Adjusted for Remaining Predictors
Using Mulreg @EXPT@MULREG, Model DESIGN_AUTO_AVA



Case Order Graph of Residuals of AVALA
Using Studentized Residuals in Model DESIGN_AUTO_AVA

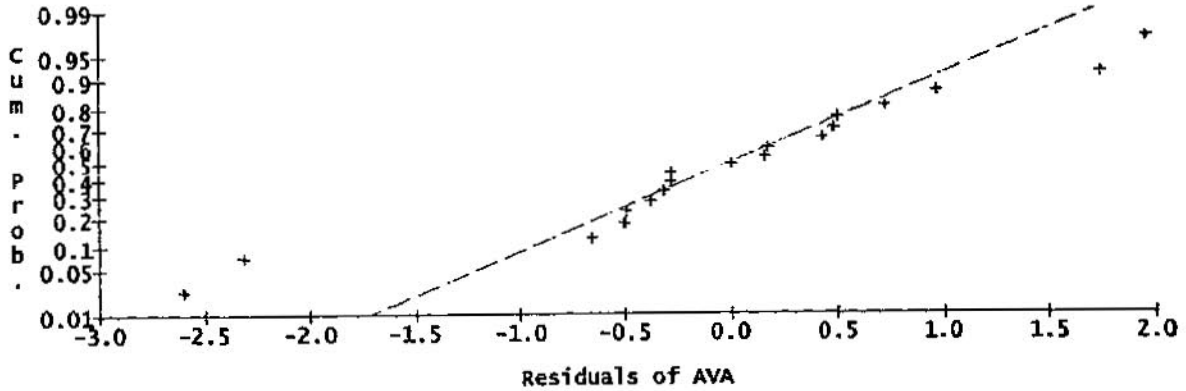


Residuals of AVALA vs Fitted Values
Using Studentized Residuals in Model DESIGN_AUTO_AVA

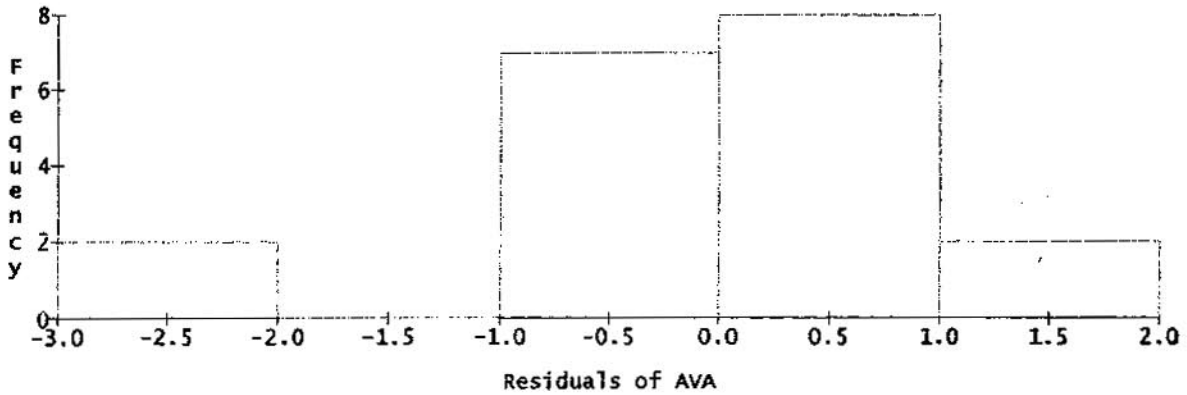


Appendix A-5C (cont.)

Normal Probability Plot of Residuals of AVA
Using Studentized Residuals in Model DESIGN_AUTO_AVA
(Sample size = 19)



Histogram of Residuals of AVA
Using Studentized Residuals in Model DESIGN_AUTO_AVA
(Sample size = 19)



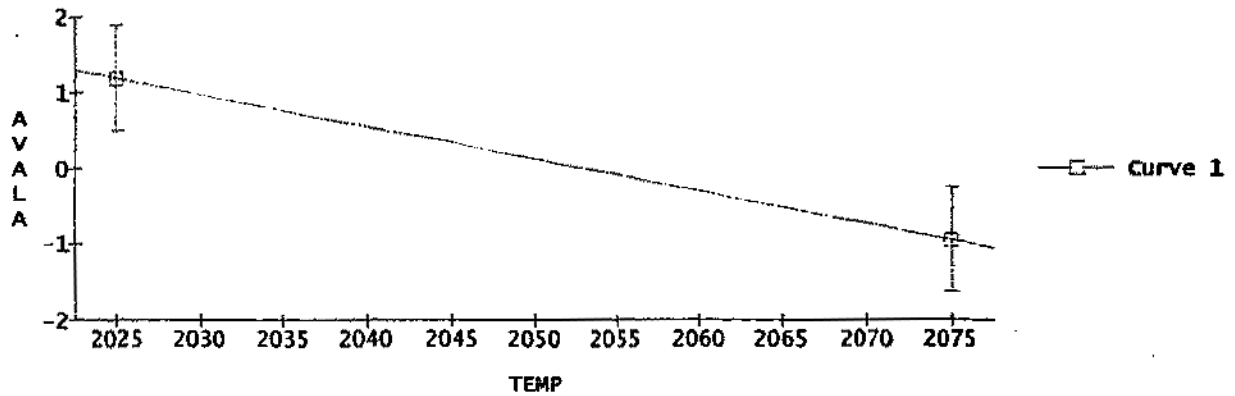
0 Factor, Response or Formula	1 Range	2 Initial Setting	3 Optimal Value

1 Factors			
2 TEMP	2025 TO 2075	2050	2025
3 PRESOAK	1 TO 10	5.5	1.0001
4 LOGSTRART	-4 TO -3	-3.5	-3.0015
5			
6 Responses			
7 AVALA	MAX		1.1916

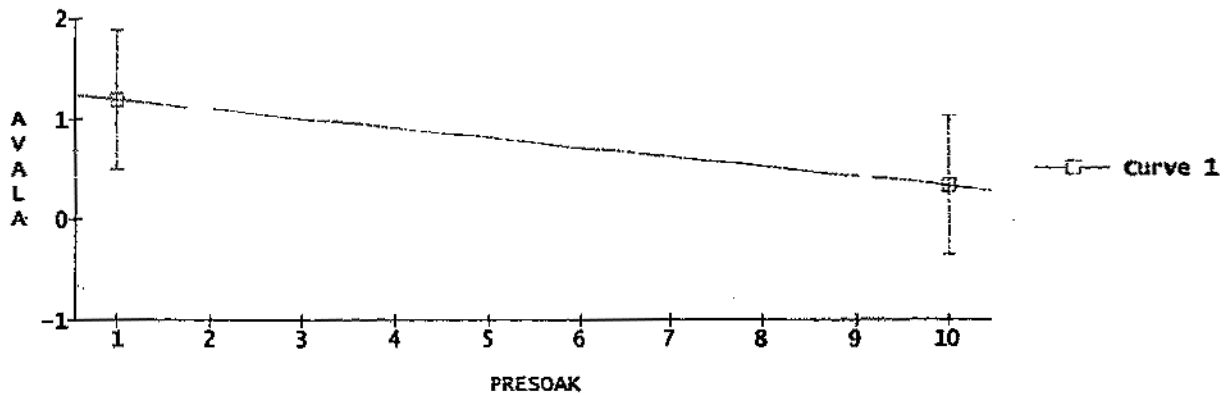
Converged to a tolerance of 0.0004 after 65 steps.

Appendix A-5C (cont.)

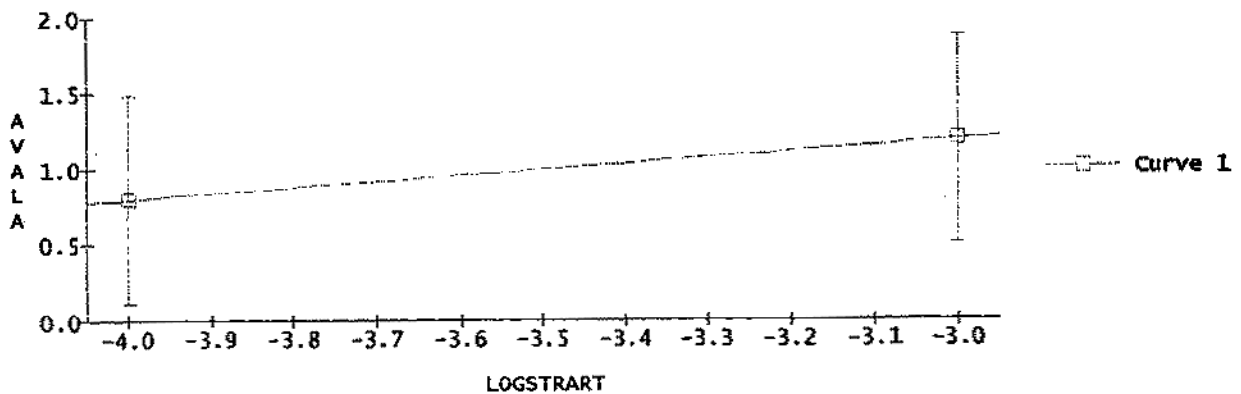
Predictions and 95% simultaneous confidence intervals
for mean responses of AVALA using model DESIGN_AUTO_AVA
P = 1.0001, LSR = -3.0015



Predictions and 95% simultaneous confidence intervals
for mean responses of AVALA using model DESIGN_AUTO_AVA
LSR = -3.0015, T = 2025

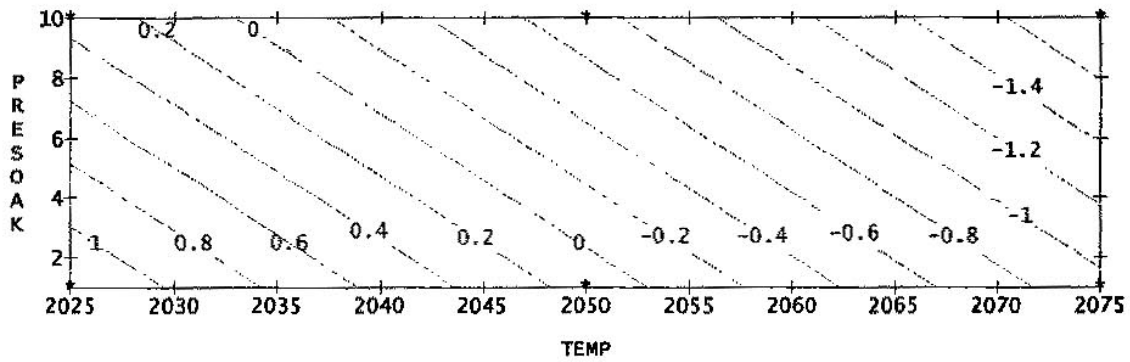


Predictions and 95% simultaneous confidence intervals
for mean responses of AVALA using model DESIGN_AUTO_AVA
T = 2025, P = 1.0001

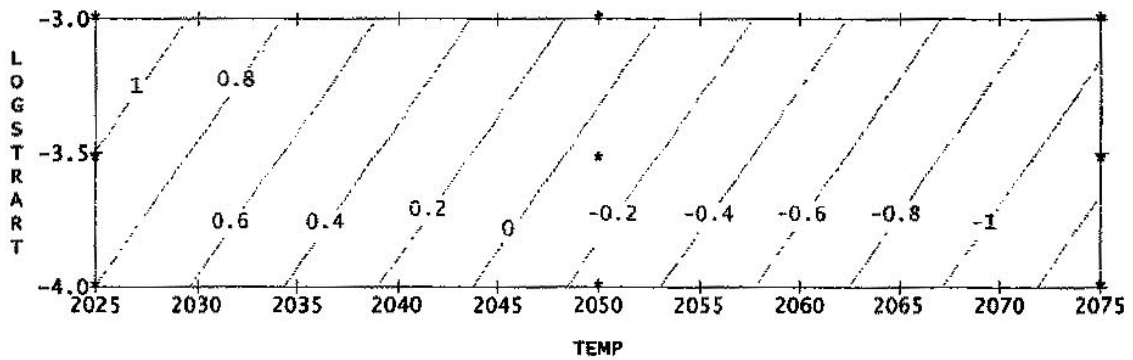


Appendix A-5C (cont.)

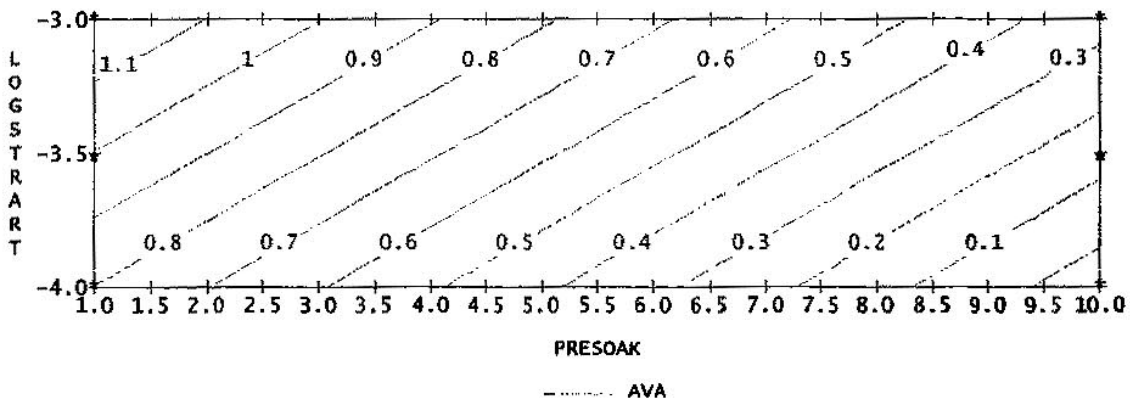
AVALA
LOGSTRART = -3.0015



AVALA
PRESOAK = 1.0001



AVALA
TEMP = 2025



Predictions and 95% simultaneous confidence intervals
for mean responses of AVALA using model DESIGN_AUTO_AVA
LSR = -3

P	T=2025
Lower	0.193091
5 Predicted	0.812742
Upper	1.432393

Appendix A-5U

Least Squares Coefficients, Response AVA, Model DESIGN_AUTO_AVA

0 Term	1 Coeff.	2 Std. Error	3 T-value	4 Signif.	5 Transformed Term
1 1	-0.496379	0.066884			
2 ~T	-1.062500	0.084141			((T-2.05e+03)/2.5e+01)
3 ~P	-0.425361	0.068678			((P-5.5)/4.5)
4 ~LSR	0.206261	0.084108	2.45	0.0197	((LSR+3.5)/5e-01)
5 ~T*P	-0.179167	0.084141	-2.13	0.0408	((T-2.05e+03)/2.5e+01)*((P-5.5)/4.5)

No. cases = 38 R-sq. = 0.8633 RMS Error = 0.4122
 Resid. df = 33 R-sq-adj. = 0.8467 Cond. No. = 1.022
 ~ indicates factors are transformed.

Least Squares Summary ANOVA, Response AVA Model DESIGN_AUTO_AVA

0 Source	1 df	2 Sum Sq.	3 Mean Sq.	4 F-Ratio	5 Signif.
1 Total(Corr.)	37	41.00974			
2 Regression	4	35.40267	8.85067	52.09	0.0000
3 Linear	3	34.63225	11.54408	67.94	0.0000
4 Non-linear	1	0.77042	0.77042	4.53	0.0408
5 Residual	33	5.60707	0.16991		

R-sq. = 0.8633

R-sq-adj. = 0.8467

Model obeys hierarchy. The sum of squares for each term is computed assuming higher order terms are first removed.

Least Squares Components ANOVA, Response AVA Model DESIGN_AUTO_AVA

0 Source	1 df	2 Sum Sq.	3 Mean Sq.	4 F-Ratio	5 Signif.	6 Transformed Term
1 Constant	1	9.40026				
2 ~T	1	27.09375	27.09375	159.50	0.0000	((T-2.05e+03)/2.5e+01)
3 ~P	1	6.51780	6.51780	38.36	0.0000	((P-5.5)/4.5)
4 ~LSR	1	1.02183	1.02183	6.01	0.0197	((LSR+3.5)/5e-01)
5 ~T*P	1	0.77042	0.77042	4.53	0.0408	((T-2.05e+03)/2.5e+01)*((P-5.5)/4.5)
6 Residual	33	5.60707	0.16991			

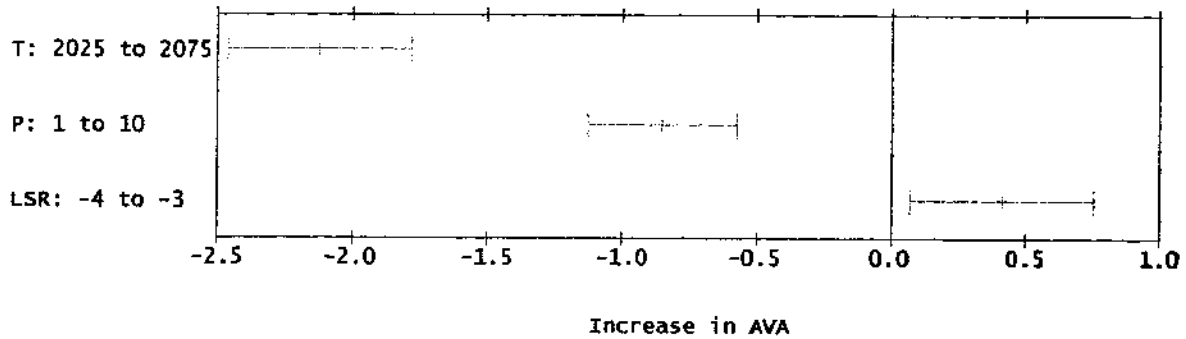
~ indicates factors are transformed. R-sq. = 0.8633
 R-sq-adj. = 0.8467

Default sum of squares.

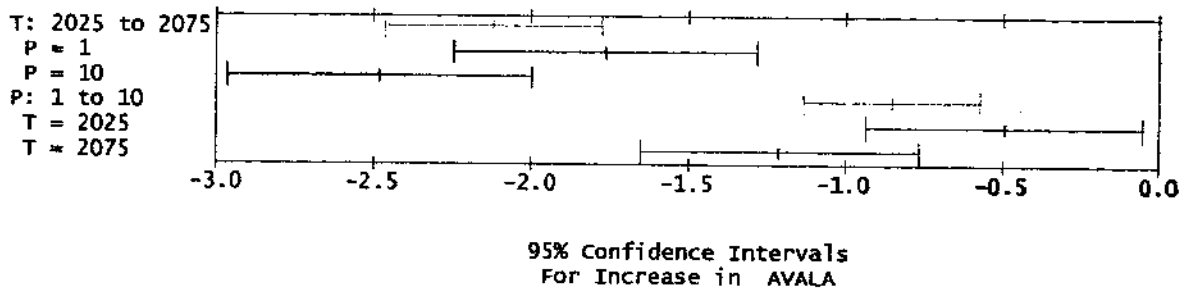
Model obeys hierarchy. The sum of squares for each term is computed assuming higher order terms are first removed.

Appendix A-5U (cont.)

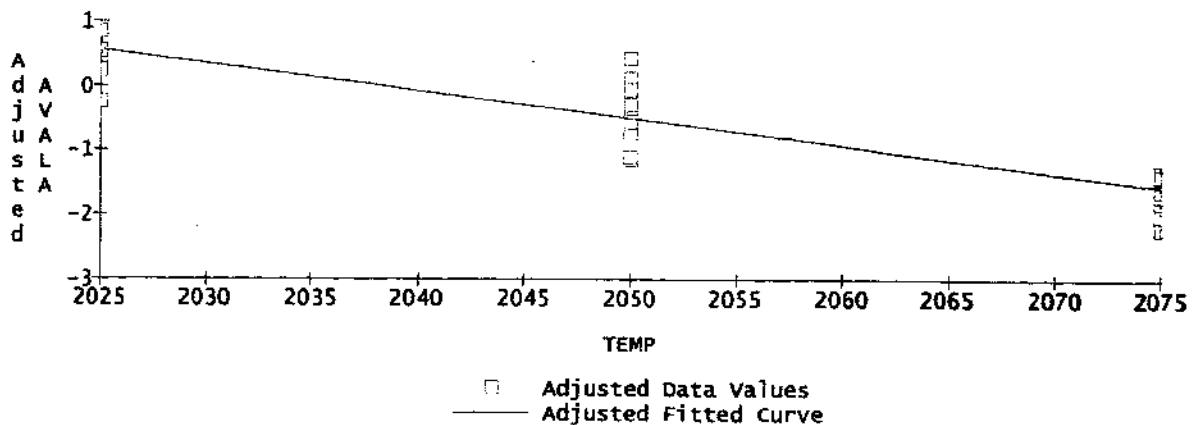
Mulreg @EXPT@MULREG, Model DESIGN_AUTO_AVA
Main Effects on Response AVALA
(with 95% Confidence Intervals)



Mulreg @EXPT@MULREG, Model DESIGN_AUTO_AVA
Interaction Effects of TEMP with PRESOAK
On Response AVALA

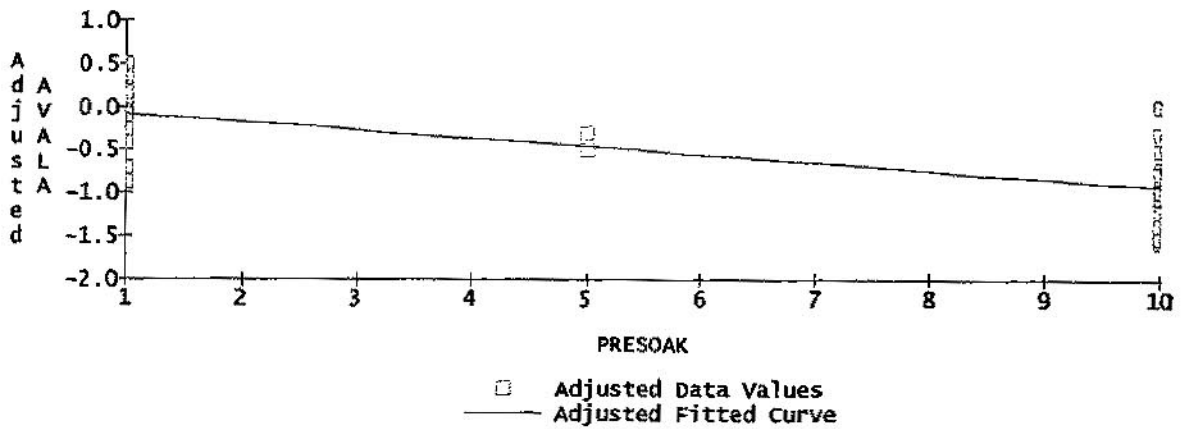


AVALA vs TEMP, Adjusted for Remaining Predictors
Using Mulreg @EXPT@MULREG, Model DESIGN_AUTO_AVA

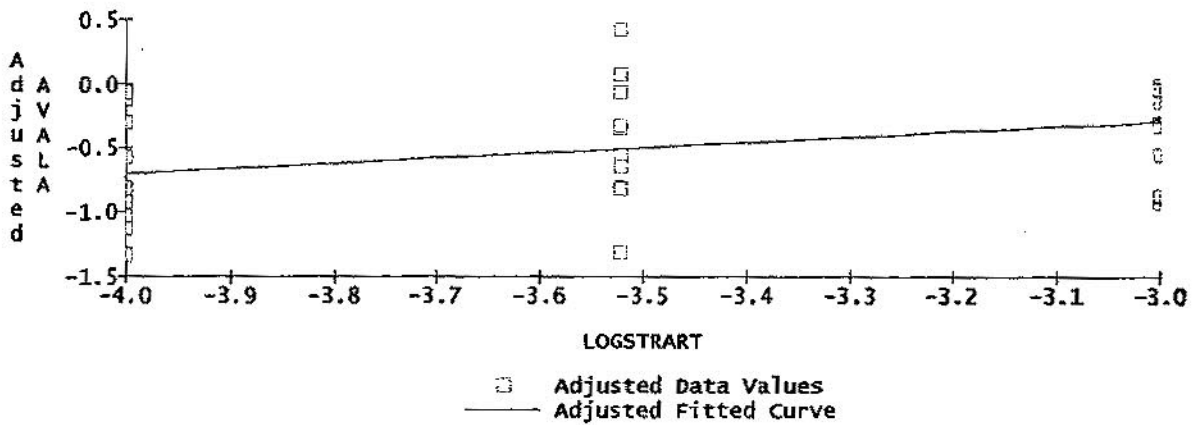


Appendix A-5U (cont.)

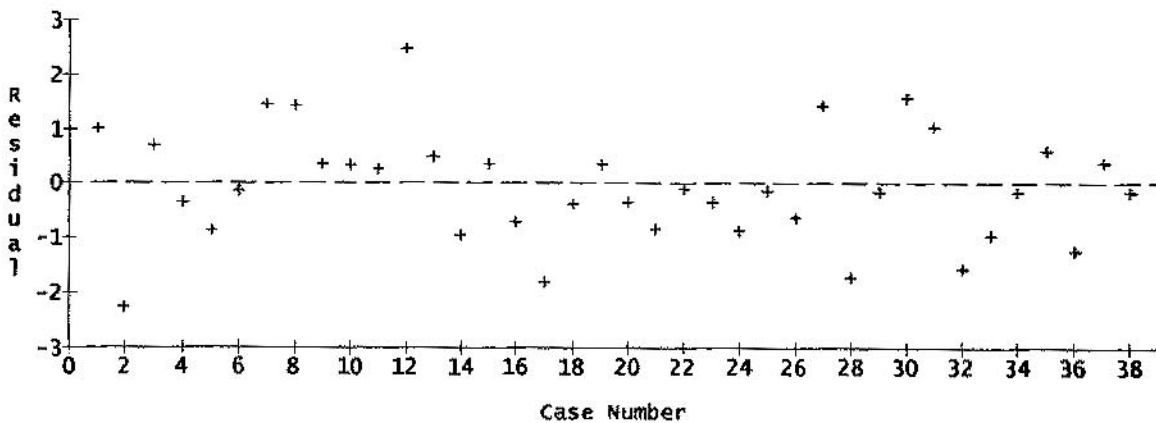
AVALA vs PRESOAK, Adjusted for Remaining Predictors
Using Mulreg @EXPT@MULREG, Model DESIGN_AUTO_AVA



AVALA vs LOGSTART, Adjusted for Remaining Predictors
Using Mulreg @EXPT@MULREG, Model DESIGN_AUTO_AVA

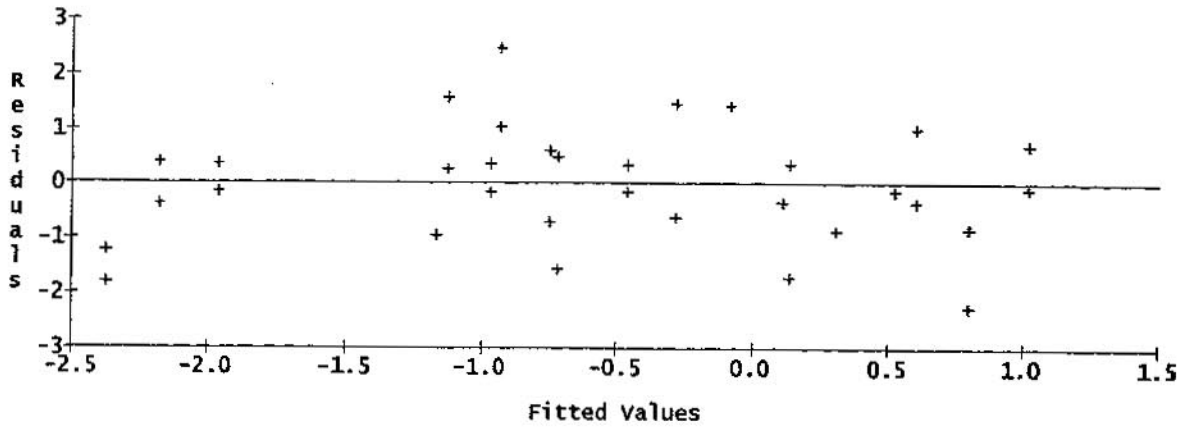


Case Order Graph of Residuals of AVA
Using Studentized Residuals in Model DESIGN_AUTO_AVA

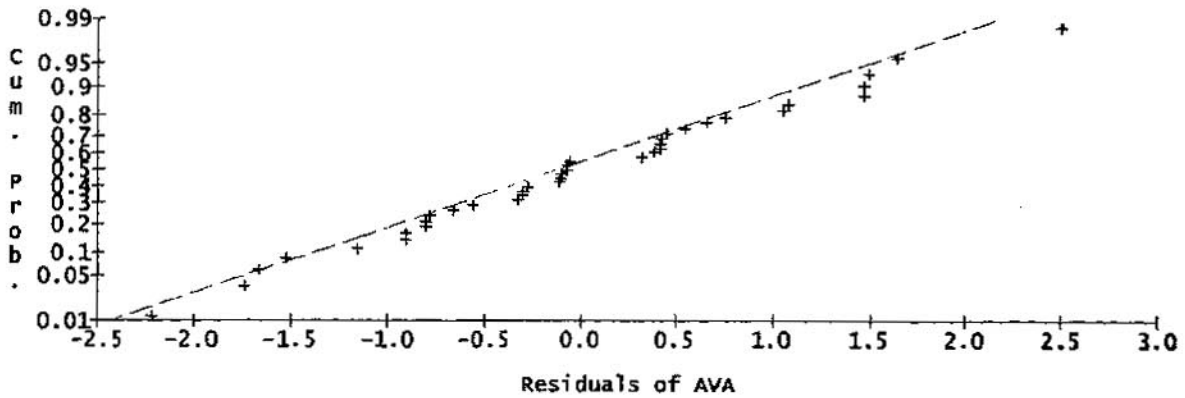


Appendix A-5U (cont.)

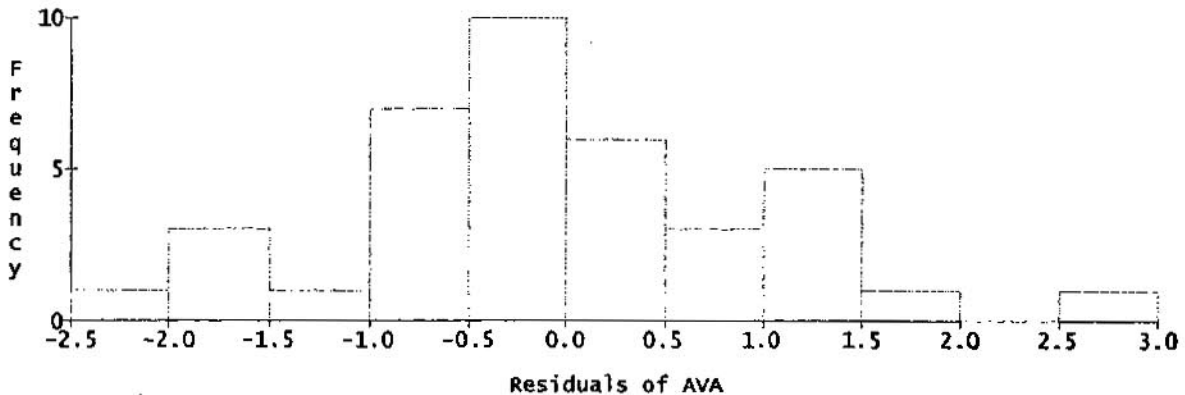
Residuals of AVA vs Fitted Values
Using Studentized Residuals in Model DESIGN_AUTO_AVA



Normal Probability Plot of Residuals of AVA
Using Studentized Residuals in Model DESIGN_AUTO_AVA
(Sample size = 38)



Histogram of Residuals of AVA
Using Studentized Residuals in Model DESIGN_AUTO_AVA
(Sample size = 38)

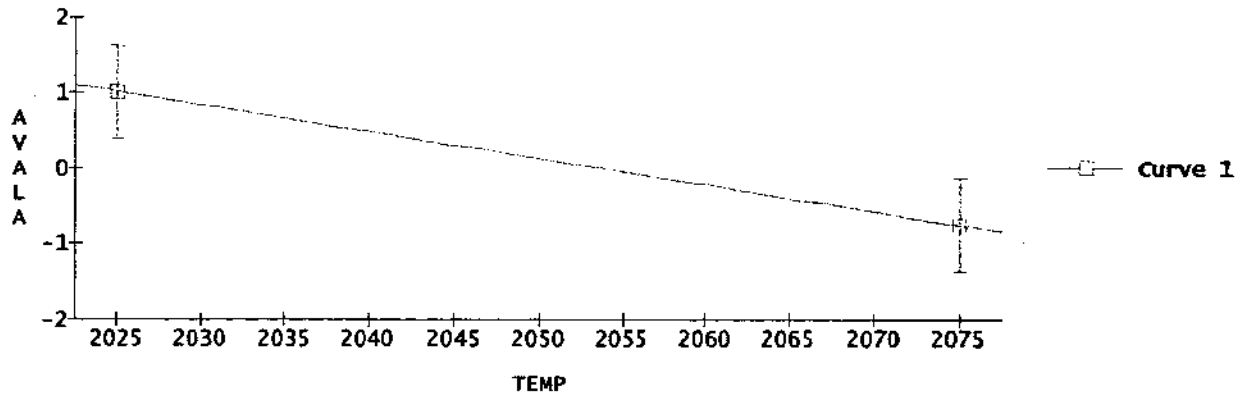


Appendix A-5U (cont.)

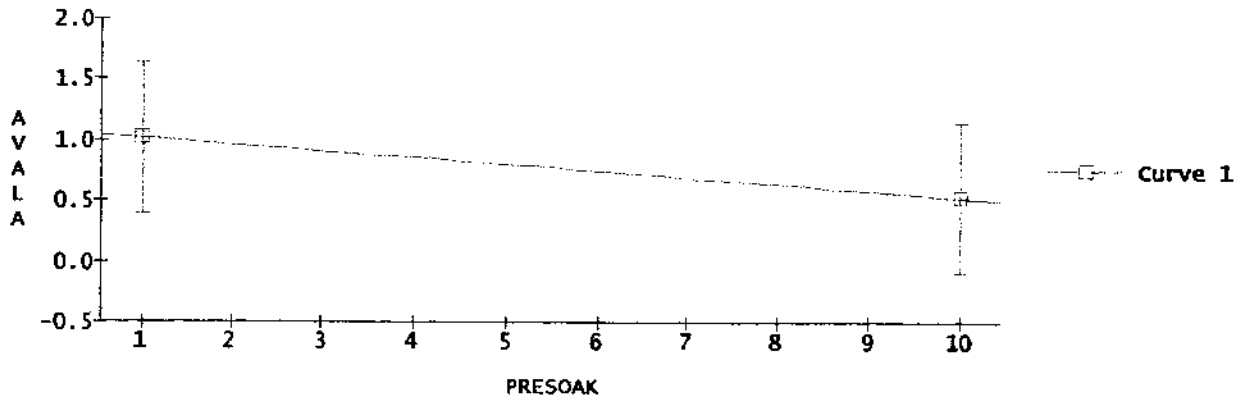
0 Factor, Response or Formula	1 Range	2 Initial Setting	3 Optimal Value
1 Factors			
2 TEMP	2025 to 2075	2050	2025
3 PRESOAK	1 to 10	5.5	1.0016
4 LOGSTRART	-4 to -3	-3.5	-3.0003
5			
6 Responses			
7 AVALA	MAX		1.0176

Converged to a tolerance of 0.00043 after 69 steps.

Predictions and 95% simultaneous confidence intervals
for mean responses of AVALA using model DESIGN_AUTO_AVA
P = 1.0016, LSR = -3.0003

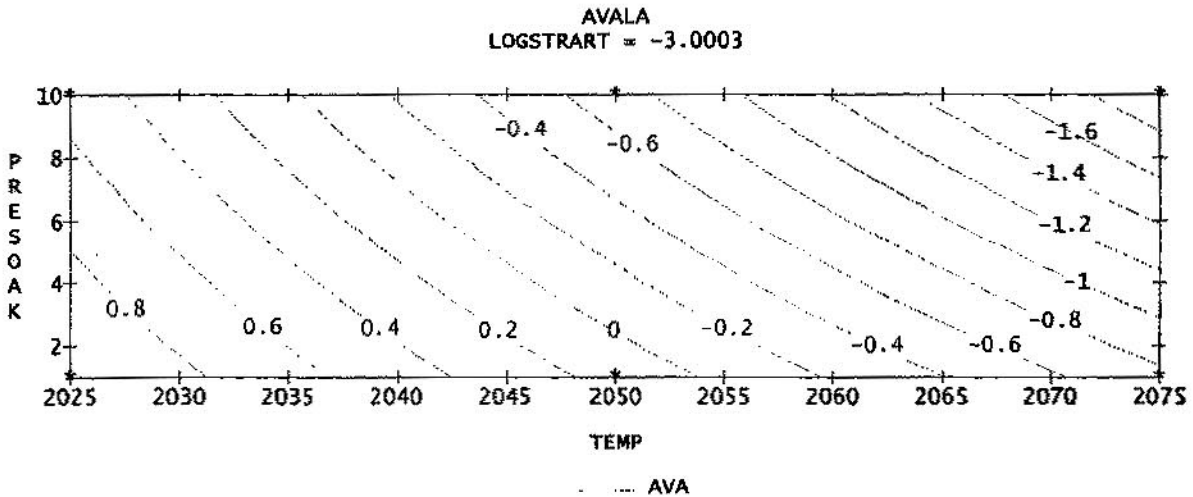
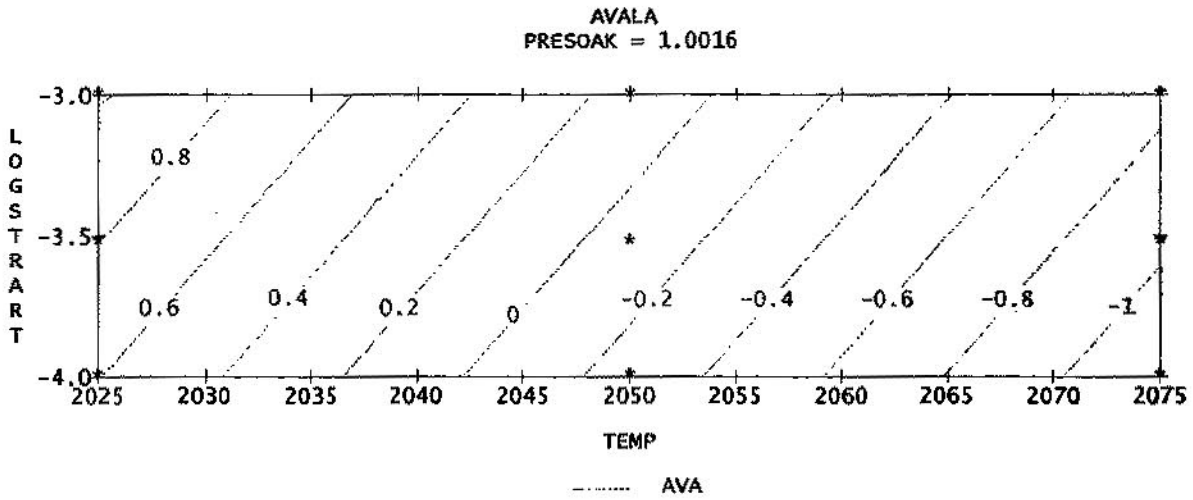
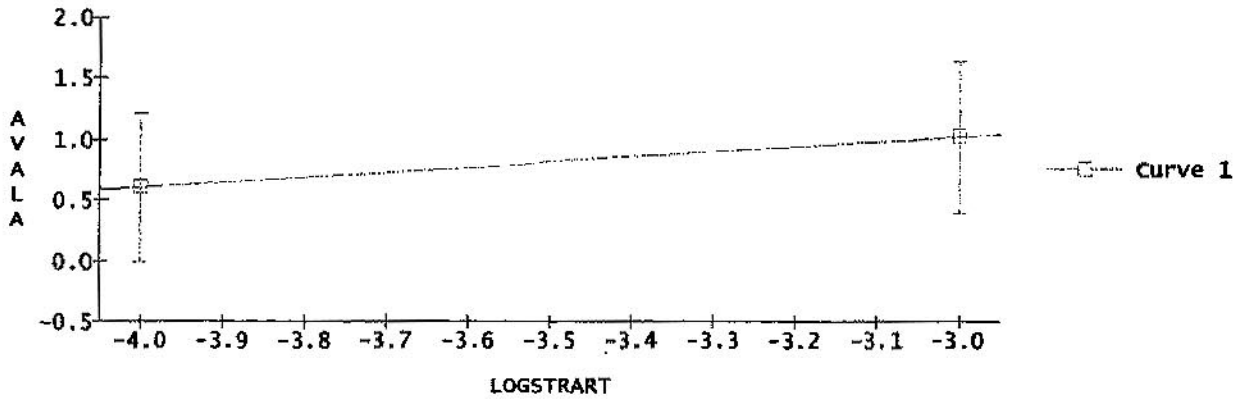


Predictions and 95% simultaneous confidence intervals
for mean responses of AVALA using model DESIGN_AUTO_AVA
LSR = -3.0003, T = 2025

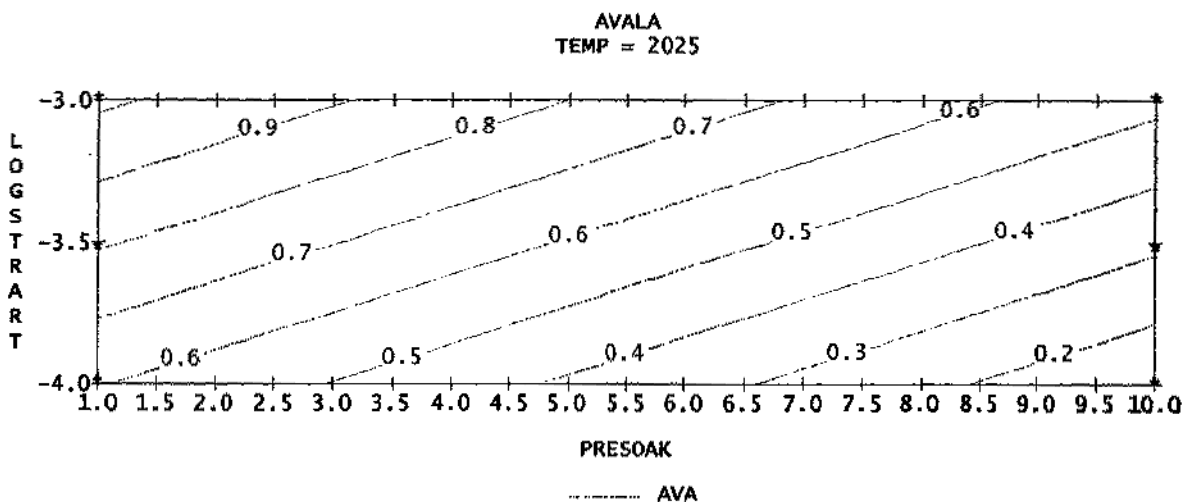


Appendix A-5U (cont.)

Predictions and 95% simultaneous confidence intervals
 for mean responses of AVALA using model DESIGN_AUTO_AVA
 T = 2025, P = 1.0016



Appendix A-5U (cont.)



Predictions and 95% simultaneous confidence intervals
for mean responses of AVALA using model DESIGN_AUTO_AVA
LSR = -3

P	T=2025
	Lower 0.312069
5	Predicted 0.799737
	Upper 1.287406

Appendix A-6C

Least Squares Coefficients, Response SDG, Model DESIGN__AUTO__SDG

0 Term 1 Coeff. 2 Std. Error 3 T-value 4 Signif.

 1 1 0.357895 0.068105 5.26 0.0001

No. cases = 19 R-sq. = 0.0000 RMS Error = 0.2969
 Resid. df = 18 R-sq-adj. = 0.0000 Cond. No. = 1

Least Squares Summary ANOVA, Response SDG Model DESIGN__AUTO__SDG

0 Source 1 df 2 Sum Sq. 3 Mean Sq. 4 F-Ratio 5 Signif.

 1 Total(Corr.) 18 1.586316
 2 Regression 0 0.000000
 3 Residual 18 1.586316 0.088129

R-sq. = 0.0000
 R-sq-adj. = 0.0000

Model obeys hierarchy. The sum of squares for each term is computed assuming higher order terms are first removed.

Least Squares Coefficients, Response SDA, Model DESIGN__AUTO__SDA

0 Term 1 Coeff. 2 Std. Error 3 T-value 4 Signif.

 1 1 0.247368 0.042830 5.78 0.0001

No. cases = 19 R-sq. = 0.0000 RMS Error = 0.1867
 Resid. df = 18 R-sq-adj. = 0.0000 Cond. No. = 1

Least Squares Summary ANOVA, Response SDA Model DESIGN__AUTO__SDA

0 source 1 df 2 Sum Sq. 3 Mean Sq. 4 F-Ratio 5 signif.

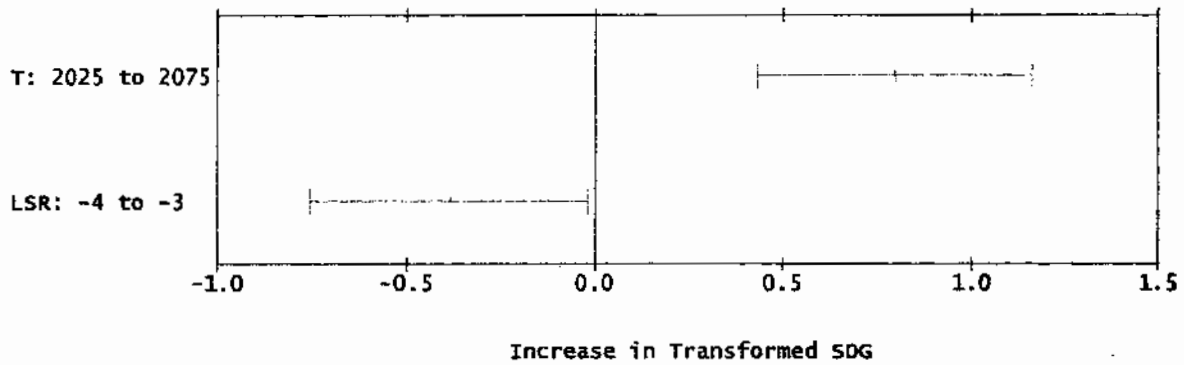
 1 Total(Corr.) 18 0.6273684
 2 Regression 0 0.0000000
 3 Residual 18 0.6273684 0.0348538

R-sq. = 0.0000
 R-sq-adj. = 0.0000

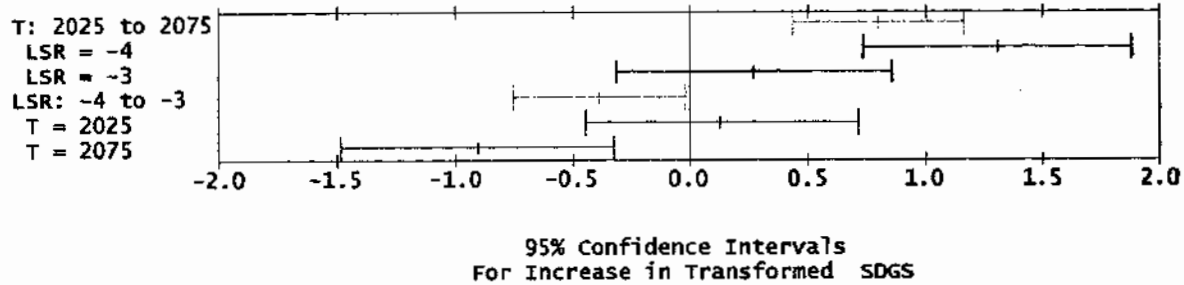
Model obeys hierarchy. The sum of squares for each term is computed assuming higher order terms are first removed.

Appendix A-6U (cont.)

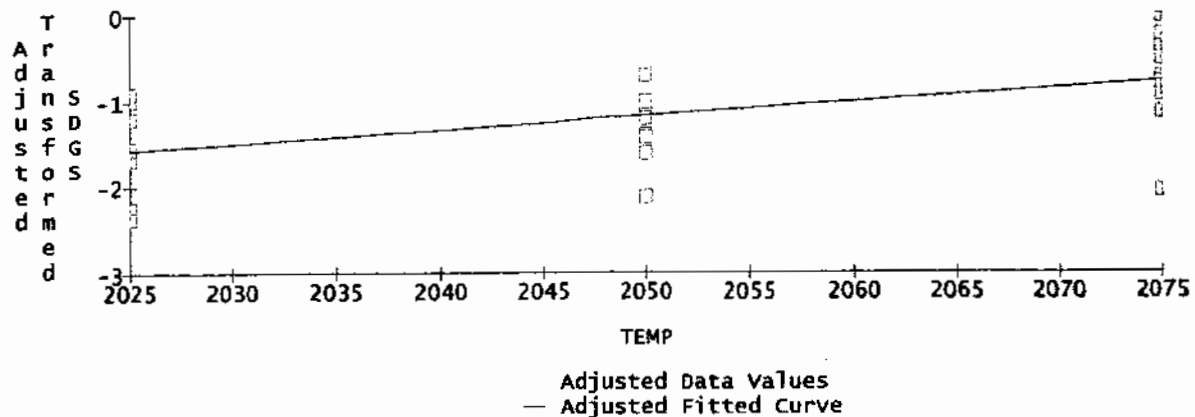
Mulreg @EXPT@MULREG, Model DESIGN_AUTO_SDG
Main Effects on Transformed Response SDGS
(with 95% Confidence Intervals)



Mulreg @EXPT@MULREG, Model DESIGN_AUTO_SDG
Interaction Effects of TEMP with LOGSTART
On Transformed Response SDGS

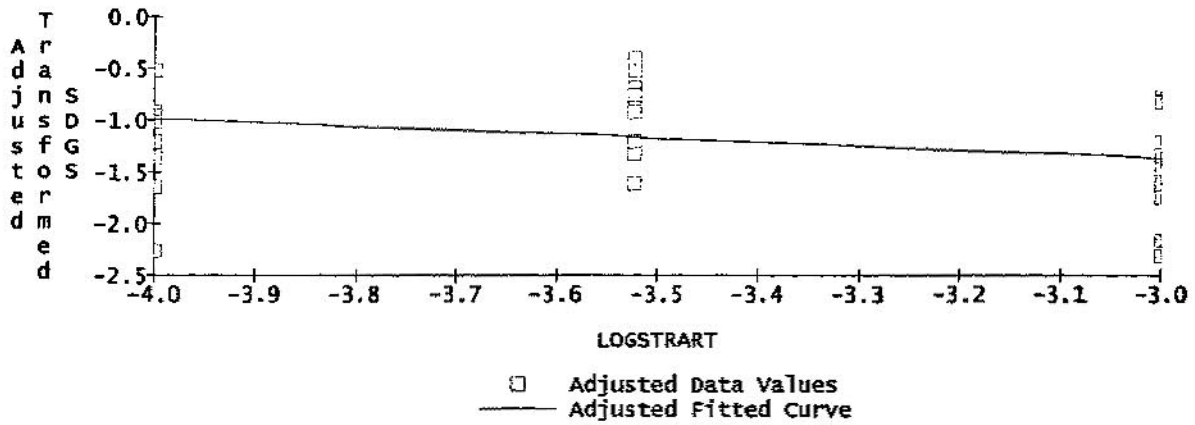


SDGS vs TEMP, Adjusted for Remaining Predictors
using Mulreg @EXPT@MULREG, Model DESIGN_AUTO_SDG

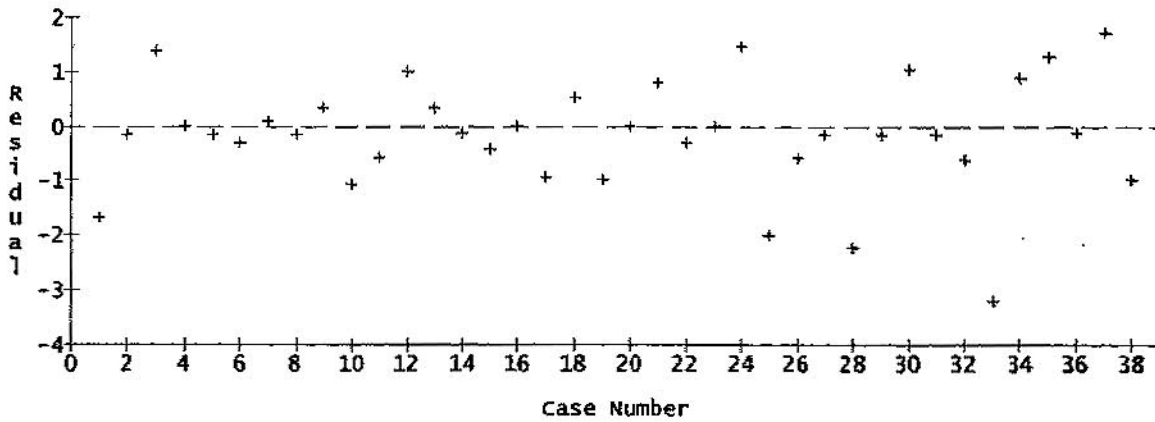


Appendix A-6U (cont.)

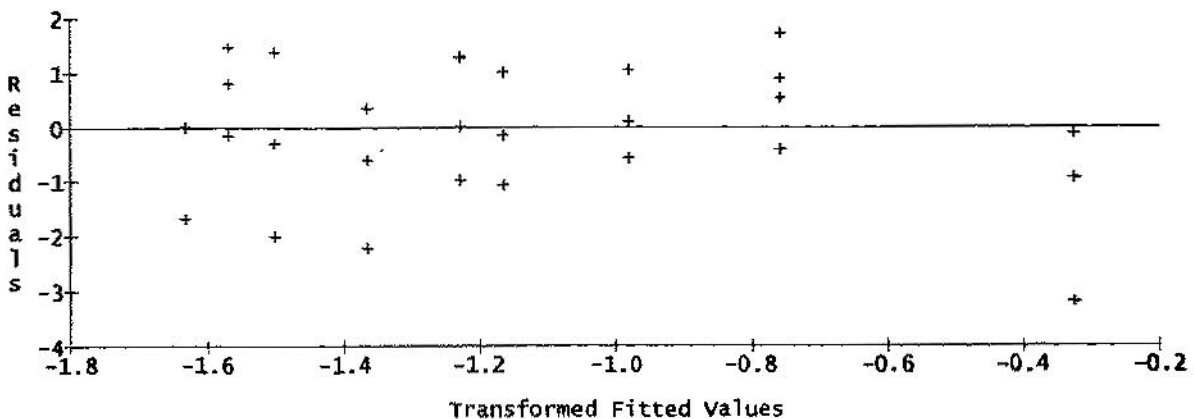
SDGS vs LOGSTART, Adjusted for Remaining Predictors
Using Mulreg @EXPT@MULREG, Model DESIGN_AUTO_SDG



Case Order Graph of Residuals of Transformed SDG
Using Studentized Residuals in Model DESIGN_AUTO_SDG

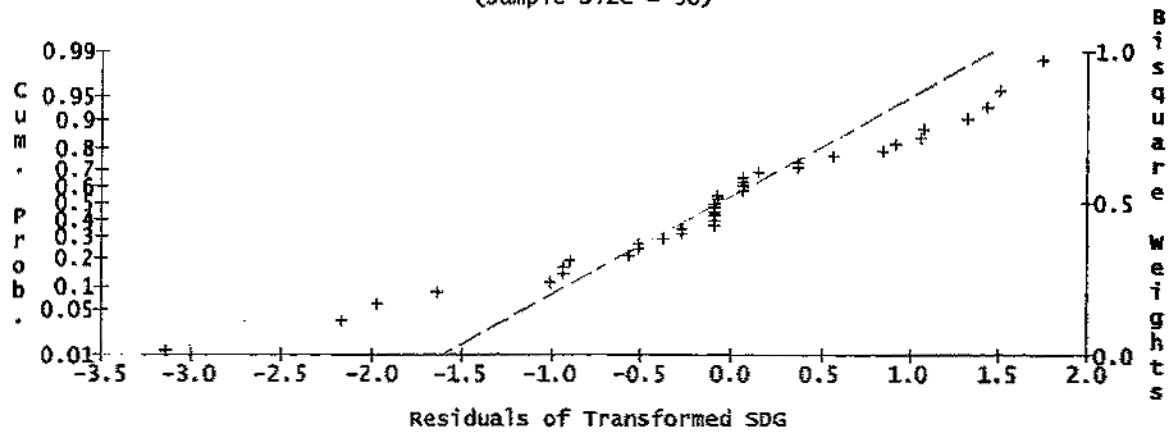


Residuals of Transformed SDG vs Fitted Values
Using Studentized Residuals in Model DESIGN_AUTO_SDG

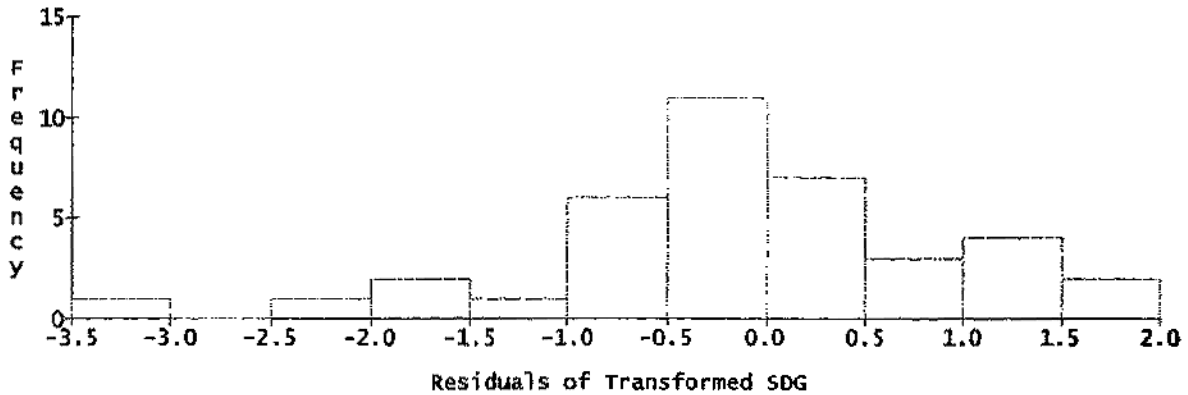


Appendix A-6U (cont.)

Normal Probability Plot of Residuals of Transformed SDG
Using Studentized Residuals in Model DESIGN_AUTO_SDG
(sample size = 38)



Histogram of Residuals of Transformed SDG
Using Studentized Residuals in Model DESIGN_AUTO_SDG
(sample size = 38)



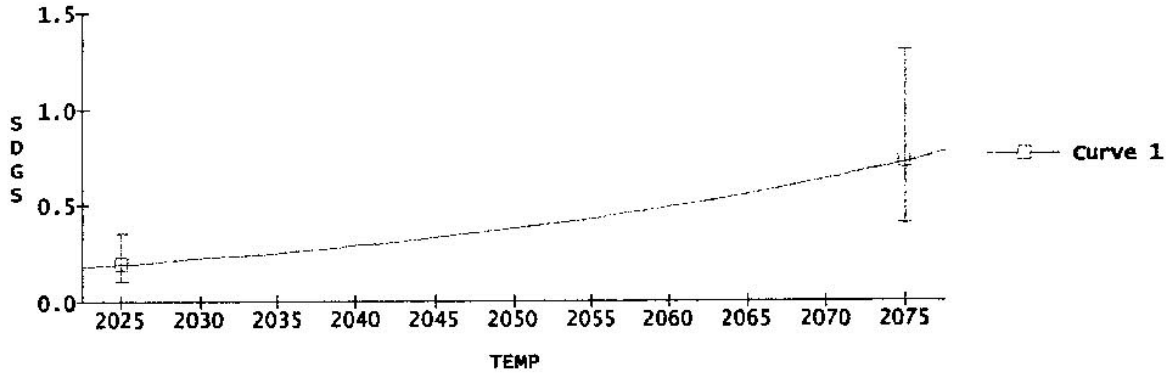
0 Factor, Response or Formula	1 Range	2 Initial Setting	3 Optimal Value

1 Factors			
2 TEMP	2025 to 2075	2050	2025
3 LOGSTRART	-4 to -3	-3.5	-3.9999
4			
5 Responses			
6 SDGS	MIN		0.19518

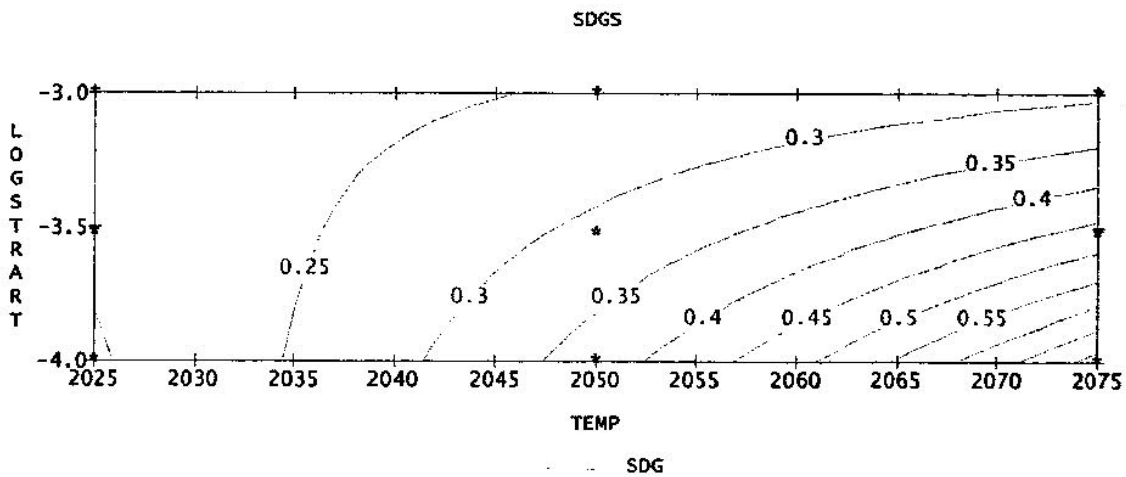
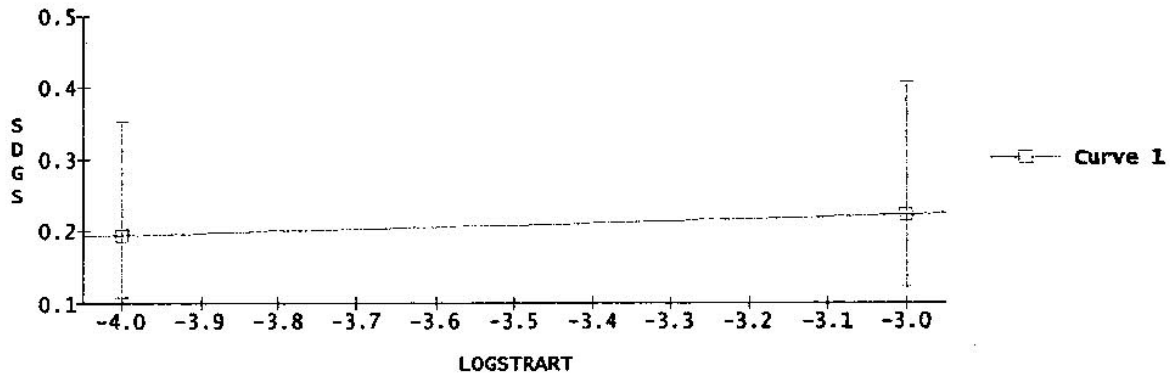
Converged to a tolerance of 0.00009 after 43 steps.

Appendix A-6U (cont.)

Predictions and 95% simultaneous confidence intervals
for mean responses of SDGS using model DESIGN_AUTO_SDG
LSR = -3.9999



Predictions and 95% simultaneous confidence intervals
for mean responses of SDGS using model DESIGN_AUTO_SDG
T = 2025



Predictions and 95% simultaneous confidence intervals
for mean responses of SDGS using model DESIGN_AUTO_SDG

LSR	T=2025
-3	Lower 0.122143
	Predicted 0.223081
	Upper 0.407435

REPORT DOCUMENTATION PAGE

Form Approved
OMB No. 0704-0188

Public reporting burden for this collection of information is estimated to average 1 hour per response, including the time for reviewing instructions, searching existing data sources, gathering and maintaining the data needed, and completing and reviewing the collection of information. Send comments regarding this burden estimate or any other aspect of this collection of information, including suggestions for reducing this burden, to Washington Headquarters Services, Directorate for Information Operations and Reports, 1215 Jefferson Davis Highway, Suite 1204, Arlington, VA 22202-4302, and to the Office of Management and Budget, Paperwork Reduction Project (0704-0188), Washington, DC 20503.

1. AGENCY USE ONLY (<i>Leave blank</i>)		2. REPORT DATE August 2001	3. REPORT TYPE AND DATES COVERED Technical Memorandum	
4. TITLE AND SUBTITLE High Temperature, Slow Strain Rate Forging of Advanced Disk Alloy ME3			5. FUNDING NUMBERS WU-714-04-10-00	
6. AUTHOR(S) Timothy P. Gabb and Kenneth O'Connor				
7. PERFORMING ORGANIZATION NAME(S) AND ADDRESS(ES) National Aeronautics and Space Administration John H. Glenn Research Center at Lewis Field Cleveland, Ohio 44135-3191			8. PERFORMING ORGANIZATION REPORT NUMBER E-12778	
9. SPONSORING/MONITORING AGENCY NAME(S) AND ADDRESS(ES) National Aeronautics and Space Administration Washington, DC 20546-0001			10. SPONSORING/MONITORING AGENCY REPORT NUMBER NASA TM-2001-210901	
11. SUPPLEMENTARY NOTES Responsible person, Timothy P. Gabb, organization code 5120, 216-433-3272.				
12a. DISTRIBUTION/AVAILABILITY STATEMENT Unclassified - Unlimited Subject Category: 26 Available electronically at http://gltrs.grc.nasa.gov/GLTRS This publication is available from the NASA Center for AeroSpace Information, 301-621-0390.			12b. DISTRIBUTION CODE	
13. ABSTRACT (<i>Maximum 200 words</i>) The advanced disk alloy ME3 was designed in the HSR/EPM disk program to have extended durability at 1150 to 1250 °F in large disks. This was achieved by designing a disk alloy and process producing balanced monotonic, cyclic, and time-dependent mechanical properties, combined with robust processing and manufacturing characteristics. The resulting baseline alloy, processing, and supersolvus heat treatment produces a uniform, relatively fine mean grain size of about ASTM 7, with as-large-as (ALA) grain size of about ASTM 3. There is a long term need for disks with higher rim temperature capabilities than 1250 °F. This would allow higher compressor exit (T3) temperatures and allow the full utilization of advanced combustor and airfoil concepts under development. Several approaches are being studied that modify the processing and chemistry of ME3, to possibly improve high temperature properties. Promising approaches would be applied to subscale material, for screening the resulting mechanical properties at these high temperatures. An obvious path traditionally employed to improve the high temperature and time-dependent capabilities of disk alloys is to coarsen the grain size. A coarser grain size than ASTM 7 could potentially be achieved by varying the forging conditions and supersolvus heat treatment. The objective of this study was to perform forging and heat treatment experiments ("thermomechanical processing experiments") on small compression test specimens of the baseline ME3 composition, to identify a viable forging process allowing significantly coarser grain size targeted at ASTM 3-5, than that of the baseline, ASTM 7.				
14. SUBJECT TERMS Forging; Superalloy; Disk; Grain size; Thermomechanical processing			15. NUMBER OF PAGES 96	
			16. PRICE CODE	
17. SECURITY CLASSIFICATION OF REPORT Unclassified	18. SECURITY CLASSIFICATION OF THIS PAGE Unclassified	19. SECURITY CLASSIFICATION OF ABSTRACT Unclassified	20. LIMITATION OF ABSTRACT	